CU/CoA-9612

Cranfield UNIVERSITY

Low Speed Aerodynamic Characteristics of 60° Rounded Leading-Edge Delta Wing with Vortex Flaps Part 2 1.15m Span Delta Wing

(Effect of Flap Deflection Angle and Leading-Edge Radius)

K. Rinoie

COA report No.9612
December 1996

College of Aeronautics
Cranfield University
Cranfield
Bedford MK43 0AL
England

College of Aeronautics Report No.9612
December 1996

ıracteristics of 60° Rounded
ing with Vortex Flaps
an Delta Wing
and Leading-Edge Radius)

RINOIE

College of Aeronautics
Cranfield University
Cranfield
Bedford MK43 0AL
England

Abstract

Low speed wind tunnel measurements have been made on a 1.15m span 60° delta wing with rounded leading-edge vortex flaps. The purpose of the measurements was to assess the benefits of the rounded leading-edge vortex flaps on the lift/drag ratio. The force and surface pressure measurements were made at a Reynolds number based on the centreline chord of $2x10^6$. The increase in the radius of the rounded leading-edge reduces the drag significantly both with and without flap deflection except in the minimum drag region. Deflecting the rounded leading-edge vortex flap improves the lift/drag ratio compared with the sharp edged vortex flap at relatively higher lift coefficients. The greatest percentage improvement in the lift/drag ratio compared with the sharp edged flat delta wing is more than 50% at a lift coefficient of 0.5 for the rounded edge delta wing with flap deflected.

Nomenclature

b	local span, m
C_D	drag coefficient
C_L	lift coefficient
C_m	pitching moment coefficient non-dimensionalised using Cr and measured about x/Cr=0.4
Cp	pressure coefficient
Cr	wing centre-line chord, m
D	rounded leading-edge diameter, m
L/D	lift/drag ratio
U_∞	free stream velocity, m/s
x	chordwise coordinate measured from the apex of the delta wing, m
y	spanwise coordinate orthogonal to x, measured from the wing centre-line, m
α	wing angle of attack, degrees
δ_f	vortex flap deflection angle measured normal to the hinge line for original wing without leading-edge modification, degrees
δ_{fc}	corrected vortex flap deflection angle for the wing with leading-edge modification, degrees

Notations

SLE Sharp Leading-edge
R05 Rounded Leading-edge D=0.005m
R15 Rounded Leading-edge D=0.015m
R30 Rounded Leading-edge D=0.03m
/n δ_f= n (n=0° - 60°)
/45 U_∞=45m/s
/R45 U_∞=45m/s with roughness

1. Introduction

A leading-edge vortex flap (LEVF) is a device that improves the low speed aerodynamic characteristics of a delta wing[1]. A pair of leading-edge separation vortices formed over the sharp edged delta wing produce an upward suction force that increases the drag component and consequently decreases the lift/drag ratio (Fig.1a). The LEVF is a leading-edge deflectable surface. When the LEVF is deflected downward, a leading-edge separation vortex is formed over the forward facing surface. The suction force produced by this vortex is expected to reduce the drag component and to increase the lift/drag ratio that plays a major role in improving the take-off and climb performance of delta wing aircraft (Fig.1b). Many tests have confirmed the benefit of the LEVF[2-4]. The present author also conducted research on the LEVF[5,6].

Another way to improve delta wing performance is to use a rounded leading-edge. A large fraction of the leading-edge suction force will act on the rounded leading-edge and so reduce the drag component of the delta wing (Fig.1c). Numerous tests have been done to investigate the effect of the rounded leading-edge[7-10]. These confirmed the benefit of the rounded leading-edge but revealed the dominance of Reynolds number effect on the rounded edged wing performance.

These studies on the rounded leading-edge delta wings led to the idea that the combination of the LEVF and the rounded leading-edge might improve the LEVF characteristics much further. By deflecting the rounded leading-edge LEVF, suction forces caused both by the leading-edge separation

vortex over the flap surface and by the rounded leading-edge are expected to reduce the drag component and to increase the lift/drag ratio (Fig.1d).

Some wind tunnel tests[11-13] were conducted at the College of Aeronautics to investigate the rounded edge vortex flap. A 60° rounded leading-edge delta wing model with 10% thickness aerofoil section was tested at a Reynolds number based on the centre line chord of $8x10^5$. Results indicated that the rounded leading-edge delta wing with a 30° vortex flap deflection improves the lift/drag ratio at lift coefficients higher than 0.4, when compared with the sharp edged flat delta wing. These results encouraged us to make further wind tunnel studies to confirm the benefit of the rounded LEVF for the 60° delta wing. Differences in the vortex flap deflection angle and in the radius of the rounded leading-edge are thought to affect the performance of the delta wing. The Reynolds number effect that is dominant for the rounded edge delta wing, as noted above, would also be important for the performance of the rounded edged vortex flap. In this paper these effects are investigated.

Here, tests were conducted in the Cranfield 2.4 x 1.8 m low-speed wind tunnel. The 60° delta wing model used in Ref.6 was again used by modifying the originally sharp leading-edge into a rounded one. The force and surface pressure measurements were made on this delta wing model with different LEVF deflection angles and with three different rounded leading-edges. Measurements were made in the incidence range of -4° to +36°. In order to examine the Reynolds number effect, two different wind tunnel speeds of U_∞=30 and 45m/s were tested. Leading-edge roughness was also applied in some cases.

In summary, the purpose of this study is
1) to confirm the benefit of rounded leading-edge vortex flaps,
2) to study the effect of the difference in the rounded leading-edge radius on wing performance,
3) to investigate the optimum vortex flap deflection angle giving the maximum lift/drag ratio,
4) to examine the Reynolds number effect.

2. Experimental Details

Fig.2 shows the model details. This model is the same one that was tested in Ref.6, except for the leading-edge modification. The original model is a sharp edged 60° delta wing with a centre line chord length Cr of 1m. It has a symmetrical convex aerofoil section with a maximum thickness/chord ratio of 4.8%. The spanwise thickness distribution varies linearly from centreline to tip. Details of this original wing section are described in Ref.6. Two rows of pressure tappings are located on the upper surface. The model has the LEVF hinge lines running from the wing apex to 75% of the trailing-edge semispan station. The flap deflection angle δ_f is defined as the angle between the mean line of the original wing and that of the vortex flap without leading-edge modification, measured in the plane normal to the hinge line (see section B-B in Fig.2). Nine different flap deflections of δ_f =0° - 60° were tested.

Rounded leading-edge modifications were made by attaching rounded leading-edge sections to the lower surface of the original wing (Fig.3). The plan shape of this section is the same as that of the vortex flap, so that the vortex flap is deflectable. It has a constant leading-edge diameter D between the chordwise stations of x/Cr=0.3 and 0.8. The diameter is defined in the plane normal to the leading-edge line (see section C-C in Fig.2). This diameter decreases linearly to zero from x/Cr=0.3 towards the apex and from x/Cr=0.8 towards the trailing-edge. The thickness of this section in a spanwise direction also decreases to zero towards the flap hinge line. Three different leading-edge diameters of D=5mm, 15mm and 30mm were tested. The ratio of rounded leading-edge radius to the root chord length is 0.25%, 0.75% and 1.5% for D=5mm, 15mm and 30mm, respectively. Two pressure tappings are located on the D=15mm and 30mm rounded leading-edge sections (Fig.3). The chordwise positions of the pressure tappings are the same as those of the main wing. Any irregularities along the intersection between the original wing and the rounded edge section were carefully blended by using Plasticine.

The experiments were made in the Cranfield 2.4m x 1.8m low-speed, closed working section, closed return wind tunnel. Most of the tests were made at a tunnel speed of U_∞=30m/s. Some tests were made at U_∞=45m/s to examine

the Reynolds number effect. The Reynolds number based on the wing centreline chord was $2x10^6$ at U_∞=30m/s and $3x10^6$ at U_∞=45m/s. The freestream turbulence intensity of the tunnel is about 0.09%. The model was mounted inverted from the overhead balance by a single shielded strut and a tail wire at the tunnel centre line. A picture of the model mounted in the wind tunnel is shown in Fig.4. The incidence range covered was from -4° to +36° for U_∞=30m/s. The incidence range at U_∞=45m/s was limited by the tunnel balance performance. Lift, drag and pitching moment were measured using the overhead six-component electromechanical balance. The aerodynamic coefficients were obtained using the same tunnel boundary correction methods used in Refs.5 and 6. All aerodynamic coefficients were calculated based on the original delta wing area. The estimated overall accuracy of the coefficients is better than ±2% at low angles of attack. Although tunnel boundary corrections were applied, the accuracy at higher angles of attack is believed to decrease due to the higher tunnel wall interference. Surface pressure distributions were measured using a "Scanivalve" mounted within the model. The estimated overall accuracy of the pressure coefficient is ±3%. Surface pressure measurements were made for the D=15mm and D=30mm rounded edge models.

Supplementary tests were made to examine the Reynolds number effect by adding roughness to the leading-edge of the model. The roughness used is a No.120 sand paper strip whose width is 10mm. These strips were attached on both the upper and lower surfaces using double sided tape. The height including the double sided tape is 0.45mm. These strips were attached 10mm from the leading-edge. According to the estimation method based on Ref.14, the strips used here would be sufficient to cause transition to turbulent flow from the roughness position.

Examples of the notation used in this paper are as follows. At U_∞=30m/s, SLE/00 represents sharp leading-edge wing without flap deflection (δ_f=0°). R05/30 represents rounded leading-edge D=5mm with flap deflection of δ_f=30°. At U_∞=45m/s, R15/25/45 represents rounded leading-edge D=15mm for δ_f=25°. R15/30/R45 represents rounded leading-edge D=15mm for δ_f=30° with roughness strips at U_∞=45m/s. Measurements with roughness were only made for the R15 wing at U_∞=45m/s.

3. Results and Discussion

3.1 Repeatability and Comparisons with Other Experiments for Sharp-Edged Delta Wings

In order to examine the repeatability of the tests, three component force measurements for the original sharp edged wing with δ_f=0° and 30° were repeated. Figs.5a-5d show the results together with data from Ref.6 for the same wing configurations. The present lift, drag, lift/drag ratio and the pitching moment distributions agree very well with those of Ref.6.

Comparisons of lift coefficient with 60° flat delta wing data from Ref.15 are also shown in Fig.5a. In Ref.15, measurements were made using a 60°, 0.10in thickness flat delta wing with beveled sharp edges at a Reynolds number of 1 million. The lift curve is in excellent agreement with the present data (δ_f =0°) until about α=25°. The discrepancy in the C_L at α=0° is due to the presence of the shielded strut in the present measurements, as was explained in Ref.6.

3.2 Effect of Rounded Leading-Edge Radius

Three Component Balance Measurements

Figs.6a-6f show the lift, drag, lift/drag and pitching moment curves for three different rounded edge models with and without flap deflection (δ_f =0° and 30°) together with the sharp edged wing results.

The C_L vs. α curves in Fig.6a shows that as the radius of the rounded edge increases the C_L decreases slightly. Deflecting the LEVF decreases the C_L for all models, as was expected.

Fig.6b shows the C_D vs. α curves. This shows that increasing the leading-edge radius reduces the C_D except in the minimum drag region. It should be noted that even the smallest increase in the rounded edge radius (R05/00 and R05/30) decreases the C_D. The high suction effect of the rounded leading-edge is demonstrated.

Figs.6c and 6d show the lift to drag ratio (L/D) versus C_L when δ_f =0° and 30°. The effects of the R05/00 and R05/30 models are very small compared with the corresponding sharp edged models. Comparisons with SLE/00, R15/00 and R30/00 in Fig.6c show a limited improvement in the maximum L/D due to the rounded edge when δ_f =0°. However, at C_L values greater than 0.2, R15/00 and R30/00 show better L/D ratios than SLE/00. Comparisons for the δ_f =30° models (Fig.6d) show no improvement of the maximum L/D due to the leading-edge roundness. The maximum L/D value of R30/30 is significantly smaller than those of SLE/30 and R15/30. However at C_L's higher than 0.5, the L/D of R30/30 shows the best value of L/D.

In order to visualise the LEVF deflection effects on L/D more clearly, the percentage increase in L/D for R15, R30 and SLE/30 wings compared with the SLE/00 wing is plotted in Fig.6e. This shows that the L/D of no flap deflection (R15/00 and R30/00) is increased more than 10% above that of the SLE/00 wing for lift coefficients greater than 0.2. The sharp edged LEVF wing (SLE/30) shows better performance than R15/00 and R30/00 in the C_L range between 0.2 and 0.6. However Fig.6e also shows that the rounded edges with the LEVF (R15/30 and R30/30) improve the L/D more than the SLE/30 configuration for C_L's greater than 0.5. The greatest L/D improvement of more than 50% compared with the sharp flat delta wing is observed for R30/30 at about C_L=0.6

Fig.6f shows the pitching moment curves versus C_L. The LEVF and rounded edge has little effect on C_m. The aerodynamic centre position measured from the C_m-C_L slope is about 0.57Cr for all cases.

Figs.7a and 7b show the results from Ref.8. In Ref.8 experiments were made on 60° flat delta wings with sharp and two different rounded leading-edges. The models have maximum thickness to local chord ratio of 3%. The rounded leading-edge radius normalised by local chord length is 0.791% and 1.582%. Measurements were made at a Reynolds number based on mean chord of $1.6\text{x}10^6$. The C_L-α (Fig.7a) and C_D-α curves (Fig.7b) show a decrease in C_L and C_D when the rounded leading-edge radius is increased. These results are similar to the presents results when δ_f =0° in Figs.6a and 6b.

Surface Pressure Measurements

Figs.8 and 9 show surface pressure distributions in the spanwise direction for the upper surface at x/Cr=0.4 and 0.8. The spanwise coordinate is normalised by the original wing local semi span length. Figs.8a-8f compare the results for R15, R30 and sharp edge[6] wings when δ_f =0°. Figs 9a-9f are results when δ_f =30°. The formation of the leading-edge separation vortex is observed in every figure. It is noted that for the rounded edge wings, a large suction force is acting at the leading-edge (see e.g. at α=24° in Figs.8c and 9a).

In order to clarify the effect of the rounded leading-edge, pressure distributions at constant incidences of α=6°, 12° and 18° at x/Cr=0.4 are shown in Figs.10a-10c (δ_f =0°) and Figs.11a-11c (δ_f =30°). Fig.10a shows that the suction region is present on all three wings. As the radius of the rounded edge increases, the suction peak decreases and the spanwise length of the suction region shortens. A similar trend is seen at α=12° (Fig.10b) and α=18° (Fig.10c). For δ_f =30° and α=6° in Fig.11a, the effect of the rounded edge is very small. However, at higher incidences (Figs.11b and 11c) an increase in the rounded edge radius reduces the spanwise length of the suction region, very much as for δ_f =0°.

3.3 Effect of Rounded Leading-Edge Radius on Different δ_f

The C_L, C_D and L/D Distributions

Figs.12a-12c (R15) and Figs.13a-13c (R30) show the C_L, C_D and L/D distributions for nine different flap deflection angles. The C_L curves (Figs.12a, 13a) show the decrease in C_L as δ_f is deflected downward. The C_D curves (Figs.12b, 13b) show that the whole curve moves to higher values of incidence as δ_f is increased. These tendencies are the same as reported in the previous study with sharp leading-edge[5,6].

The L/D vs. C_L curves for the R15 wing (Fig.12c) indicates that the maximum L/D is attained when δ_f =15°. As the δ_f is increased above 25°, the local maximum L/D becomes smaller than that for δ_f =0°. The L/D curves for

the R30 wing (Fig.13c) show that the maximum L/D is not improved by the flap deflection when compared with the R30/00 wing. However, both figures show that the L/D is improved over wide C_L regions when compared with corresponding wings without flap deflection, except for the rounded edge wings with δ_f =40°, 50° and 60°.

Figs.14a and 14b show the L/D vs. flap deflection angle at a constant C_L of 0.25 (Fig.14a) and 0.5 (Fig.14b). The data were read from Figs. 12c and 13c. Since the rounded leading-edge section was attached to the lower surface of the sharp edged wing, the true flap deflection angle is greater than δ_f for R15 and R30 wings. The δ_{fc} in Figs.14 indicates the corrected angle. Here, the true flap deflection angle at x/Cr=0.55, which is a mid chordwise station of the constant radius rounded leading-edge section (see Fig.2), is used as δ_{fc}. Details of the definition of δ_{fc} are described in Appendix A. The L/D vs. δ_{fc} curves at C_L=0.25 in Fig.14a are similar for all three wings. However, the R15 wing shows the larger L/D for whole range of δ_{fc}. The absolute maximum L/D at C_L=0.25 is about 12.7 when R15 and δ_{fc}=21° (δ_f =15°). Compared with the sharp edged flat delta wing (SLE/00), the L/D has increased about 48%. Fig.14a also shows that the R30 wing is not so effective as the R15 wing.

Fig.14b shows L/D vs. δ_{fc} curves at C_L=0.5. The L/D vs. δ_{fc} curves are similar for the R15 and R30 wings. The absolute maximum L/D at C_L=0.5 is about 7.8, which is attained for the R30 wing between δ_{fc}=32.5° and 37.5° (δ_f=20° and 25°). The % increase in L/D compared with the SLE/00 is about 53%. Similarly, the maximum % increase in L/D compared with the SLE/00 for the R15 wing is more than 50% when δ_{fc}=36° (δ_f=30°). The measurements for the original sharp edged wing were made for a limited number of cases. However, since the results in Ref.6 indicated that δ_f greater than 40° is not as effective as δ_f smaller than 30°, it can be said that the maximum L/D for the sharp edged wing at C_L=0.5 is attained at δ_f =30°. The maximum % increase in L/D compared with the SLE/00 is about 40% when δ_f =30° (SLE/30). This means that the rounded leading-edge vortex flaps are more effective than the sharp edged vortex flaps at relatively higher lift coefficients.

Surface Pressure Distributions

Surface pressure distributions at constant incidence for different δ_f at x/Cr=0.4 are shown in Figs.15a-15c (at α=6°) and Figs.16a-16c (at α=12°) for R15 and R30 wings, together with the sharp edged wing results[6]. Effects of the rounded edge radius are the same as discussed in Figs.10 and 11. The effect of the flap deflection for the R15 and R30 wings is similar to that of the sharp edged wing. At α=6° in Figs.15, as the LEVF is deflected, the suction region over the flap surface shrinks and the suction region inboard of the flap hinge line extends. At α=12° in Figs.16, a similar tendency is observed.

Fig.17a shows pressure distributions for three wings (R15, R30 and SLE[6]) when the absolute maximum L/D was attained for each wing. As was discussed in Ref.6, the maximum L/D for the sharp edged wing is attained when the flow attaches on the flap surface without forming a large separation vortex. This figure shows that for the R15 and R30 wings only a small suction region at the leading-edge is observed. This means that for the rounded edged wing with the vortex flap, the maximum L/D is attained at the same flow condition as the sharp edged wing, when there is no large separation vortex on the flap surface. This result coincides with the one deduced in Ref.16.

Fig.17b shows the pressure distributions when the local maximum L/D is attained at constant C_L of 0.5 for three wing configurations. Since the pressure measurements were made at a specific incidence without concerning the C_L, the Cp distributions when the C_L is the nearest to the constant value of 0.5 are shown. The Cp distributions show that a separation vortex is formed on the vortex flap surface for all three configurations. The spanwise length of the vortex for the SLE/30 almost coincides with the flap span. As the rounded edge radius increases, the suction peak of the vortex decreases.

3.4 Discussion on Leading-Edge Suction Force

Axial Force Distributions

Fig.18a shows the axial force coefficients C_A versus C_L curves. The C_A is defined by

$$C_A = C_D \cos\alpha - C_L \sin\alpha.$$

A negative value of C_A suggests that there is a suction force acting on the wing. The SLE/00 wing has a small negative value of C_A at C_L's higher than 0.3. But the suction component of C_A for the R15/00 and R30/00 wings is much larger than the SLE/00, as expected.

The C_A distributions for the wing with vortex flaps show that a strong suction force is acting on the wing at C_L's higher than 0.2, even for the sharp edge wing (SLE/30). The minimum C_A is attained for the R30/30 wing. This clearly corresponds to the fact that the R30/30 attained the maximum L/D at high C_L in Fig.6d.

Fig.18b shows results from Ref.8. The C_A curves in this figure show similar distributions to those of Fig.18a for $\delta_f = 0°$ wings. As the radius of the leading-edge increases, negative value of C_A increases as in Fig.18a.

Suction Force Caused by Vortex Flap and Rounded Leading-Edge

In order to get an idea of the magnitude of the suction force caused by the separation vortex on the vortex flap and by the rounded leading-edge, a simple analysis using the surface pressure measurements is done in this section. By integrating the surface pressure coefficients over the whole upper and lower flap surface, the drag component caused by the vortex flap can be obtained. Similarly, by integrating the pressure coefficients around the rounded leading-edge, the suction force components acting to the rounded leading-edge can be obtained. However, since the number of pressure tappings is limited and since the pressure measurements were only made on the upper surface, a simplified approach was used here. By integrating the pressure coefficient along x/Cr=0.4 over the upper surface of the vortex flap normalised by the local span length, the suction force normal to the flap surface acting along x/Cr=0.4 can be estimated. The "drag force" component parallel to the free stream direction was then obtained geometrically using this suction force and is shown in Fig.19. It is noted that the integration was only made along one chordwise station. However, it is thought that this can represent the drag (suction) force caused by the separation vortex formed

over the flap surface. Hereafter, this force component is called the "vortex flap" force.

The pressure coefficients at the second tapping from the leading-edge can be thought to represent the pressure acting on the upper part of the rounded leading-edge. By integrating the pressure along the quarter circle of the upper rounded leading-edge, the leading-edge suction force parallel to the vortex flap mean line was estimated. The "suction force" component parallel to the free stream direction was then obtained geometrically. It is also noted that this "suction force" component is not the total force acting along the leading-edge from the apex to the trailing-edge. Hereafter, this force component is called the "rounded edge" force. Details of the "vortex flap" force and the "rounded edge" force are described in Appendix B. It is noted that these forces are normalised by the local semispan length and the free stream dynamic pressure. A positive value denotes that a drag force is acting on the wing.

Fig.19a shows the "vortex flap" force versus C_L for SLE/00. Since the flap deflection angle is 0°, as the C_L increases, the "vortex flap" drag force increases due to the suction force caused by the leading-edge separation vortex. Fig.19b shows results for the SLE/30. It is clear that for C_L<0.4 the vortex flap acts to reduce the drag. But at the higher C_L (C_L>0.5), the "vortex flap" force produces the drag.

Fig.19c shows the "vortex flap" force results for R15/00 together with the results of the "rounded edge" force. The "vortex flap" force shows similar values to those for SLE/00. The drag reduction due to the "rounded edge" force is seen over the whole C_L range. Fig.19d (R15/30) shows the similar "vortex flap" force values to those in Fig.19b. However, the C_L range where the suction "vortex flap" force is acting is reduced from that in Fig.19b. Figs.19e and 19f show results for the R30/00 and R30/30. The distribution patterns are similar to those in Figs.19c and 19d. It is clearly seen that the effect of the rounded-edge is larger than that of the R15 wing.

These results suggest that deflecting the vortex flap acts to reduce the drag force at lower C_L both for the sharp and rounded leading-edge wings. At higher C_L's, the rounded leading-edge helps to reduce the drag force due to

the leading-edge suction force.

3.5 Effects of Reynolds Number & Roughness

Figs.20a-20d show the three component balance results for the R15/00 wing at U_∞=45m/s with and without roughness strips together with results at U_∞=30m/s. These figures show that the increase in Reynolds number and the application of roughness does not cause any major change in the forces. The measurements for the R15/30 wing in Figs.21a-21d show similar results.

Surface pressure measurements for these conditions are shown in Fig.22a-22d (R15/00/45 & R15/30/45) and Figs.23a-23d (R15/00/R45 & R15/30/R45) at x/Cr=0.4 and 0.8. Surface pressures on the rounded leading-edge were not measured. Comparisons with Figs.8a, 8b, 9a and 9b show that the effects of Reynolds number and roughness on the pressure distributions are small.

These results indicate that the Reynolds number is not so dominant as expected in the present measurement ranges. These results also suggest that there is no benefit in deploying the roughness in the present measurements.

3.6 Effect of Nose Leading-Edge Sharpness

It is thought that the apex of the delta wing plays an important role in producing the leading-edge separation vortex. A rounded-edge at the apex might reduce the strength of the vortex. In order to investigate this effect, the rounded leading-edges were detached from the apex to the $0.1Cr$ chordwise position of the R15 wing so that the apex has sharp leading-edges. Measurements for R15 at δ_f=0° were made. Figs.24a-d show three component balance measurements compared with the results when the whole leading-edge has a rounded edge. These show that the nose leading-edge sharpness has little effect on the forces. Figs.25a-b show surface pressure distributions. Comparisons with Figs.8a and 8b show little difference between the two cases.

In this paper, the benefits of a rounded leading-edge vortex flap at low speed were investigated. A delta wing aircraft usually flies at supersonic speeds.

Study of a rounded leading-edge vortex flap at supersonic speeds will be an important subject.

4. Conclusions

Measurements were made using a 60° delta wing model to investigate the effect of rounded leading-edge with and without vortex flaps.

1) A rounded leading-edge delta wing without vortex flap deflection offers about a 10% improvement in lift/drag ratio relative to the sharp edged flat delta wing at a lift coefficient greater than about 0.2.

2) The increase in the radius of the rounded leading-edge reduces the drag significantly both with and without flap deflection except in the minimum drag region. The increase in the radius of the rounded leading-edge vortex flap also reduces the spanwise length of the suction pressure region on the flap surface. However, the maximum lift/drag ratio is not improved, when compared with the sharp edged wing at the Reynolds number tested.

3) Deflecting the rounded leading-edge vortex flap improves the lift/drag ratio compared with the sharp edged vortex flap at relatively higher lift coefficients. The greatest percentage improvement in the lift/drag ratio compared with the sharp edged flat delta wing is more than 50% at a lift coefficient of 0.5 for 20° flap deflection angle of a 30mm diameter rounded leading-edge vortex flap.

4) The maximum lift/drag ratio for the rounded edge wing is achieved when there is no large area of separation over the deflected vortex flap surface, that agrees with the observation made for the sharp edged delta wing.

5) Increasing the Reynolds number and adding roughness on the leading-edge of the wing showed no improvements in the lift/drag ratio.

6) Leading-edge sharpness at the nose section showed no significant change in the present measurements.

7) There is very little change of pitching moment for all the sharp and

rounded vortex flaps tested here.

Acknowledgements

The author would like to thank Professor J. L. Stollery for his beneficial advice in conducting the present study. He also expresses his gratitude to members of the workshop in the College for their help in performing the wind tunnel tests.

References

1) Rao, D.M., "Leading Edge Vortex-Flap Experiments on a 74deg. Delta Wing," NASA CR-159161, Nov. 1979.

2) Marchman III, J.F., "Effectiveness of Leading-Edge Vortex Flaps on 60 and 75 Degree Delta Wings," *Journal of Aircraft*, Vol.18, No.4, 1981, pp.280-286.

3) Campbell, J.F. and Osborn, R.F., "Leading-Edge Vortex Research: Some Nonplanar Concepts and Current Challenges," *Vortex Flow Aerodynamics Volume I*, NASA CP-2416, July 1986, pp.31-63.

4) Traub, L.W., "Aerodynamic Characteristics of Vortex Flaps on a Double-Delta Planform," *Journal of Aircraft*, Vol.32, No.2, 1995, pp.449-450.

5) Rinoie, K., "Experiments on a 60° Delta Wing with Vortex Flaps and Vortex Plates," *The Aeronautical Journal*, Vol.97, No.961, 1993, pp.33-38.

6) Rinoie, K. and Stollery, J.L., "Experimental Studies of Vortex Flaps and Vortex Plates," *Journal of Aircraft*, Vol.31, No.2, 1994, pp.322-329.

7) Jones, R., Miles, J.W. and Pusey, P.S., "Experiments in the Compressed Air Tunnel on Swept-back Wings Including Two Delta Wings," British Aeronautical Council (A.R.C.) R.&M. 2871, 1954.

8) Fletcher, H.S., "Low-Speed Experimental Determination of the Effects of Leading-Edge Radius and Profile Thickness on Static and Oscillatory Lateral

Stability Derivatives for a Delta Wing," NACA TN-4341, Jul., 1958.

9) Henderson, W.P., "Effects of Wing Leading-Edge Radius and Reynolds Number on Longitudinal Aerodynamic Characteristics of Highly Swept Wing-Body Configurations at Subsonic Speeds," NACA TN D-8361, Dec., 1976.

10) Chu, J. and Luckring, M., "Experimental Surface Pressure Data Obtained on 65° Delta Wing Across Reynolds Number and Mach Number Ranges," NASA TM 4645, Feb., 1996.

11) Hu, B.K. and Stollery, J.L., "The Performance of 60° Delta Wings: The Effects of Leading Edge Radius and Vortex Flaps," College of Aeronautics Rept. No.9004, Cranfield Inst. of Technology, Bedford, England, UK, Mar., 1990.

12) Rowan, C., "The Effect of Leading Edge Radius on Vortex Flap Performance," College of Aeronautics MSc Thesis, Cranfield Inst. of Technology, Bedford, England, UK, Sep. 1991.

13) Rinoie, K. and Stollery, J.L., "Low Speed Aerodynamic Characteristics of 60° Rounded Leading-Edge Delta Wing with Vortex Flaps: Part 1 457.2mm Span Delta Wing," College of Aeronautics Rep. No.9611, Cranfield Univ., Bedford, England, UK, Dec. 1996.

14) Schlichting, H., *Boundary-Layer Theory*, 7th ed., McGraw-Hill, New York, 1979, pp.538-542.

15) Wentz, Jr, W.H. and Kohlman, D.L., "Vortex Breakdown on Slender Sharp-Edged Wings," *Journal of Aircraft*, Vol.8, No.3, 1971, pp.156-161.

16) Traub, L.W., "Comparative Study of Delta Wings with Blunt Leading Edges and Vortex Flaps," *Journal of Aircraft*, Vol.33, No.4, 1996, pp.828-830.

Appendix A Corrected Vortex Flap Deflection Angle δ_{fc}

Corrected vortex flap deflection angle δ_{fc} at x/Cr=0.55 is defined as follows:

$$\delta_{fc} = \delta_f + \tan^{-1}\left(\frac{2D\sin(\varepsilon+\Lambda)}{x\sin\Lambda}\frac{1}{\tan\left(\frac{\pi}{2}-\Lambda\right)}\right),$$

where x is the chordwise station at x/Cr=0.55, ε is the semi apex angle of the main wing inboard of the flap hinge line, Λ is the wing sweepback angle.

The formulations:

$\delta_{fc} = \delta_f + 6.2°$ (D=15mm),
$\delta_{fc} = \delta_f + 12.2°$ (D=30mm),

were used in this experiment.

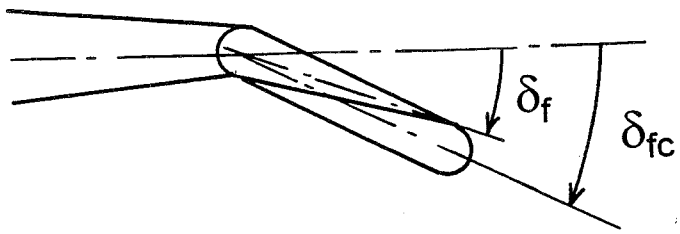

Section normal to flap hinge line

Appendix B The "Vortex Flap" Force and The "Rounded Edge" Force

(1) The "Vortex Flap" Force

The "Vortex Flap" Force, parallel to the freestream, produced by the vortex flap is represented by as follows:

$$\frac{2}{b}\int_{l_0}^{l_1} Cpdl\left(\cos\delta_f \sin\alpha - \sin\delta_f \sin\varepsilon\cos\alpha\right),$$

where Cp is the pressure coefficients over the flap surface, ε is the semi apex angle of the main wing inboard of the flap hinge line, l_0 is the leading-edge position and l_1 is the hinge line position. It is noted that this force is normalised by the local semispan length and the free stream dynamic pressure. A positive value denotes that a drag force is acting on the wing.

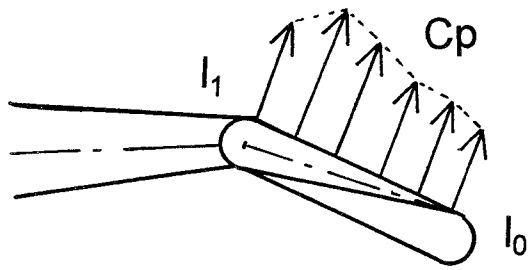

Section normal to flap hinge line

(2) The "Rounded Edge" Force

The suction force component P_2, parallel to the wing mean line, produced by the upper quarter circular part of the rounded leading-edge is assumed here to be represented by the following formulae:

$$P_2 = \frac{1}{b}\int_0^{\frac{\pi}{2}} Cp_2 \sin\theta\cos\theta D d\theta \ ,$$

where Cp_2 is the pressure coefficient at the second pressure tapping from the leading-edge at x/Cr=0.4. It was also assumed only the suction force component parallel to the wing mean line contributes to the suction force produced by the rounded leading-edge.

Then the "Rounded Edge" force parallel to the freestream produced by P_2 is:

$$P_2 (\cos\gamma \cos (\xi - \varepsilon) \cos\alpha + \sin\gamma \sin\alpha),$$

where $\gamma = \sin^{-1} (\sin\delta_f \cos\theta)$,

$$\xi = \sin^{-1}\left(\frac{\cos\delta_f}{\sqrt{(1/\cos^2\theta - \sin^2\delta_f)}} \right) ,$$

$$\theta = \pi/2 - \Lambda - \varepsilon .$$

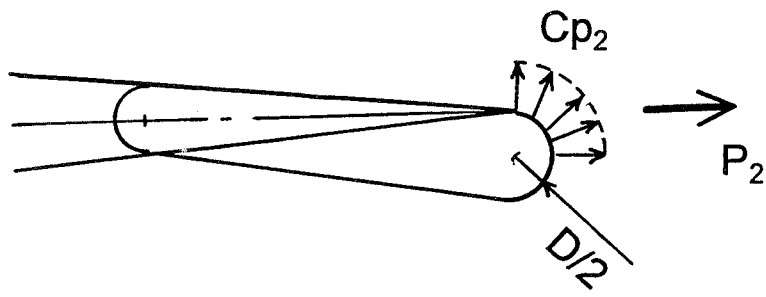

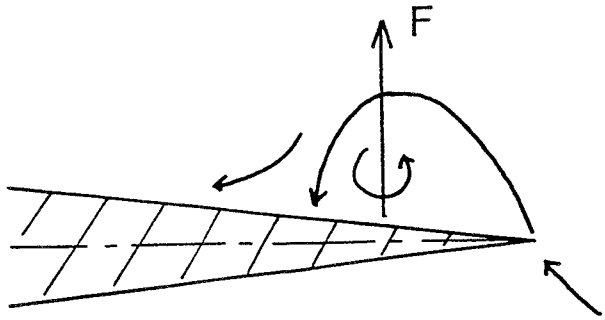

a) Flat Delta Wing (Sharp L.E.)

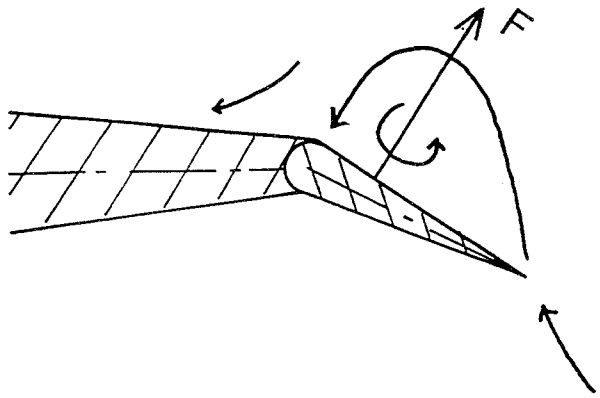

b) Delta Wing with Sharp L.E. Vortex Flap

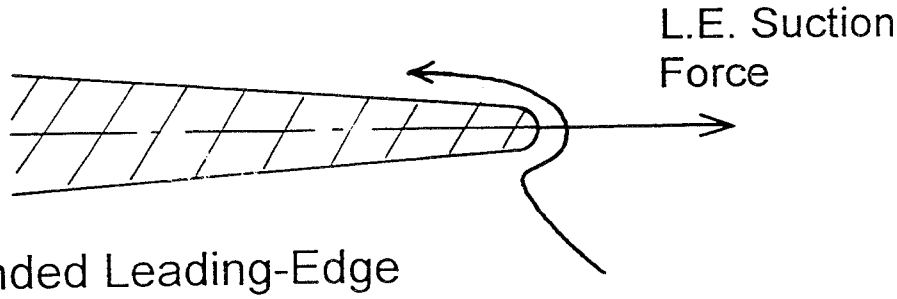

c) Rounded Leading-Edge

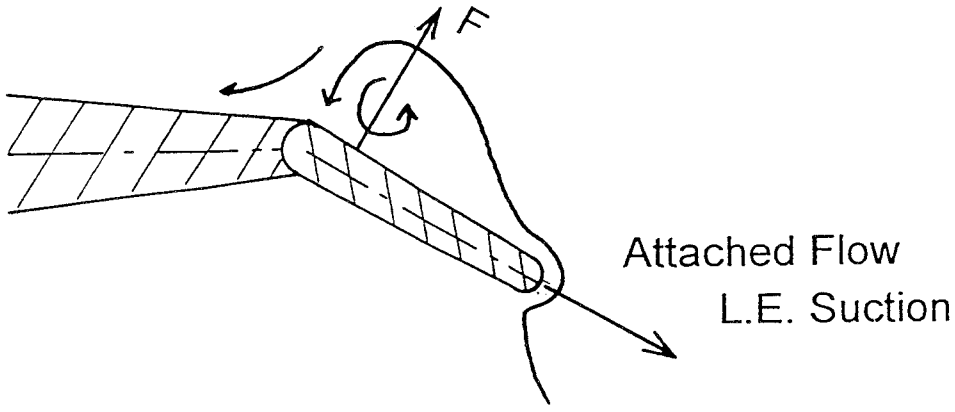

d) Delta Wing with Rounded L.E. Vortex Flap

Fig.1 Concept of Vortex Flap & Rounded L.E.

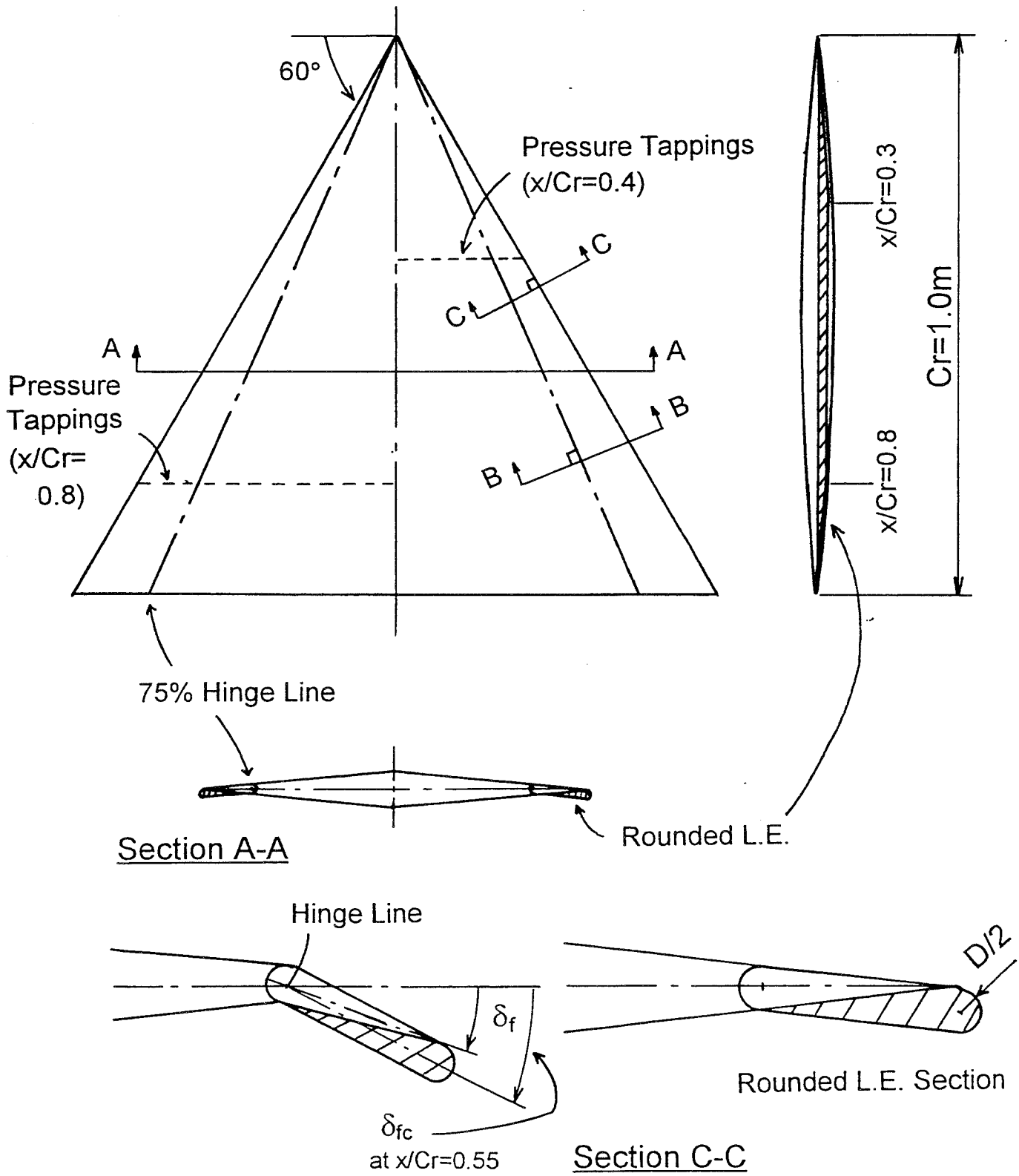

Fig.2 Delta Wing Model with Rounded L.E. LEVF

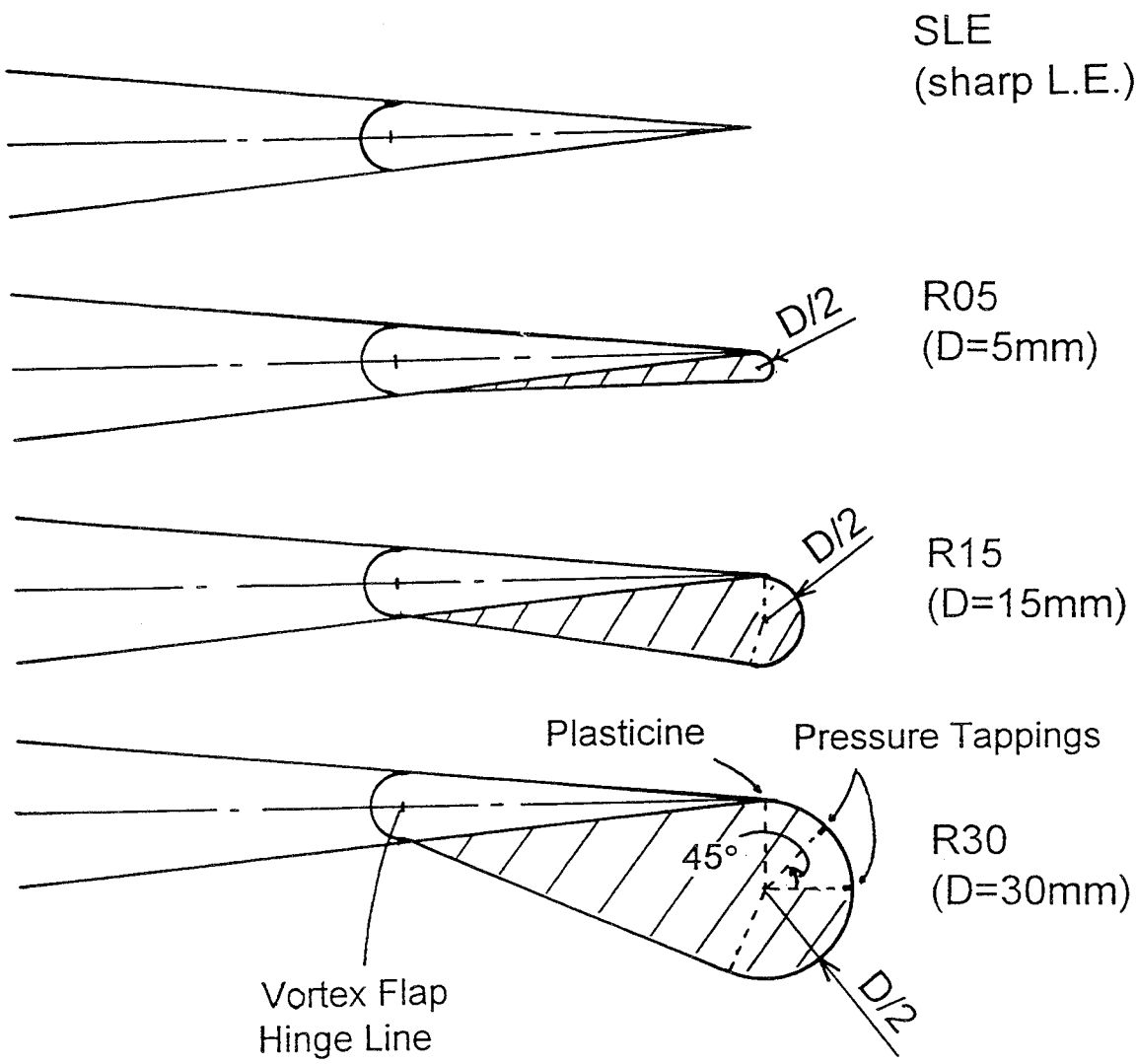

Fig.3 Different Rounded Leading-Edges

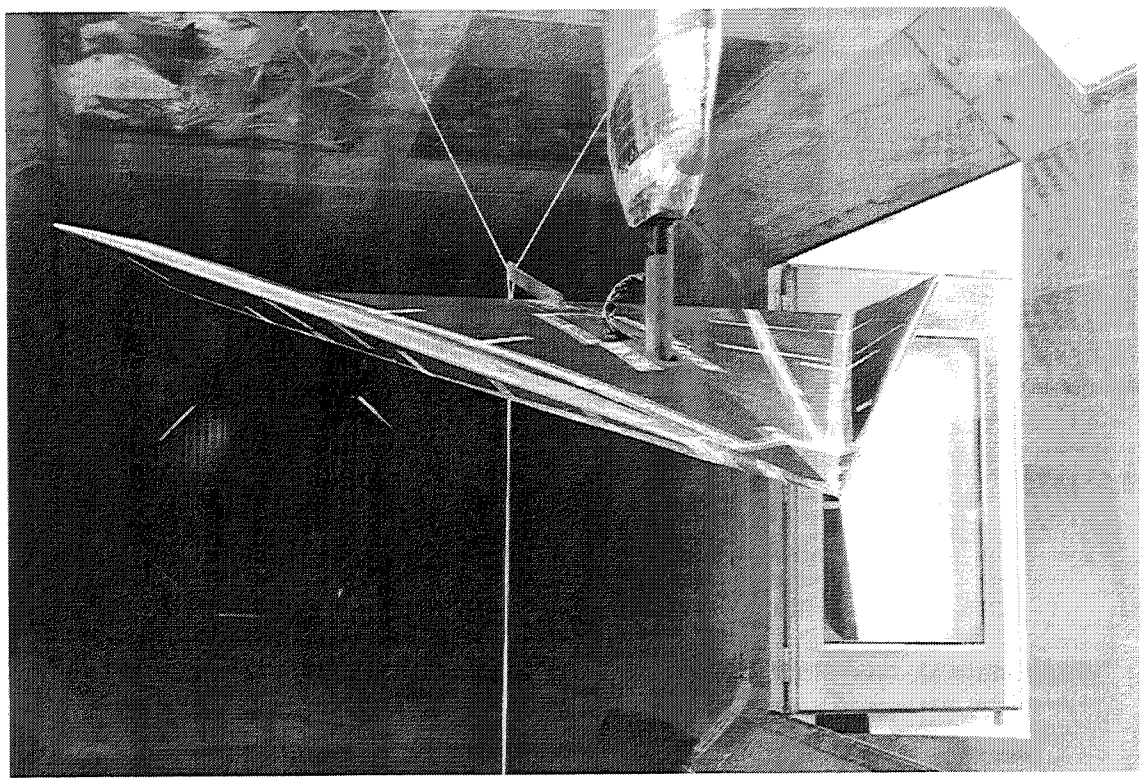

Fig.4 Delta Wing Model and Wind Tunnel

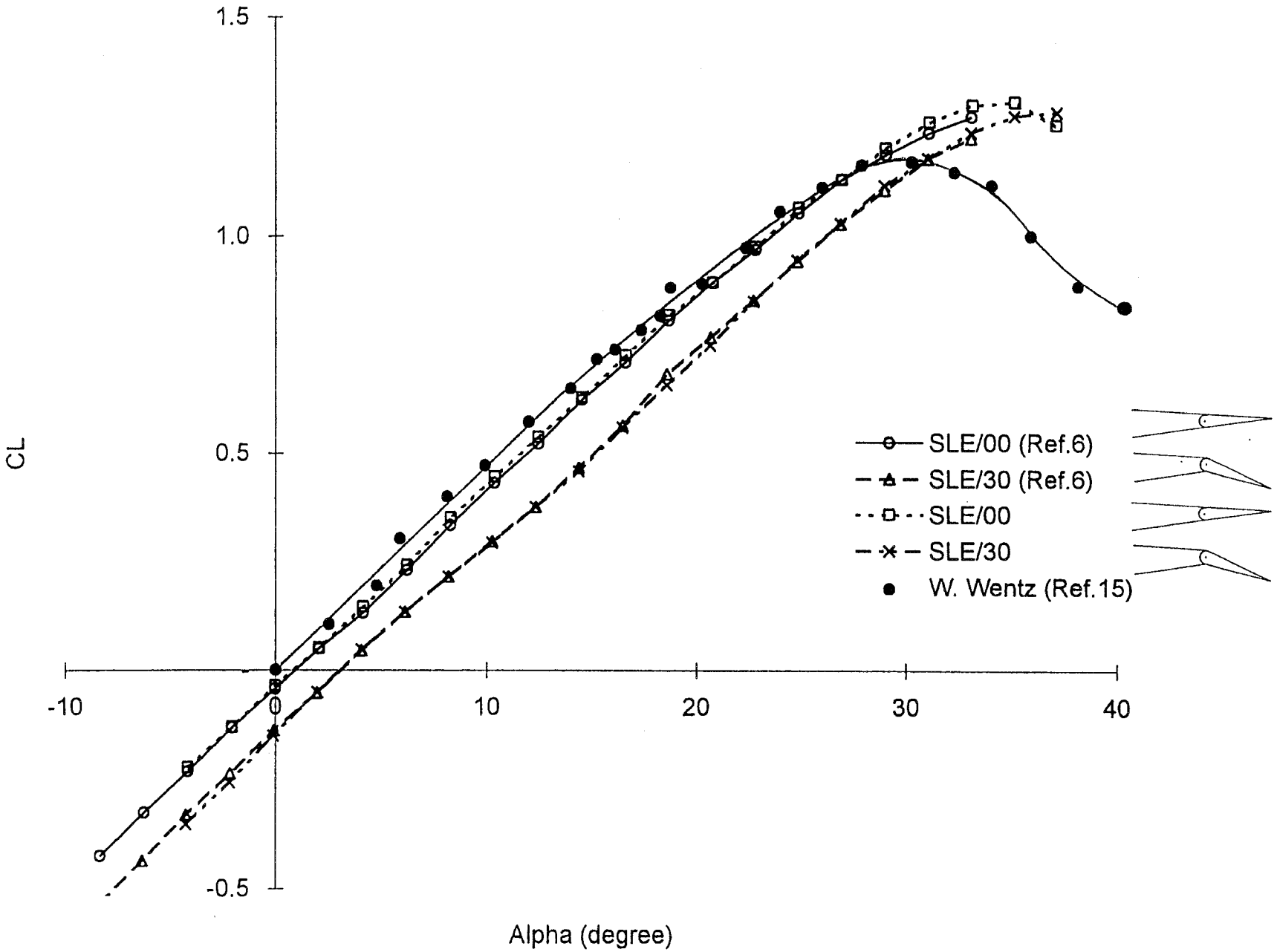

Fig.5a) C_L-α

Fig.5 Repeatability and Comparisons for Sharp L.E., δ_f=0° & 30°
(SLE/00, SLE/30)

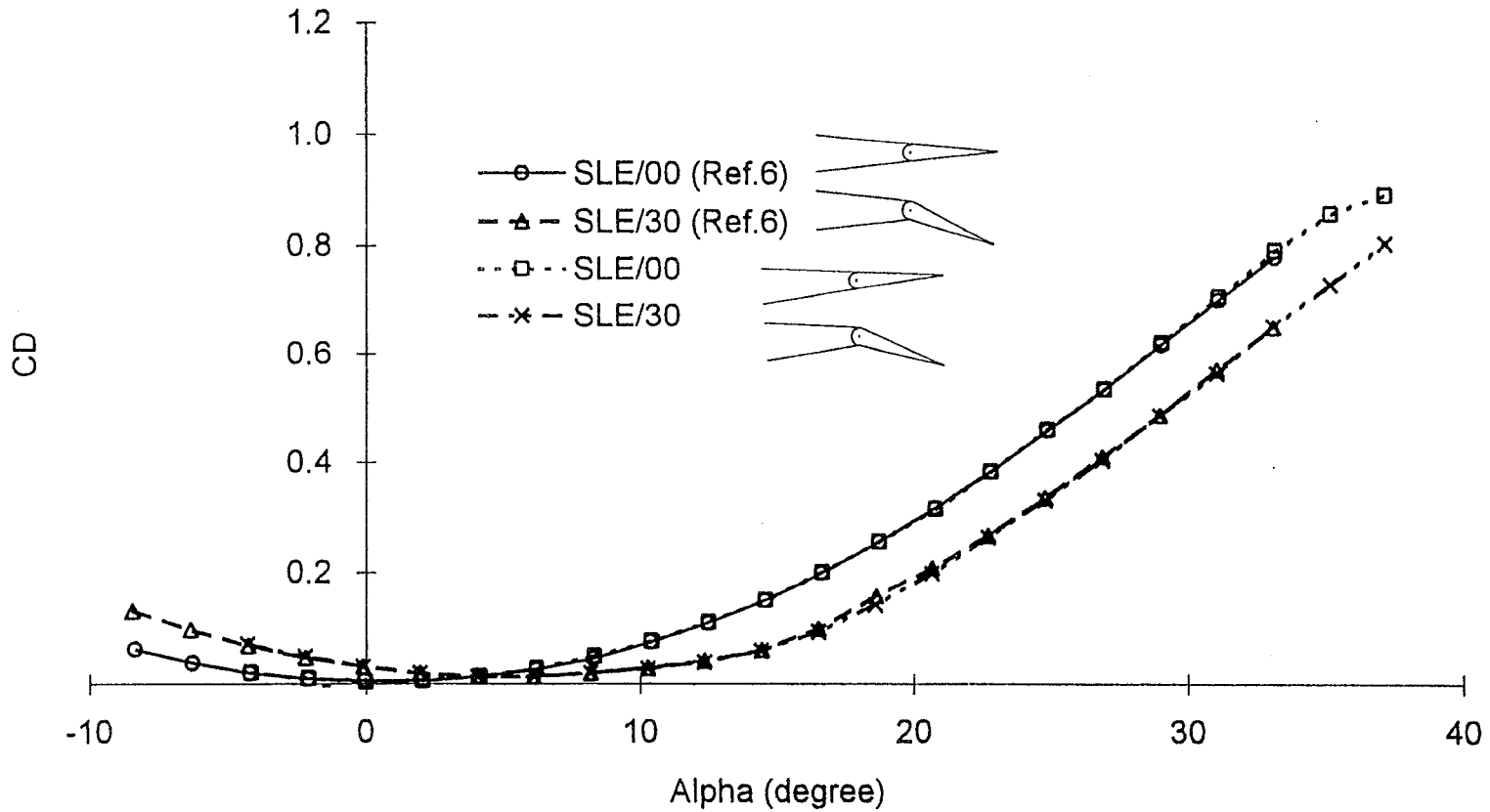

Fig.5b) C_D-α

Fig.5 Repeatability and Comparisons for Sharp L.E., δ_f=0° & 30°
(SLE/00, SLE/30)

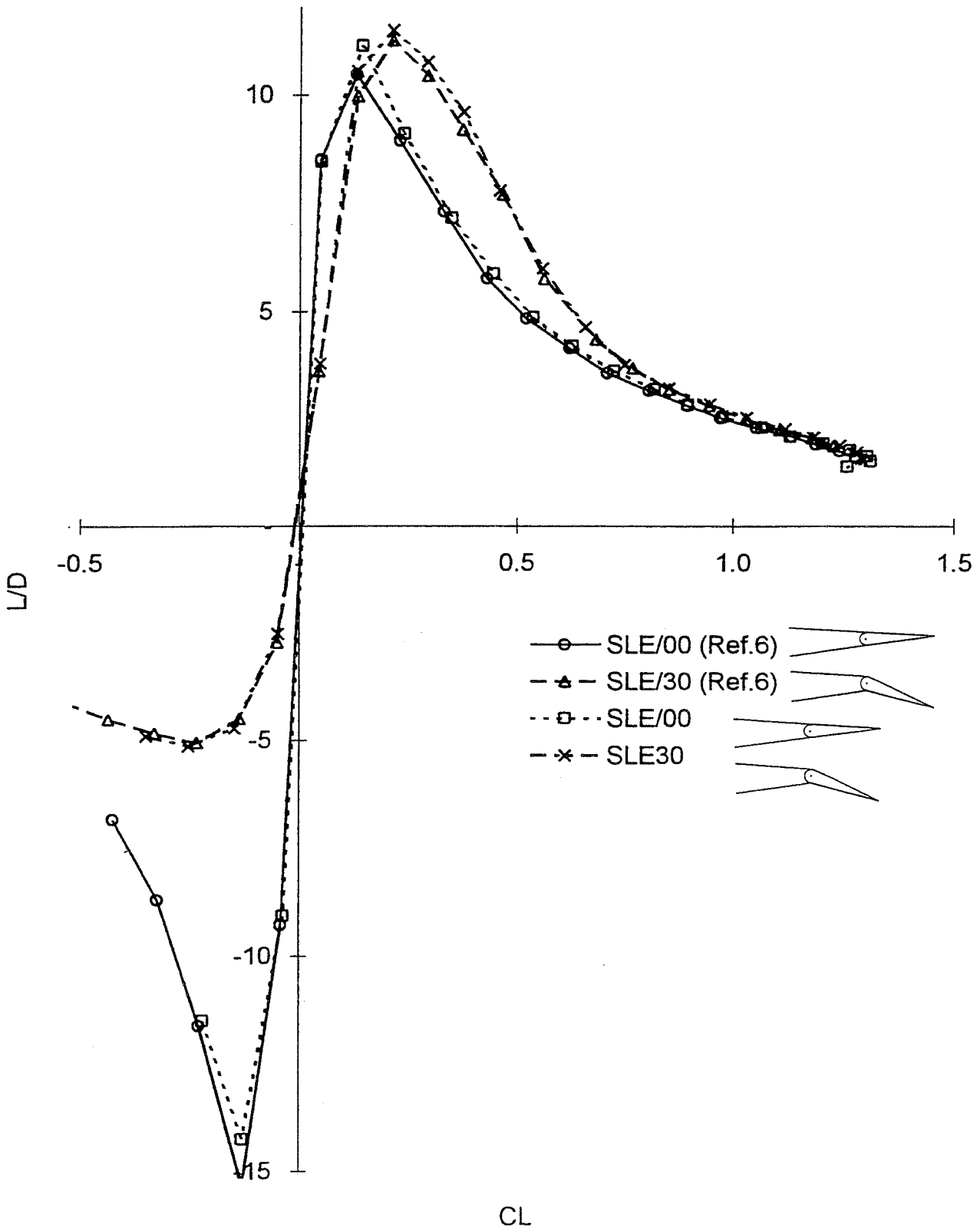

Fig.5c) L/D-C_L

Fig.5 Repeatability and Comparisons for Sharp L.E., δ_f=0° & 30° (SLE/00, SLE/30)

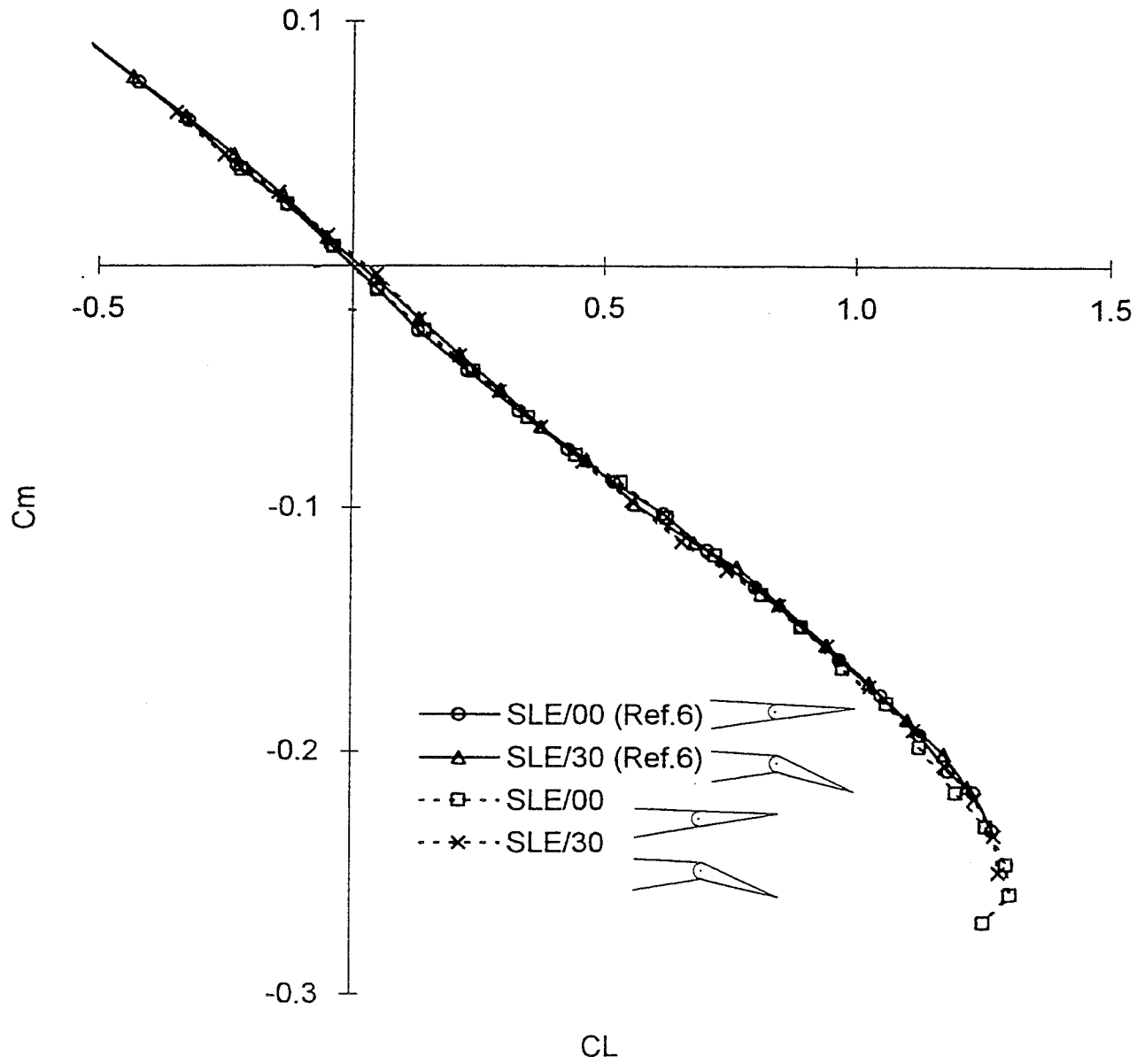

Fig.5d) C_m-C_L

Fig.5 Repeatability and Comparisons for Sharp L.E., δ_f=0° & 30° (SLE/00, SLE/30)

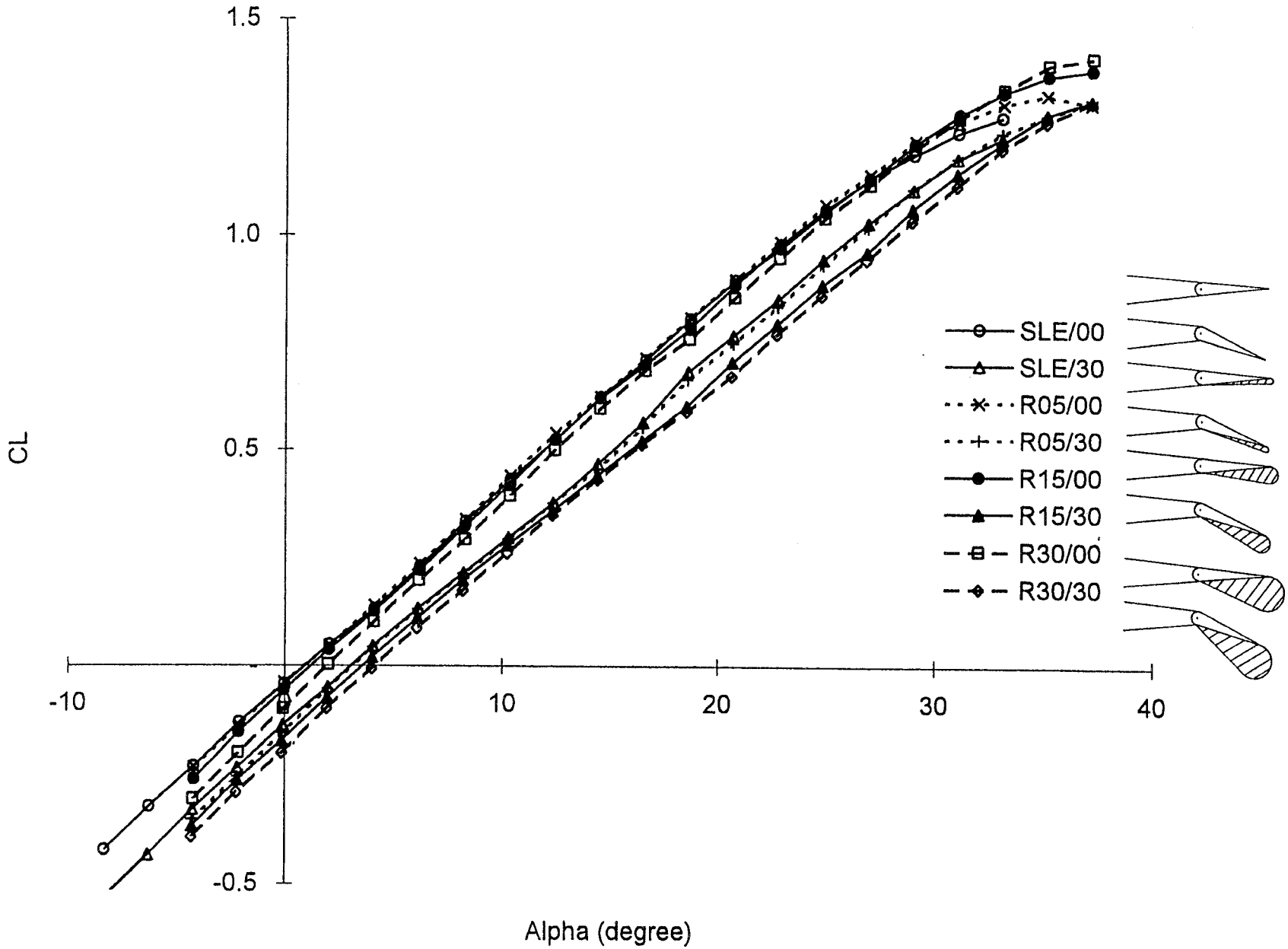

Fig.6a) C_L-α

Fig.6 Effect of Rounded L.E. with and without flap deflection

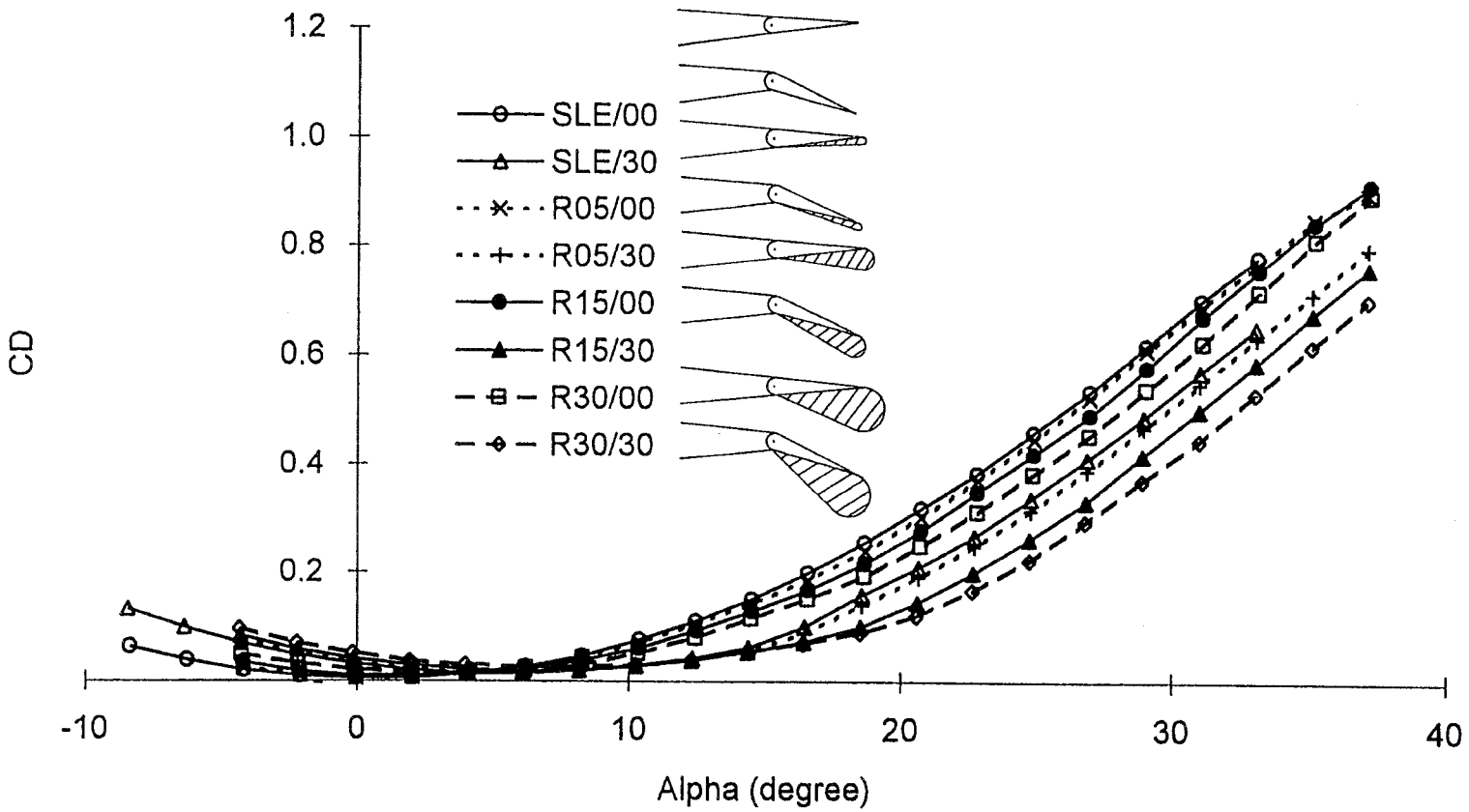

Fig.6b) C_D-α

Fig.6 Effect of Rounded L.E. with and without flap deflection

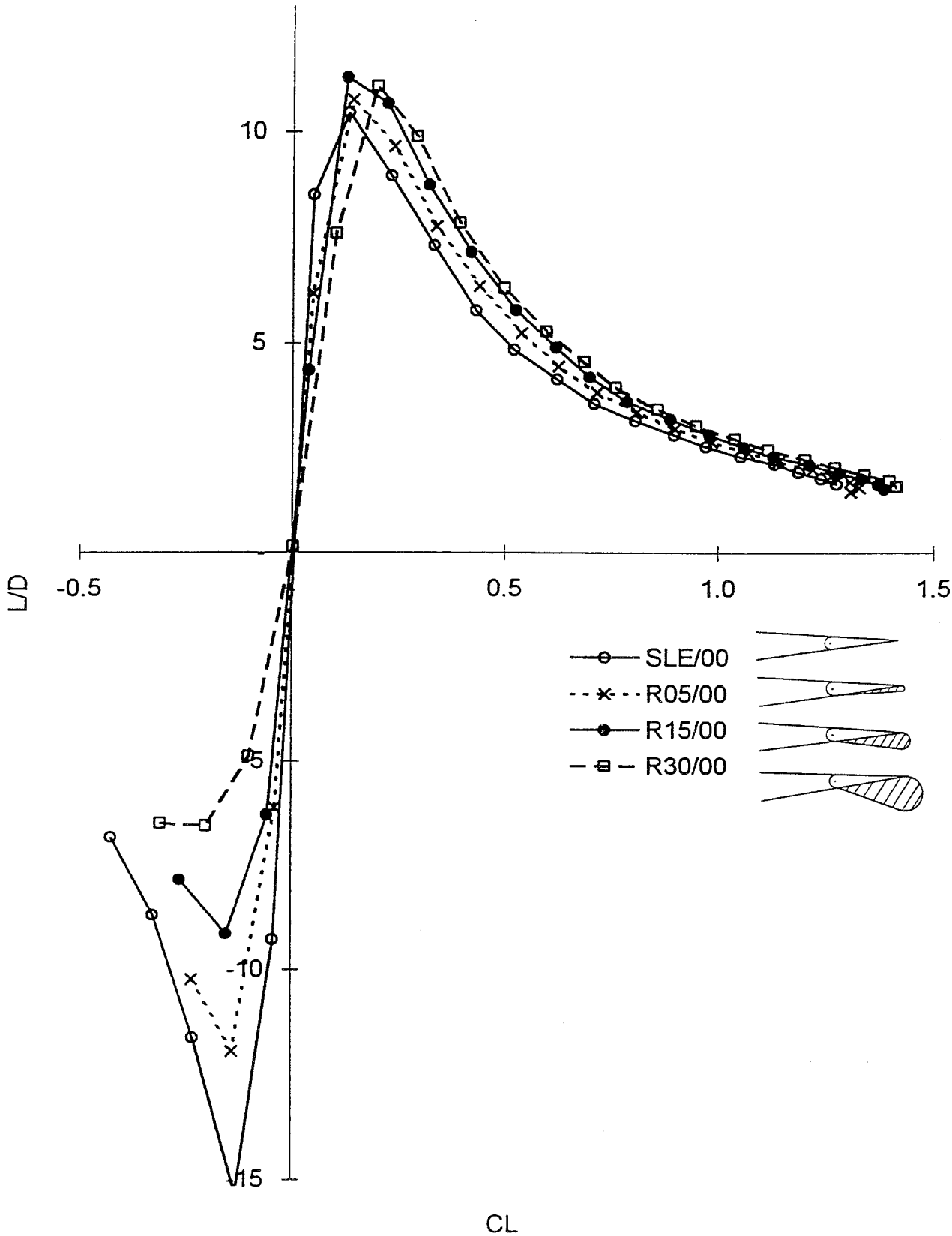

Fig.6c) L/D-C_L (δ_f=0°)

Fig.6 Effect of Rounded L.E. with and without flap deflection

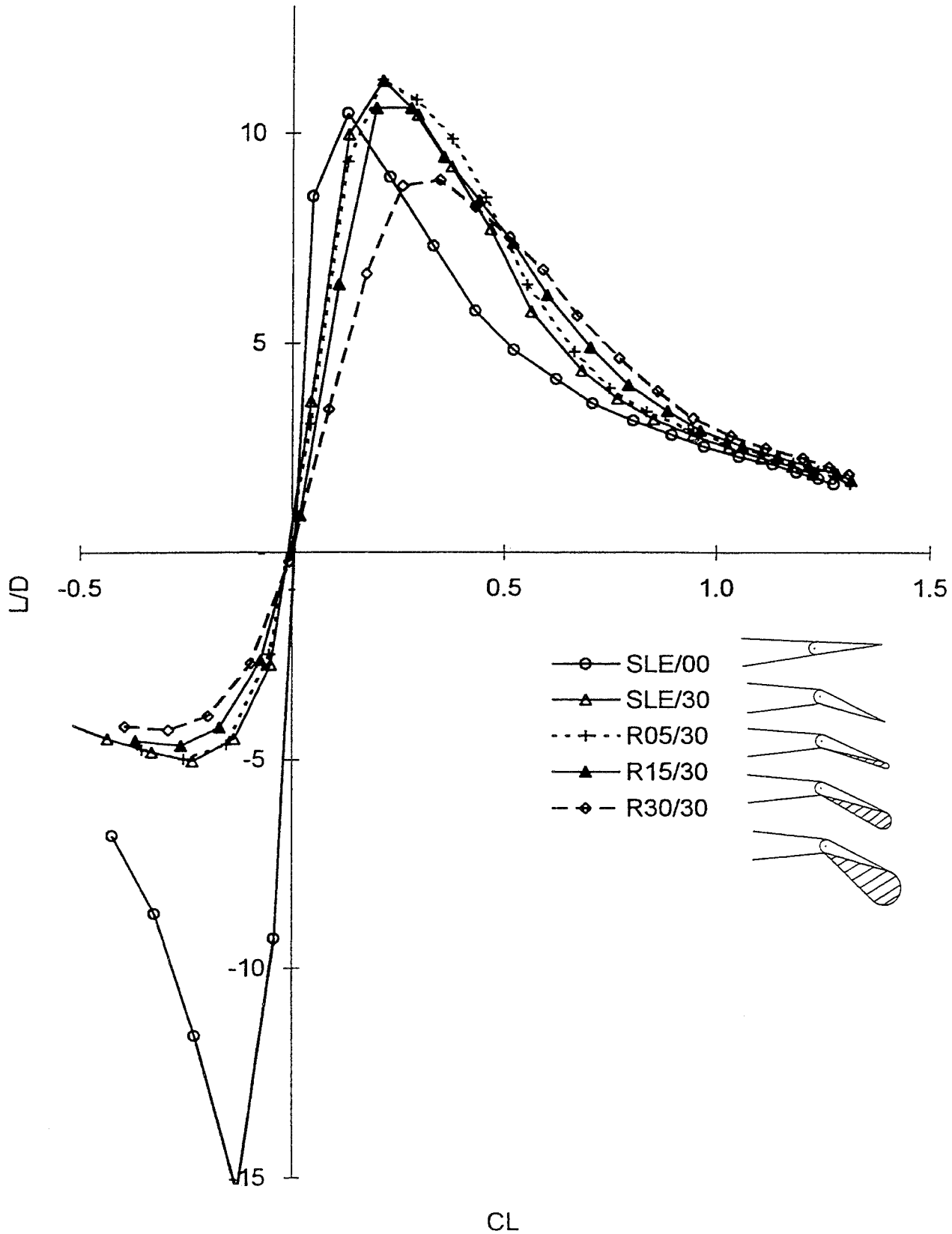

Fig.6d) L/D-C_L (δ_f=30°)

Fig.6 Effect of Rounded L.E. with and without flap deflection

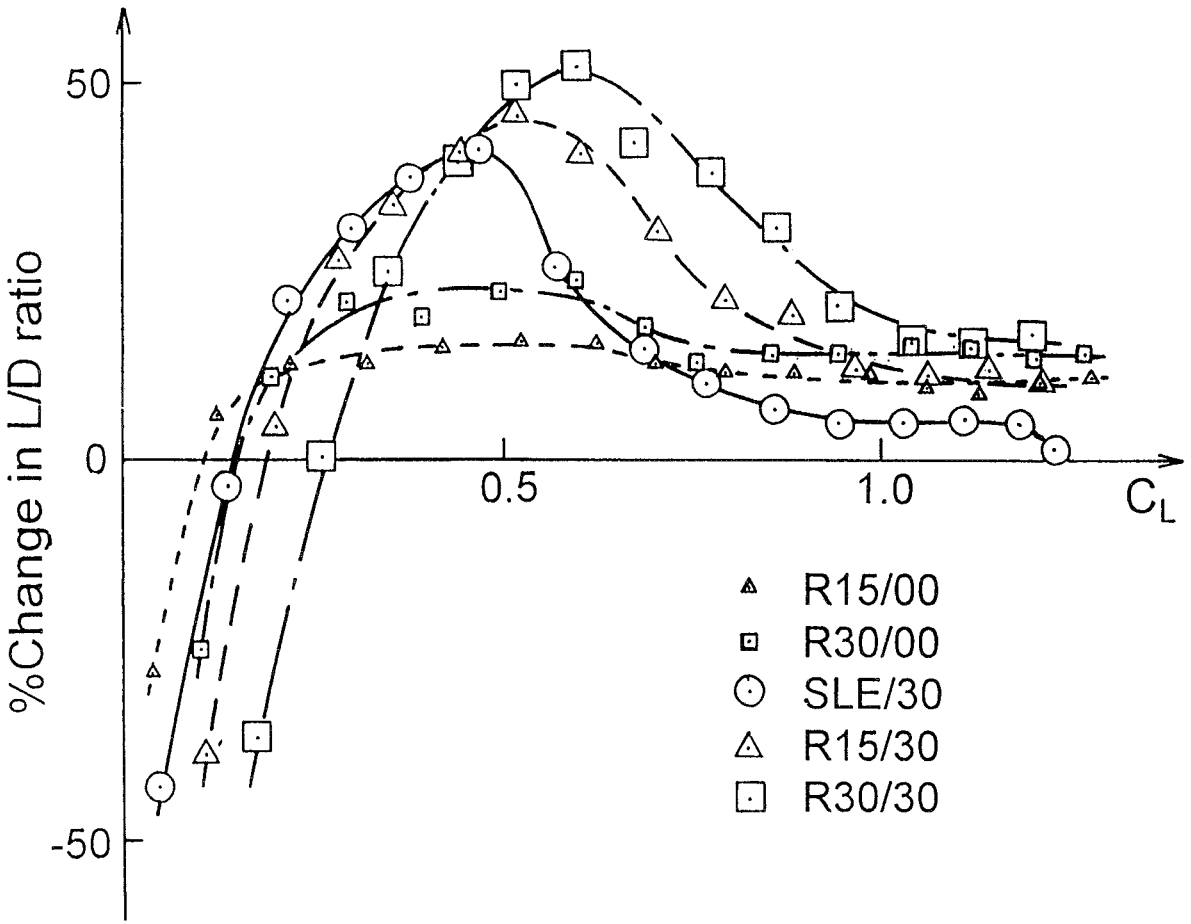

Fig.6e) % Improvement in *L/D*

Fig.6 Effect of Rounded L.E. with and without flap deflection

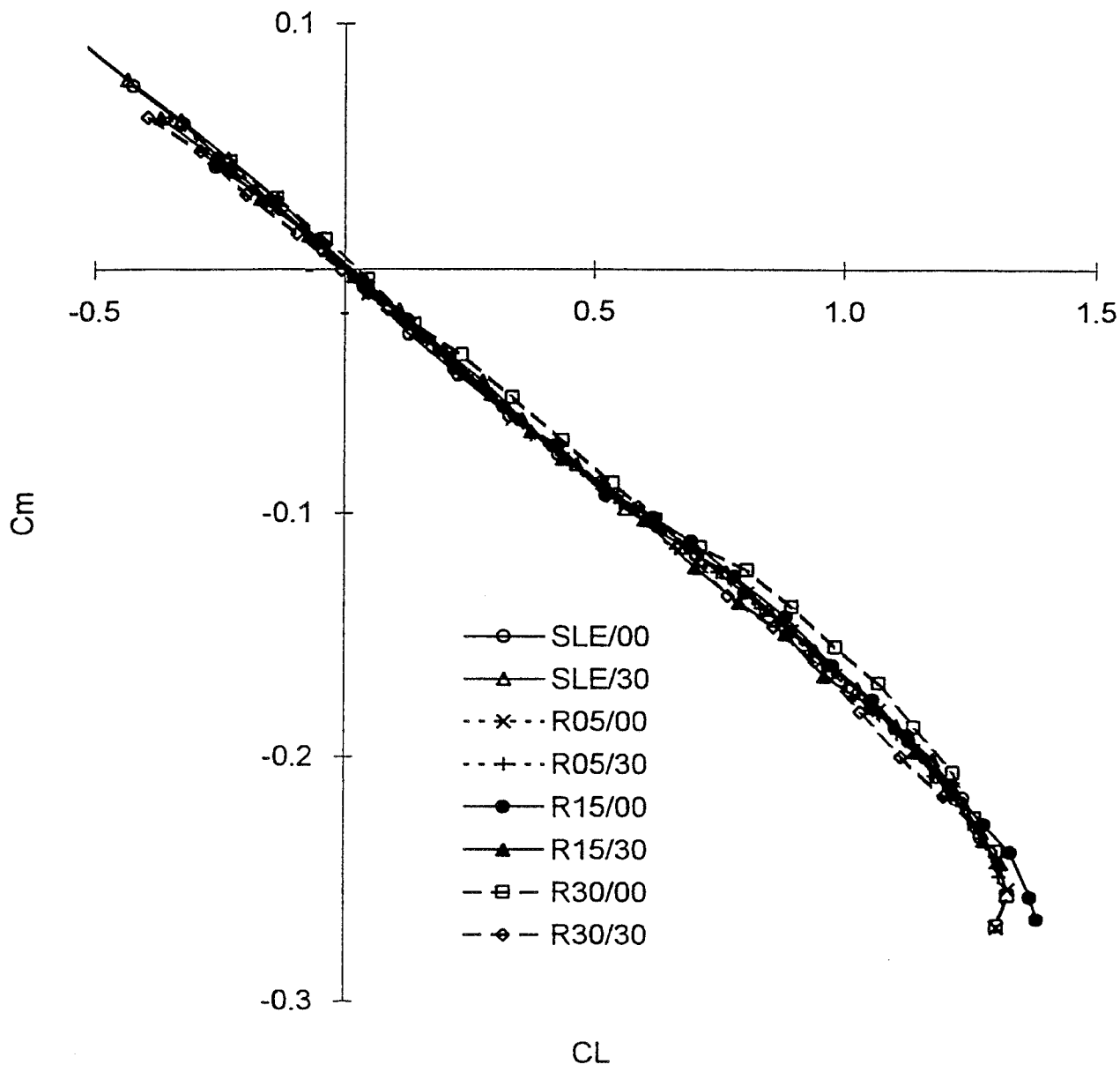

Fig.6f) C_m-C_L

Fig.6 Effect of Rounded L.E. with and without flap deflection

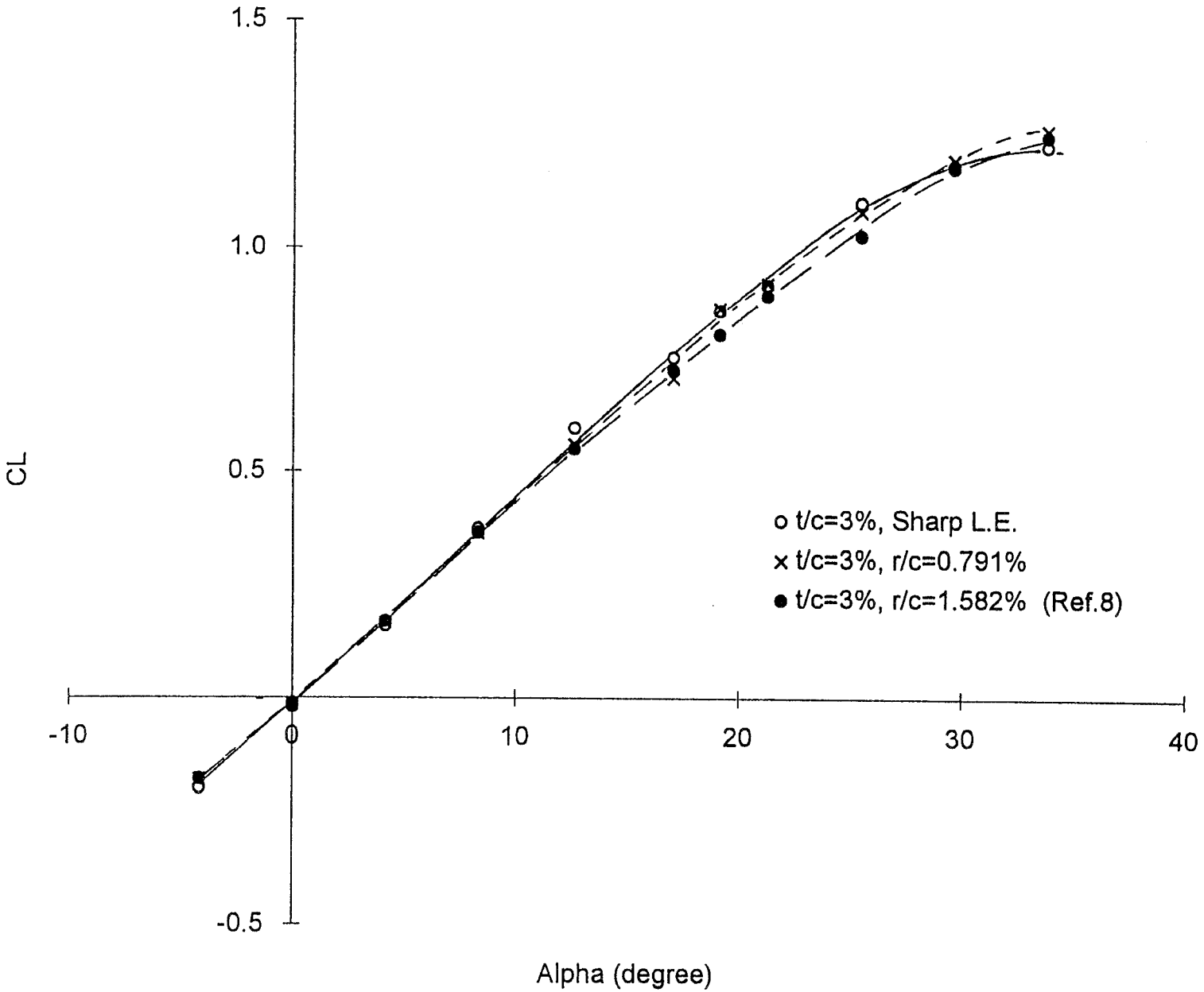

Fig.7a) C_L-α

Fig.7 Effect of Rounded L.E. data taken from Ref.8

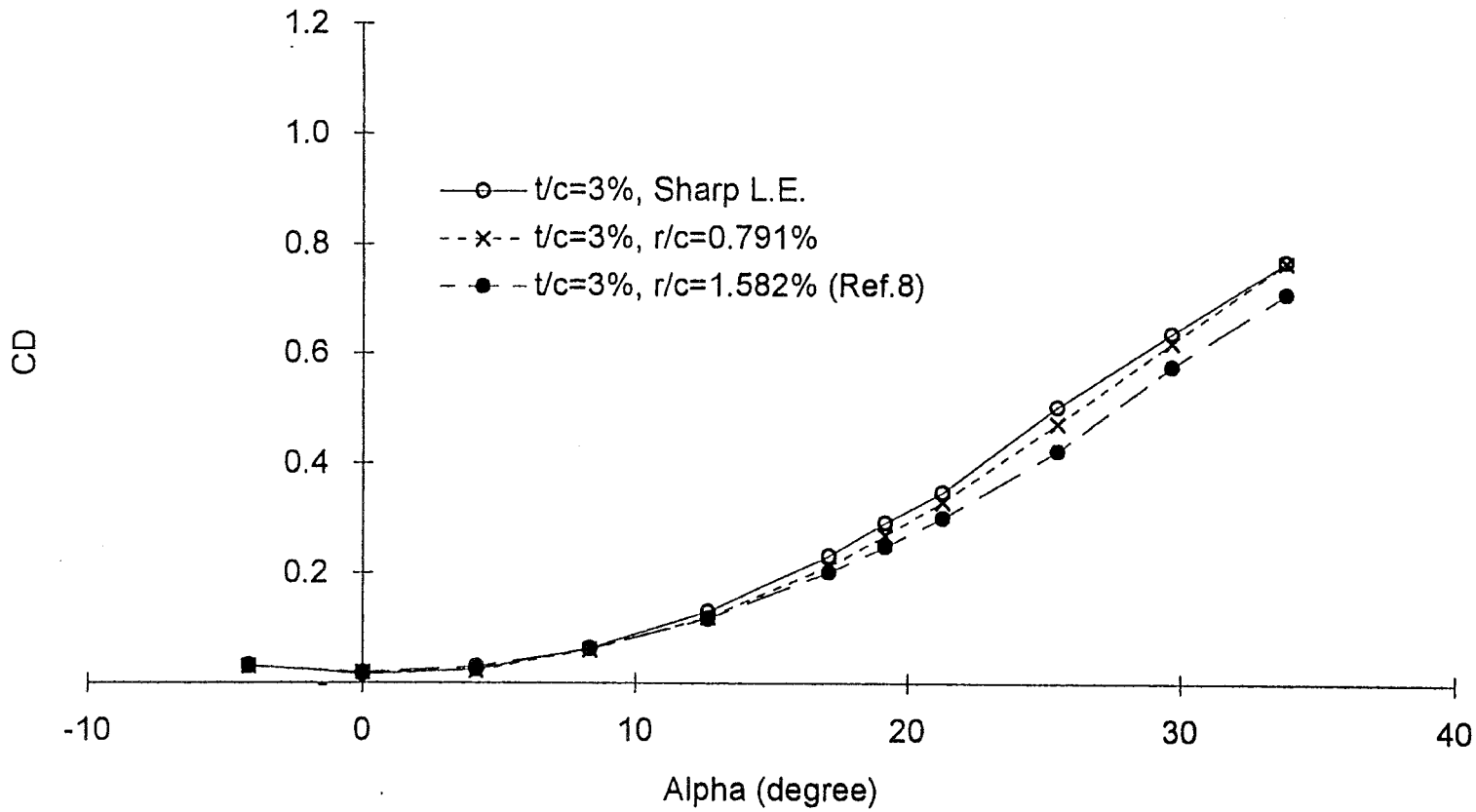

Fig.7b) C_D-α

Fig.7 Effect of Rounded L.E. data taken from Ref.8

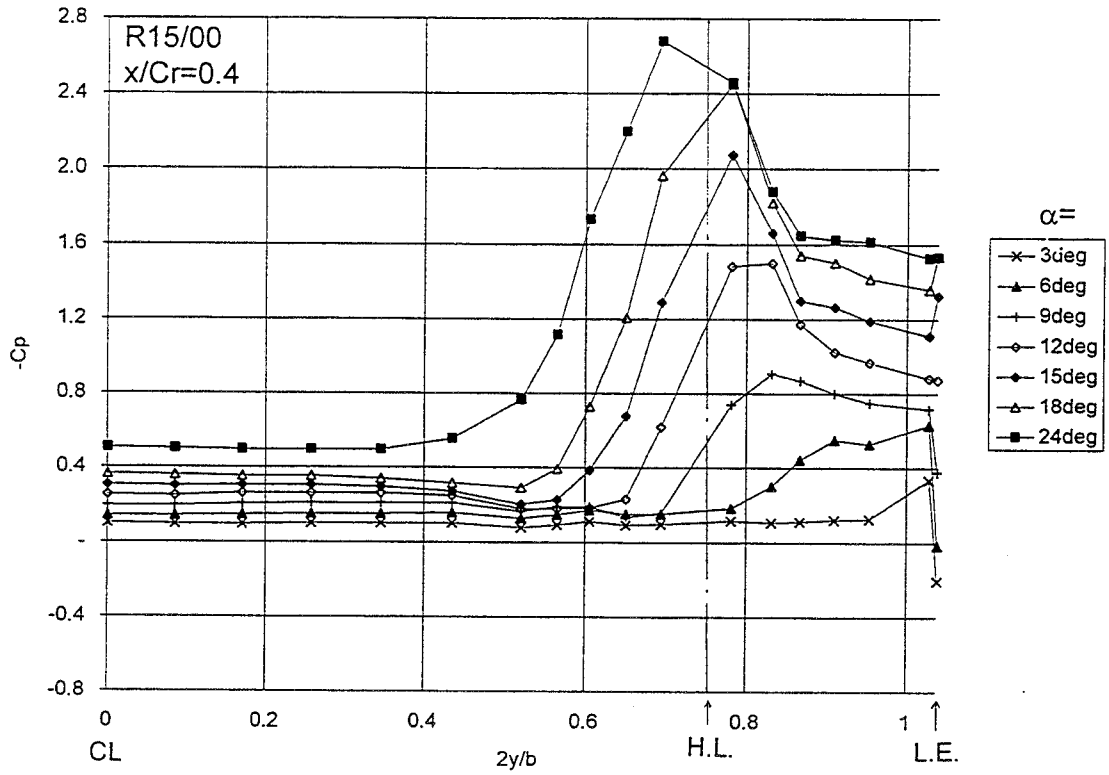

Fig.8a) R15/00, *x/Cr*=0.4

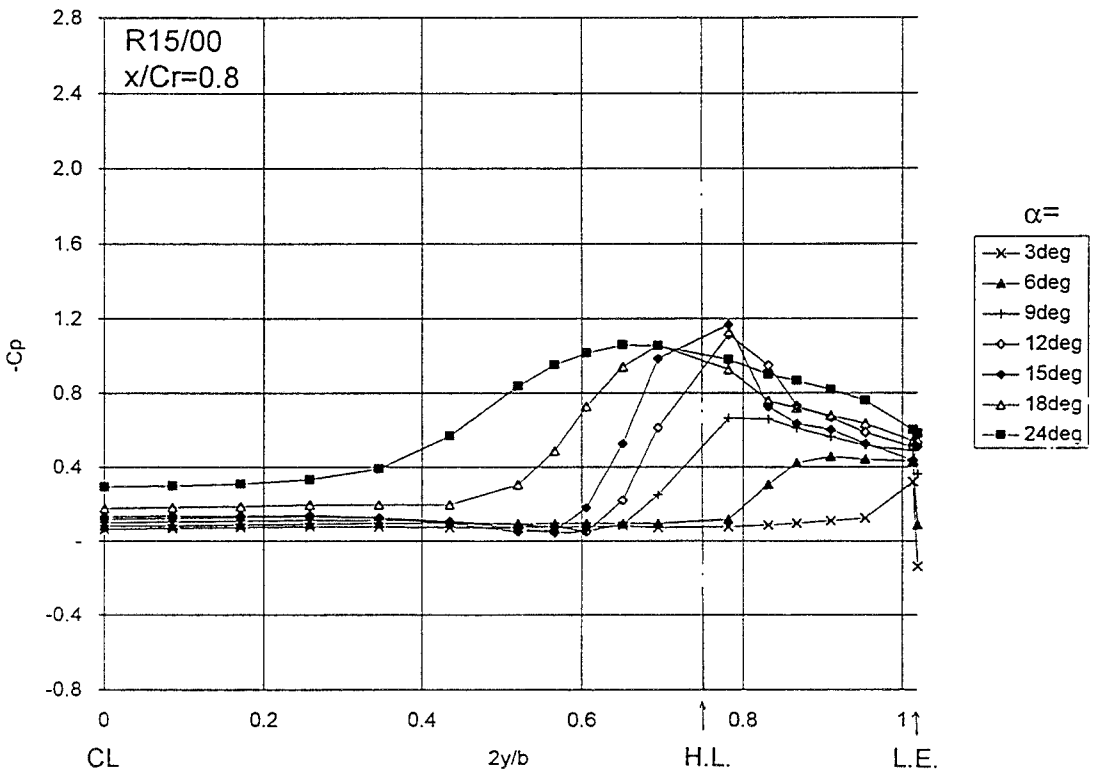

Fig.8b) R15/00, *x/Cr*=0.8

Fig.8 Surface Pressure Distributions (δ_f=0°)

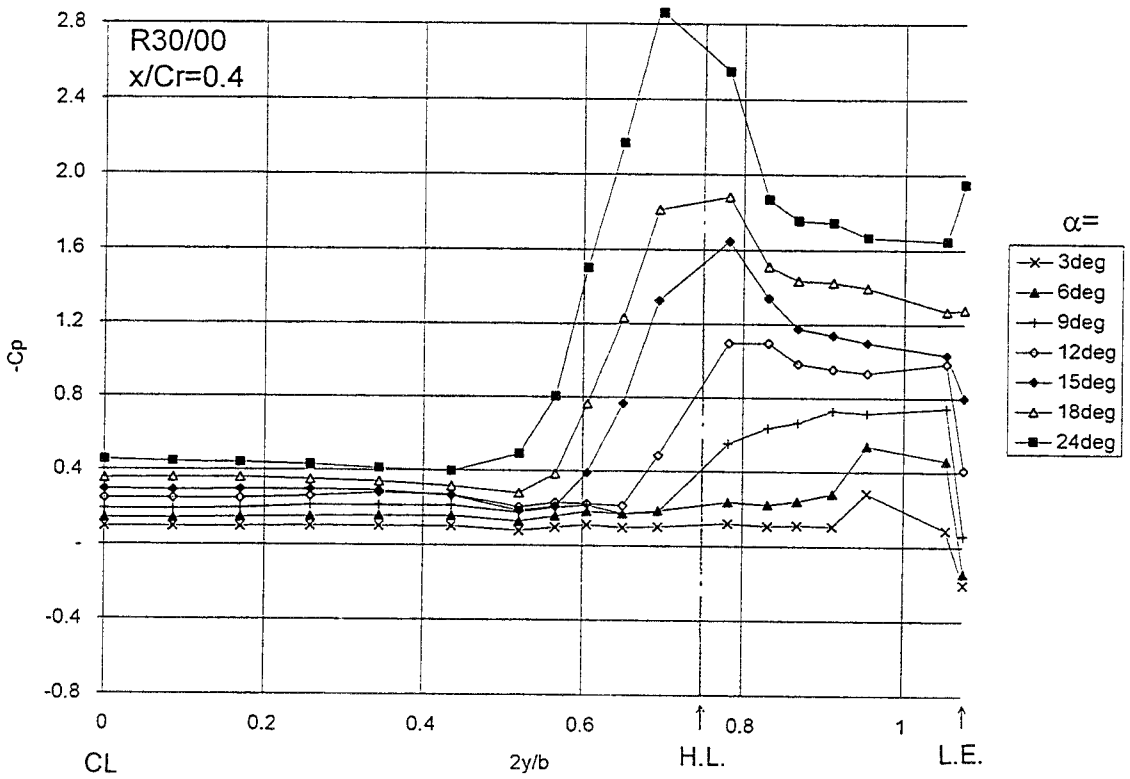

Fig.8c) R30/00, *x/Cr*=0.4

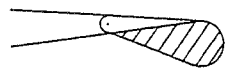

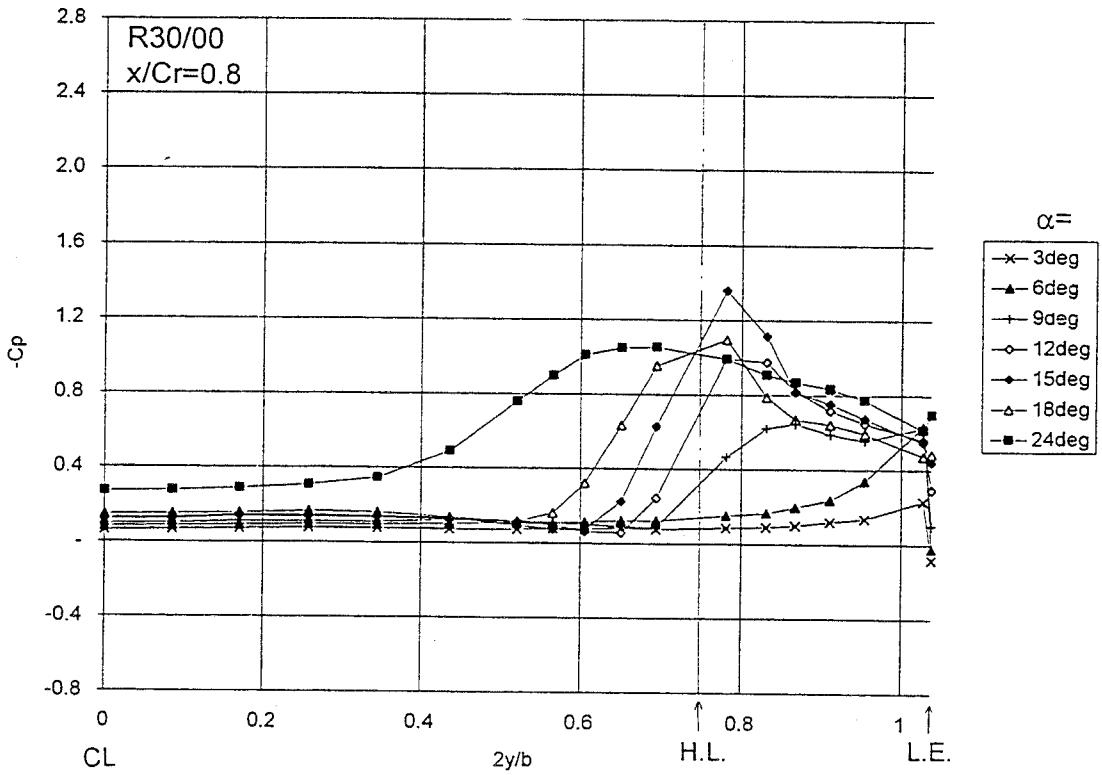

Fig.8d) R30/00, *x/Cr*=0.8

Fig.8 Surface Pressure Distributions (δ_f=0°)

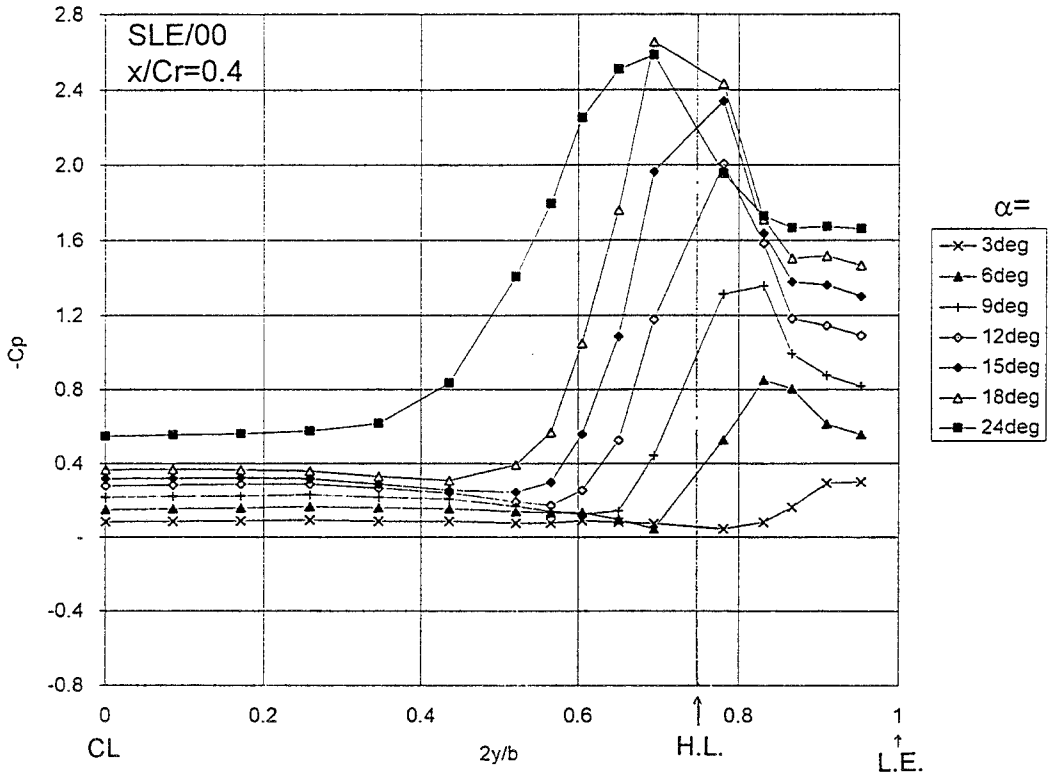

Fig.8e) SLE/00, *x/Cr*=0.4

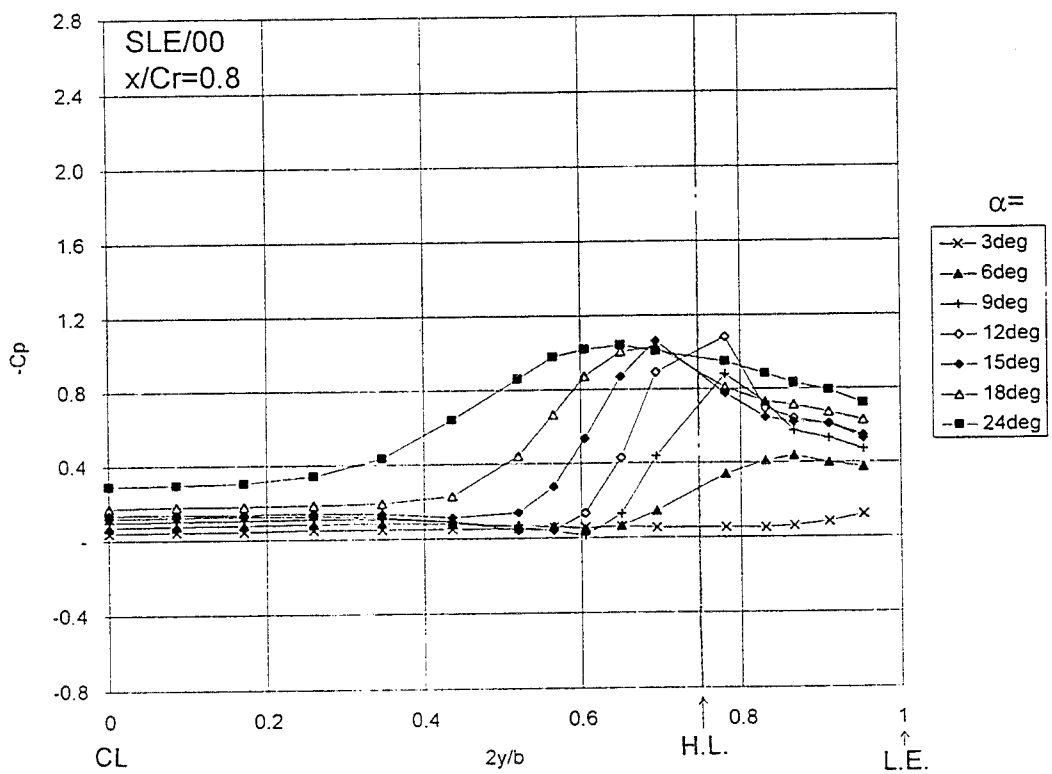

Fig.8f) SLE/00, *x/Cr*=0.8

Fig.8 Surface Pressure Distributions (δ_f=0°)

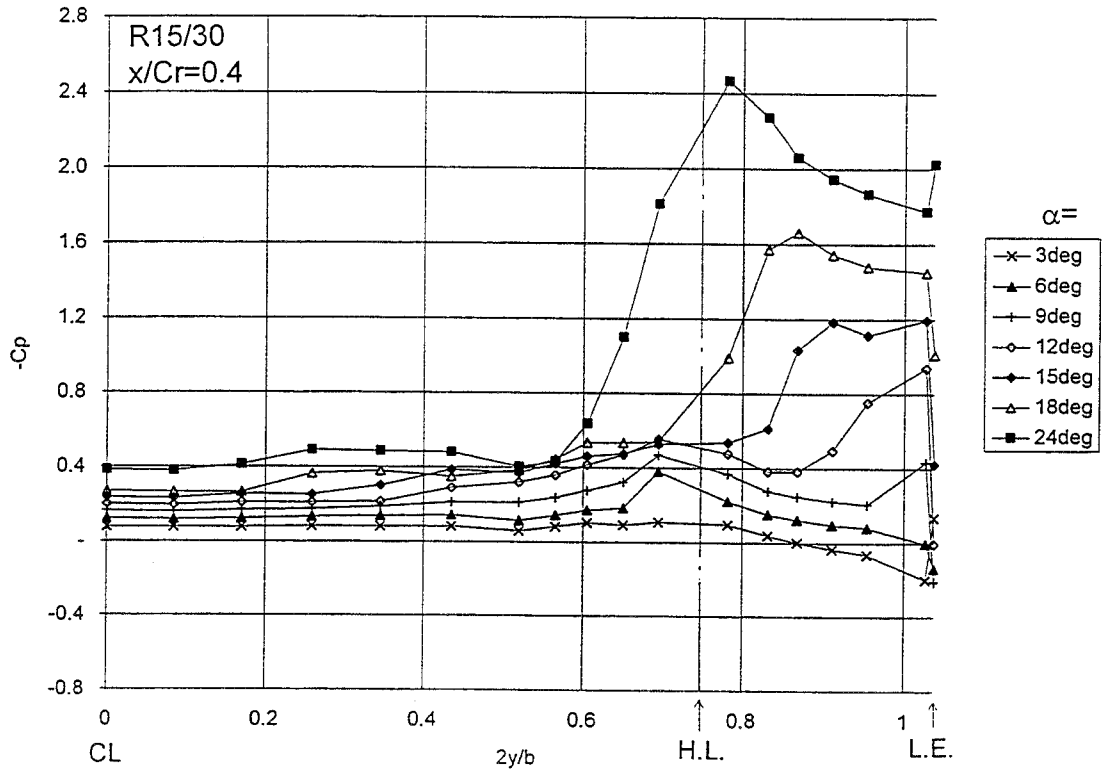

Fig.9a) R15/30, *x/Cr*=0.4

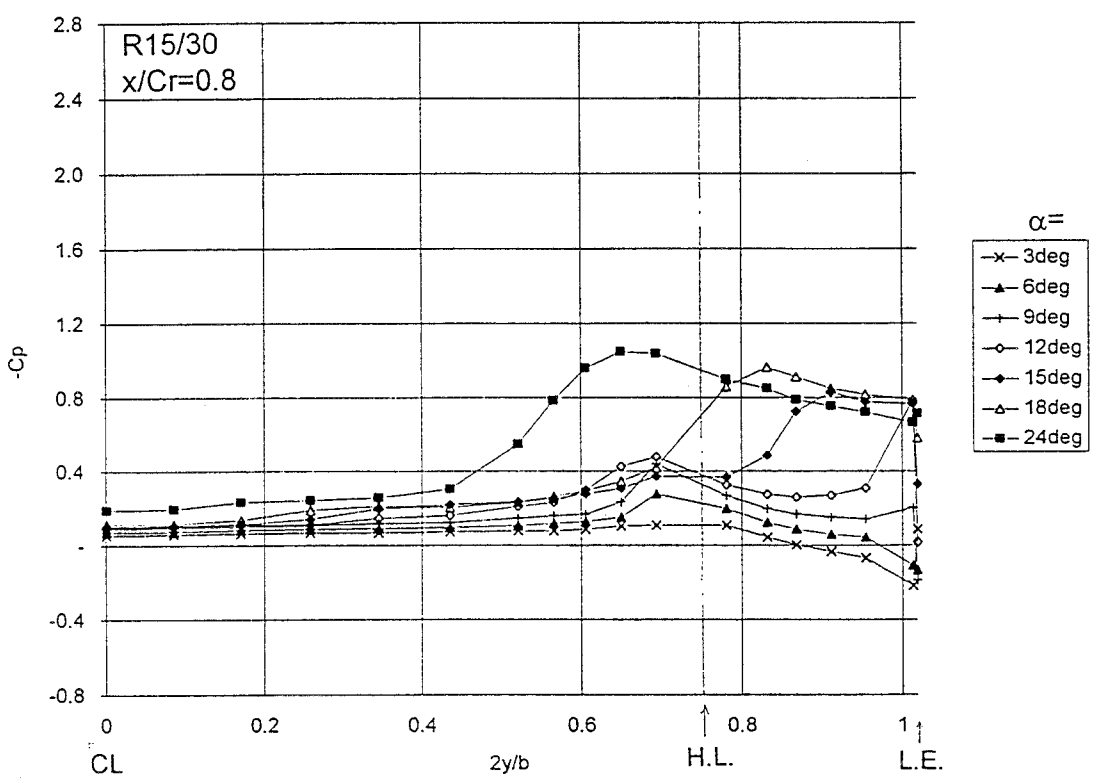

Fig.9b) R15/30, *x/Cr*=0.8

Fig.9 Surface Pressure Distributions (δ_f=30°)

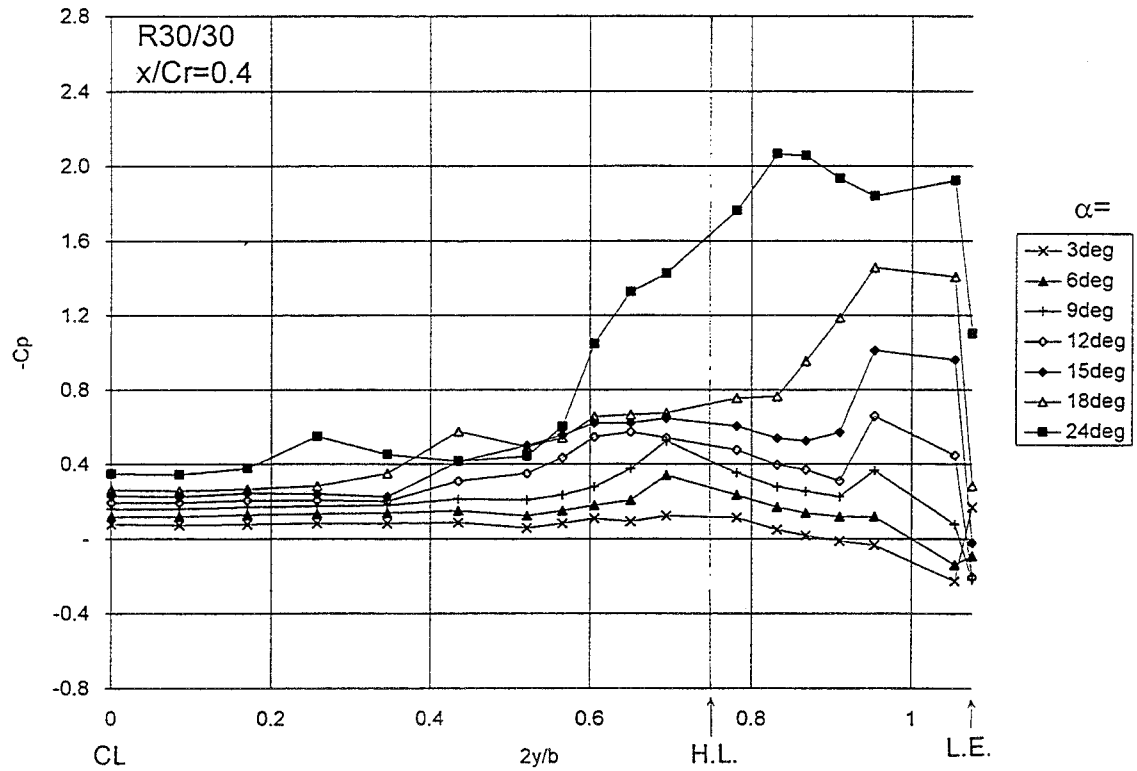

Fig.9c) R30/30, *x/Cr*=0.4

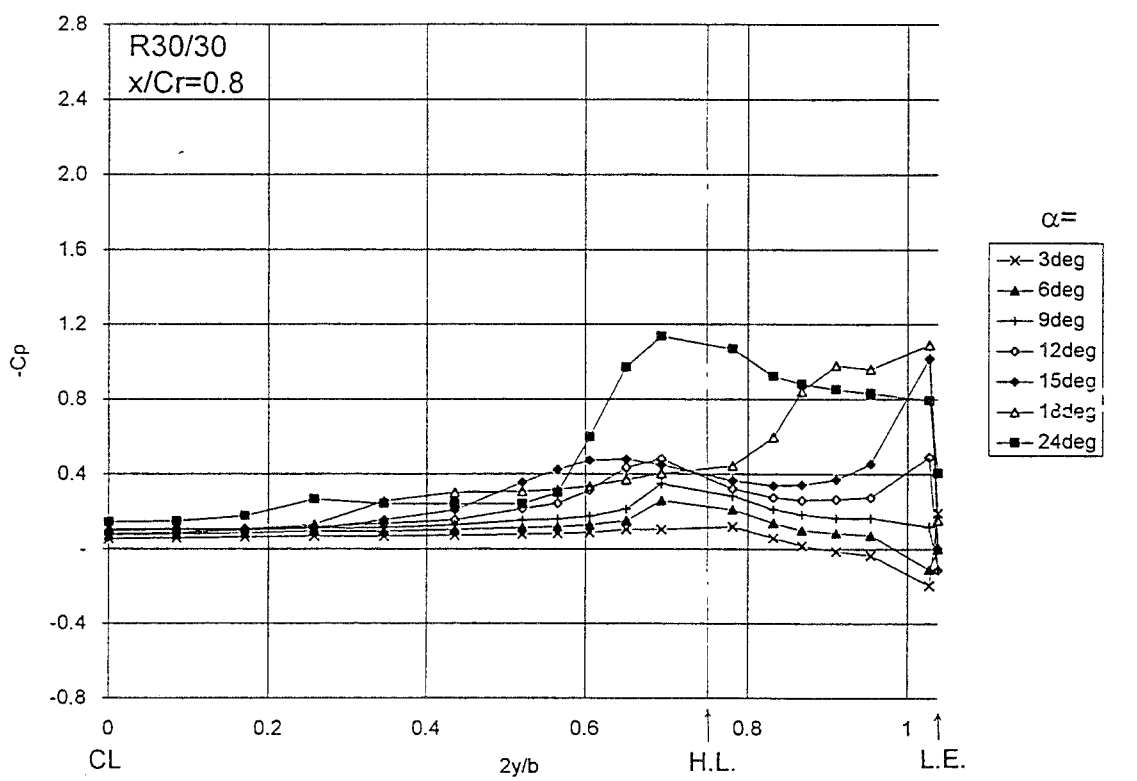

Fig.9d) R30/30, *x/Cr*=0.8

Fig.9 Surface Pressure Distributions (δ_f=30°)

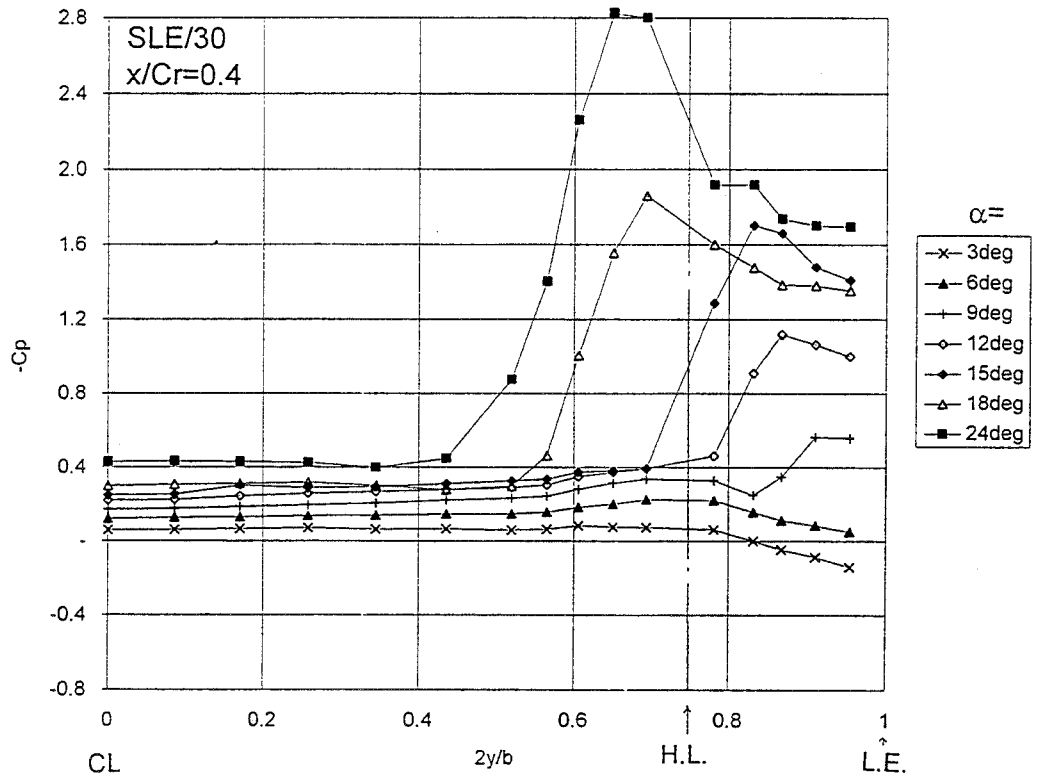

Fig.9e) SLE/30, *x/Cr*=0.4

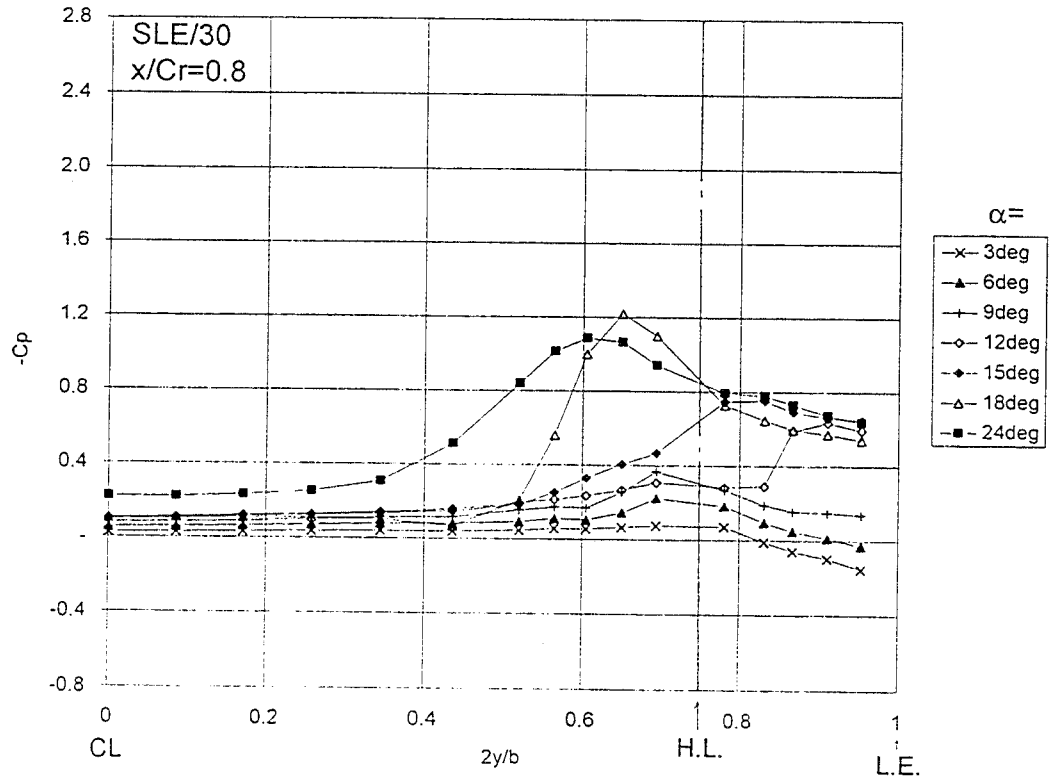

Fig.9f) SLE/30, *x/Cr*=0.8

Fig.9 Surface Pressure Distributions (δ_f=30°)

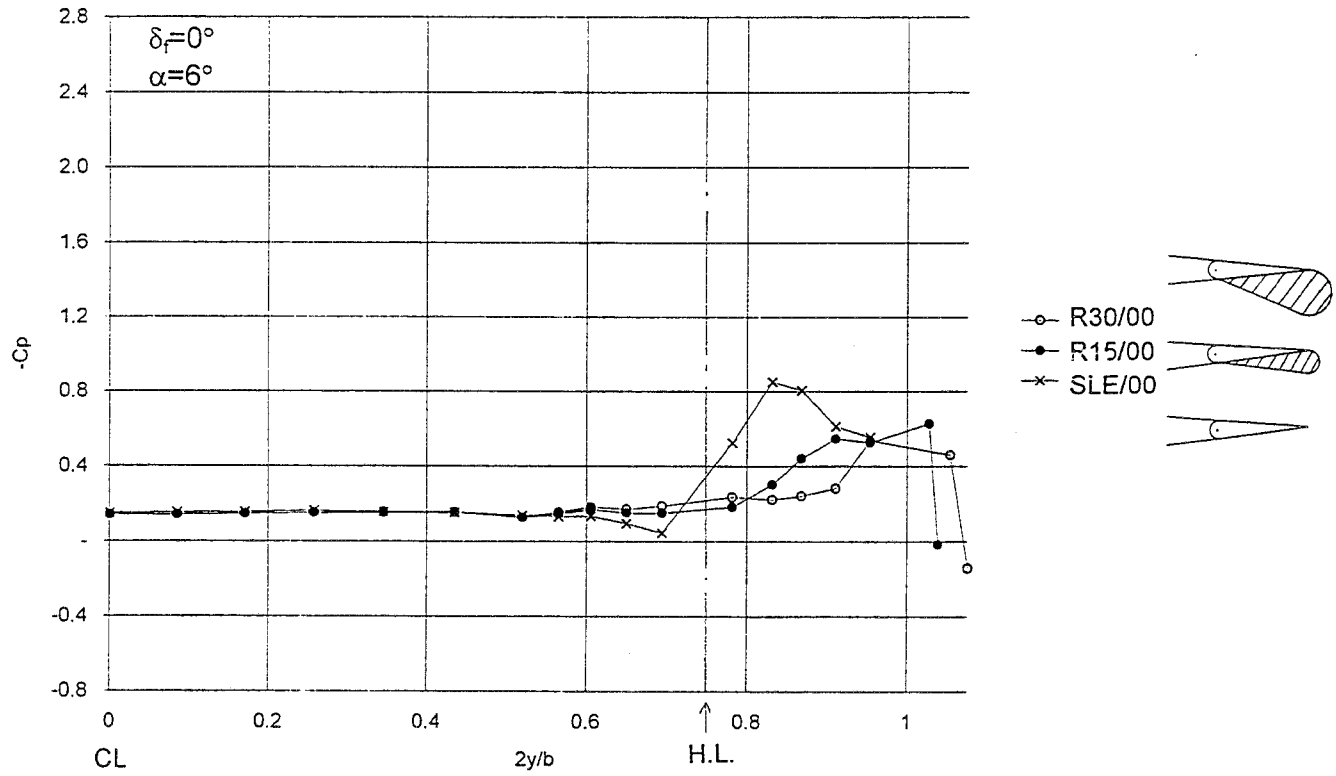

Fig.10a) α=6°

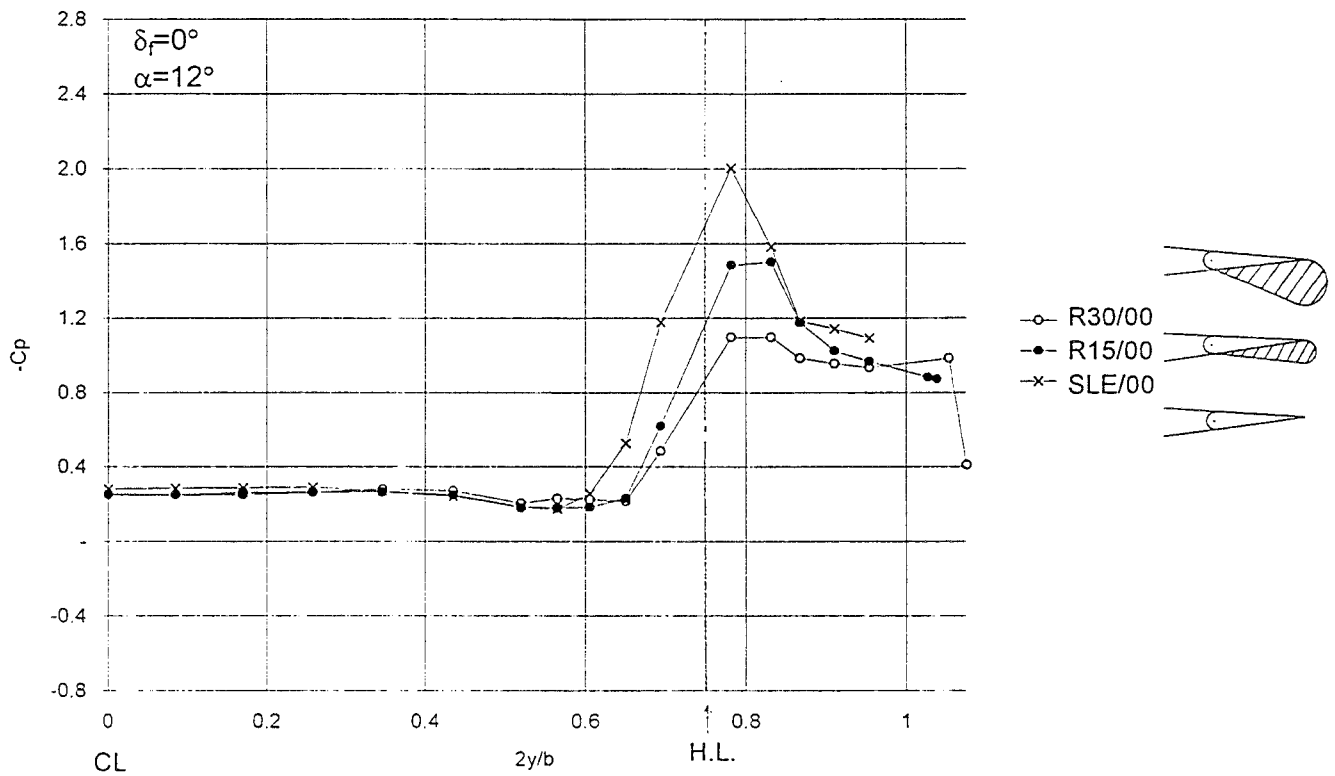

Fig.10b) α=12°

Fig.10 Surface Pressure Distributions at constant α (δ_f=0°)

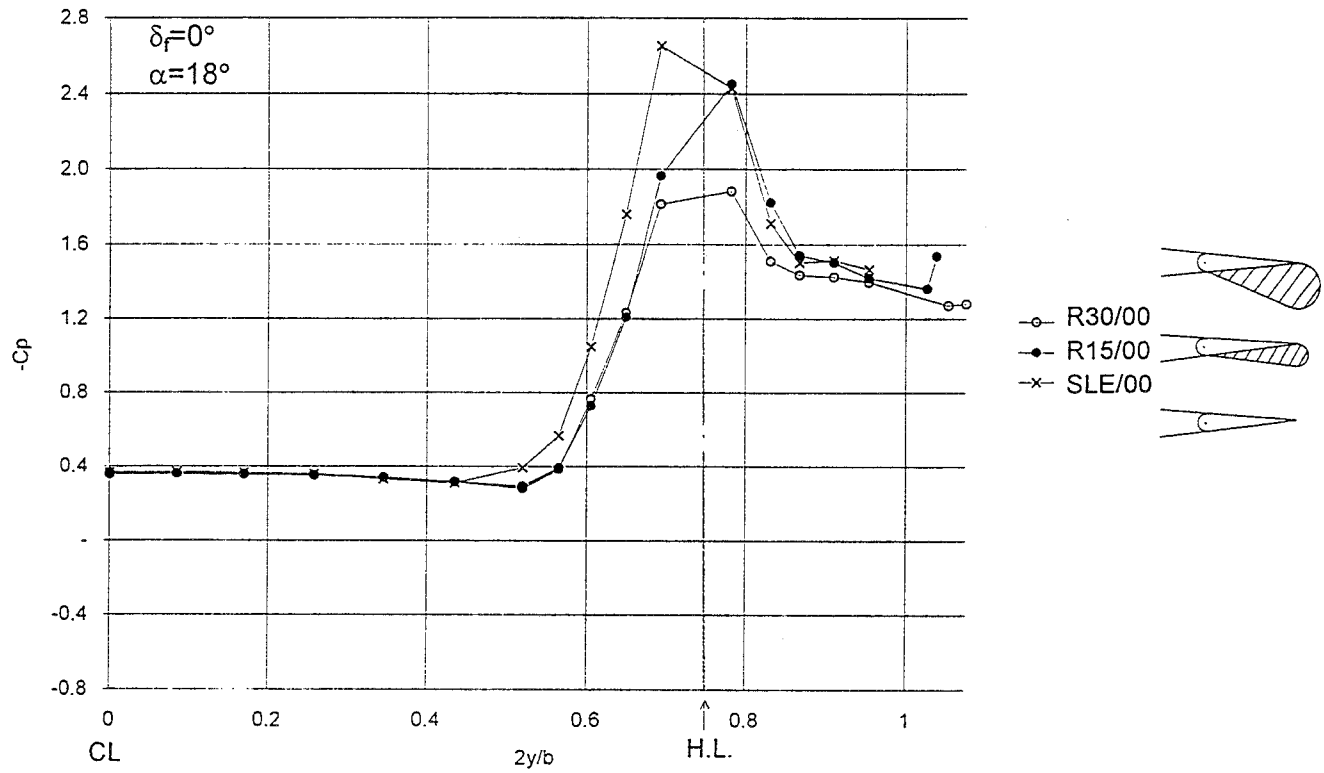

Fig.10c) α=18°

Fig.10 Surface Pressure Distributions at constant α (δ_f=0°)

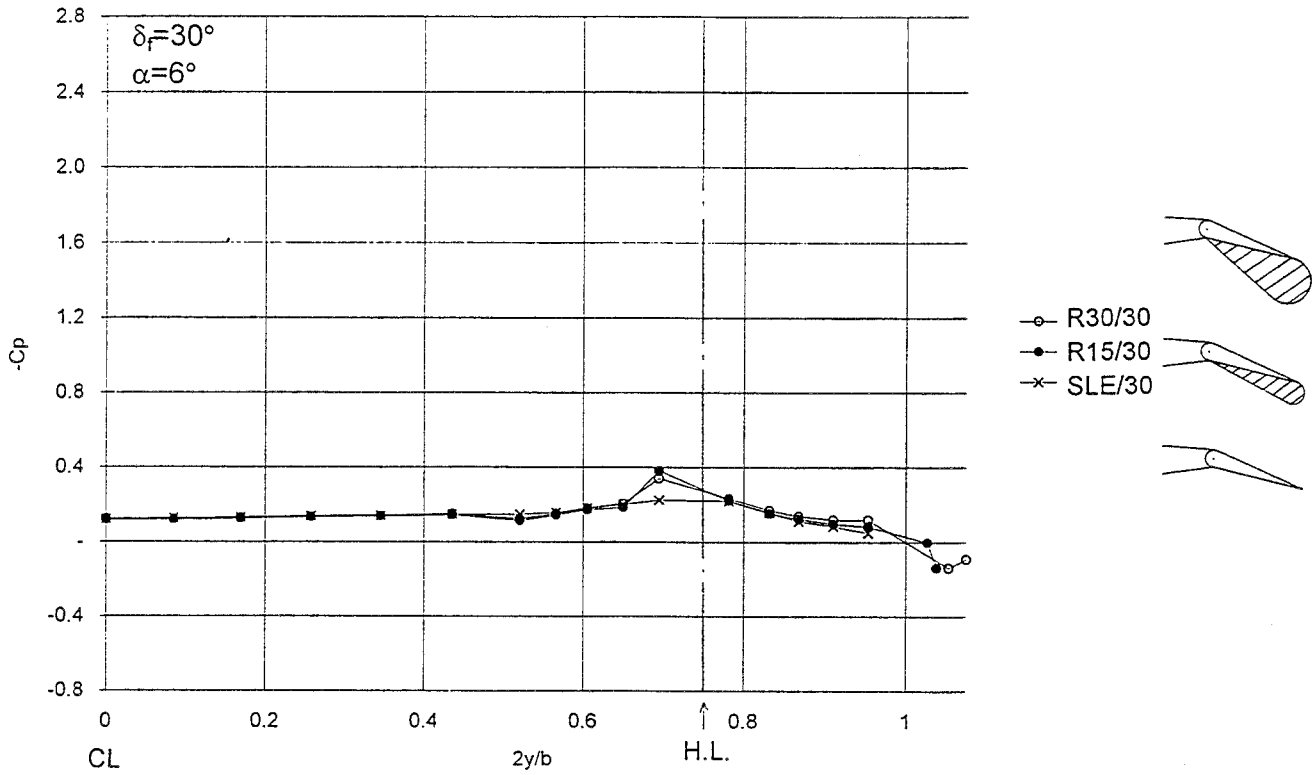

Fig.11a) α=6°

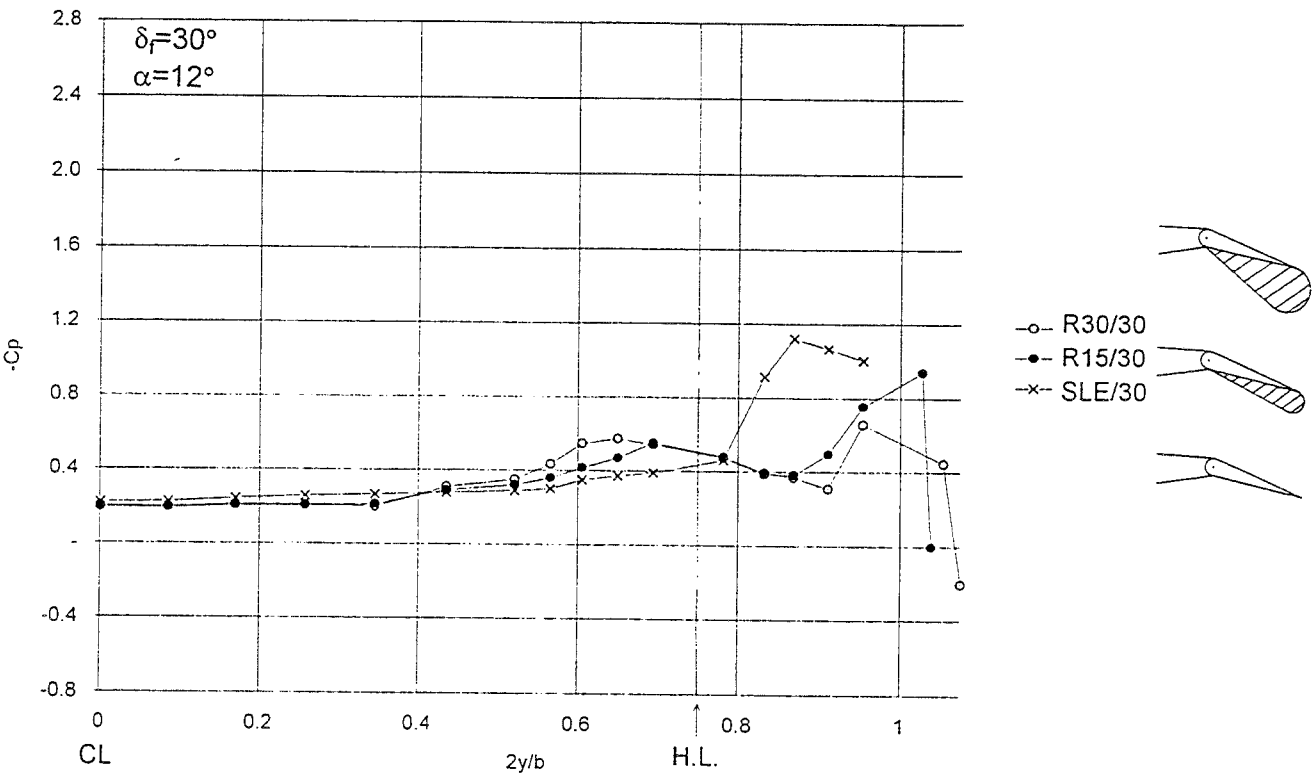

Fig.11b) α=12°

Fig.11 Surface Pressure Distributions at constant α (δ_f=30°)

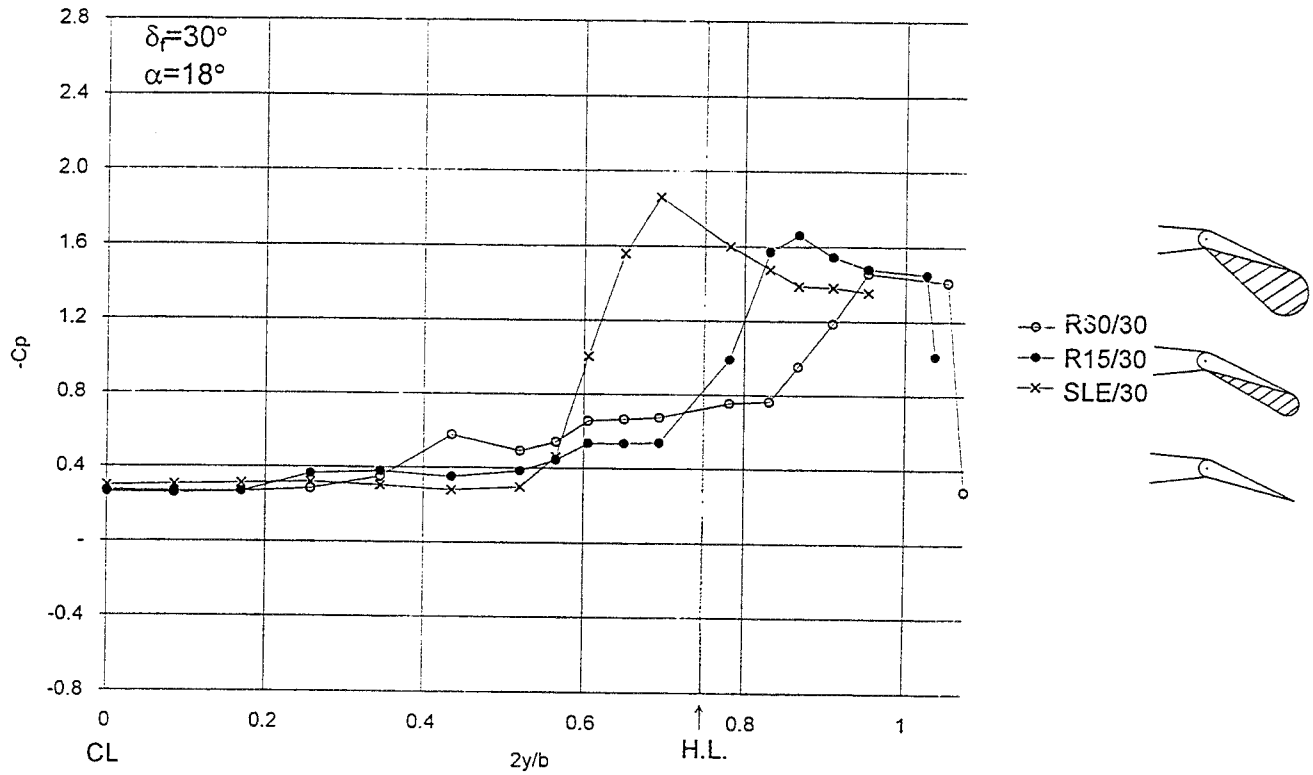

Fig.11c) α=18°

Fig.11 Surface Pressure Distributions at constant α (δ_f=30°)

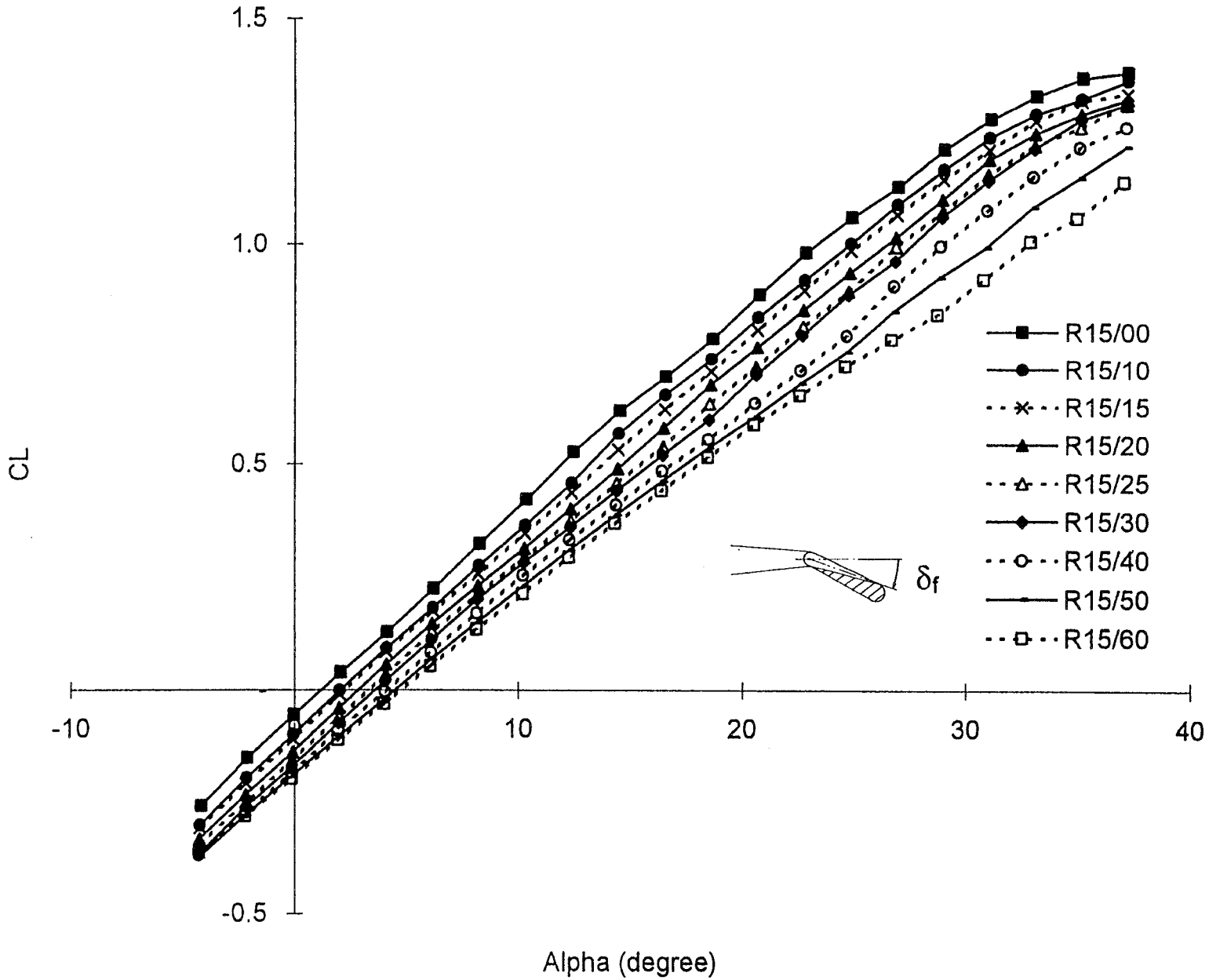

Fig.12a) C_L-α

Fig.12 Effect of Flap Deflection (R15)

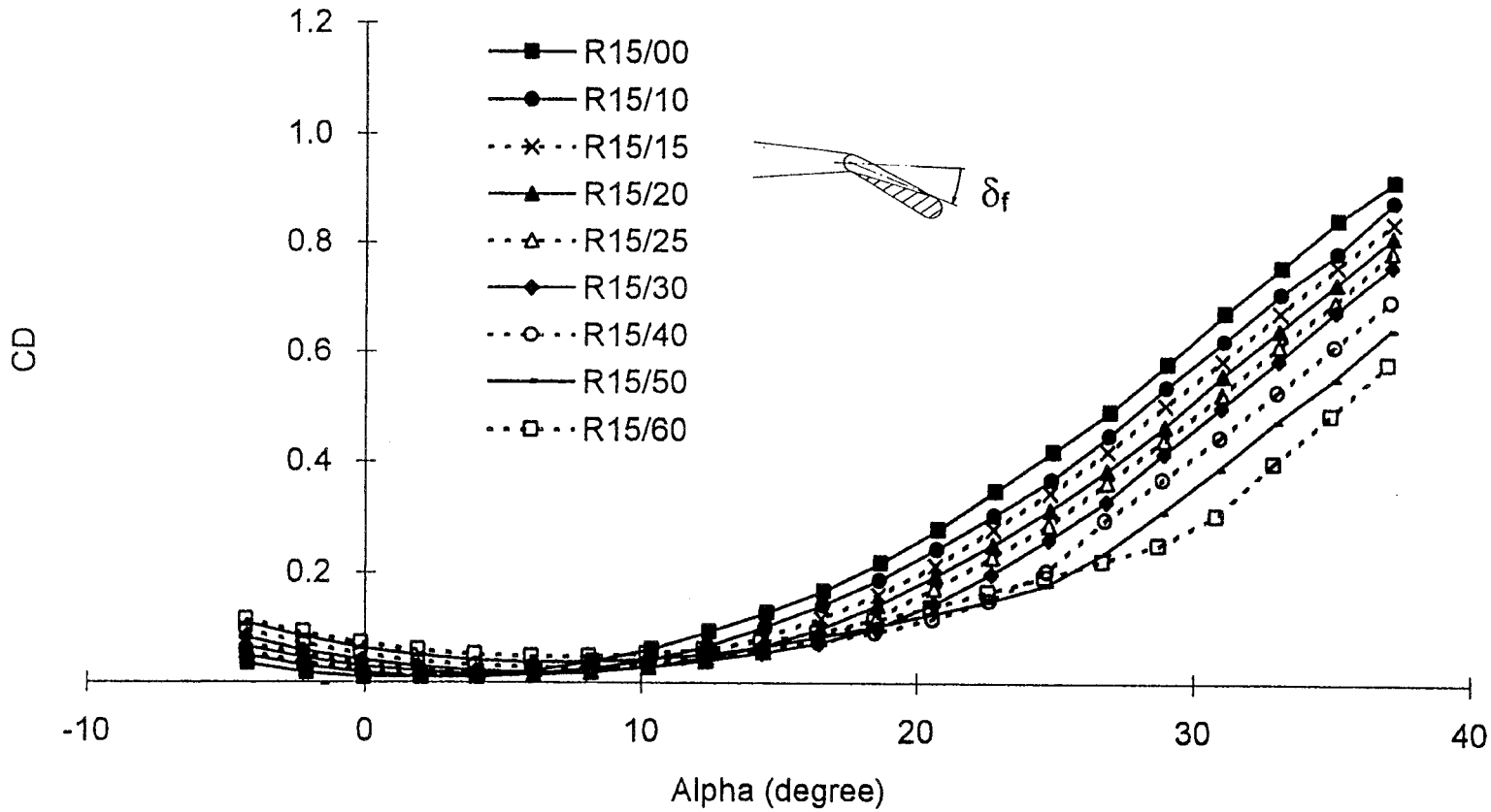

Fig.12b) C_D-α

Fig.12 Effect of Flap Deflection (R15)

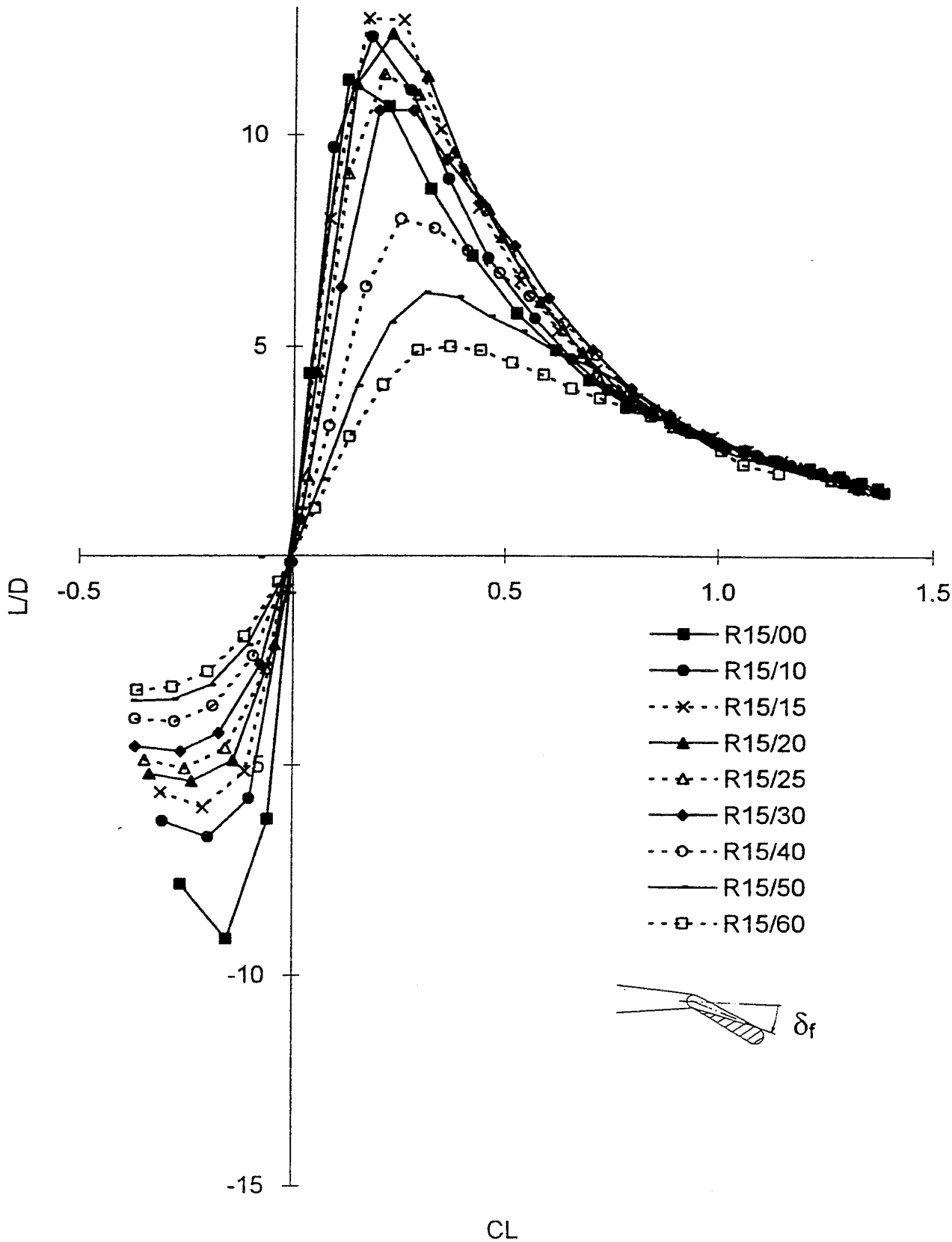

Fig.12c) *L/D-C*$_L$

Fig.12 Effect of Flap Deflection (R15)

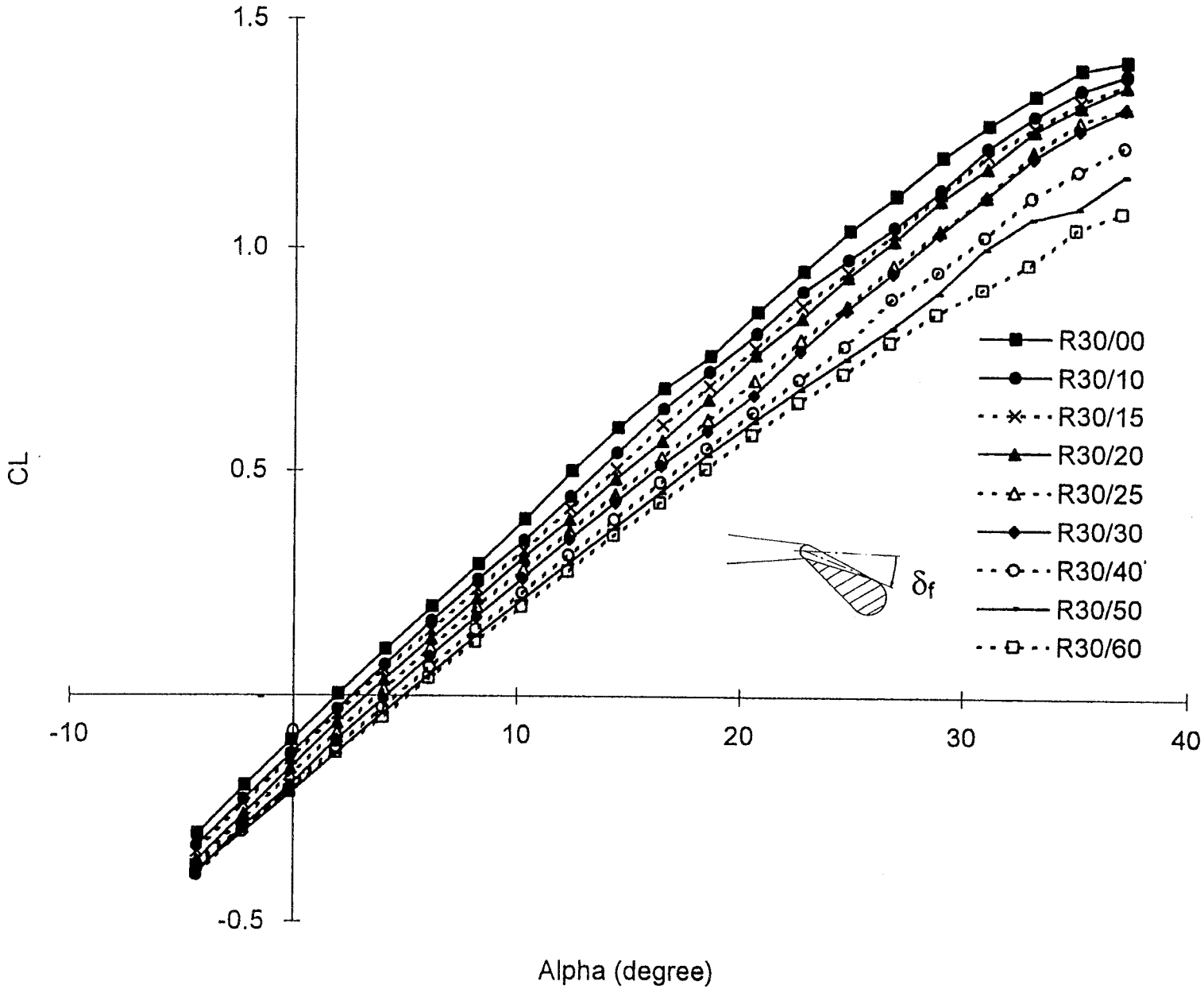

Fig.13a) C_L-α

Fig.13 Effect of Flap Deflection (R30)

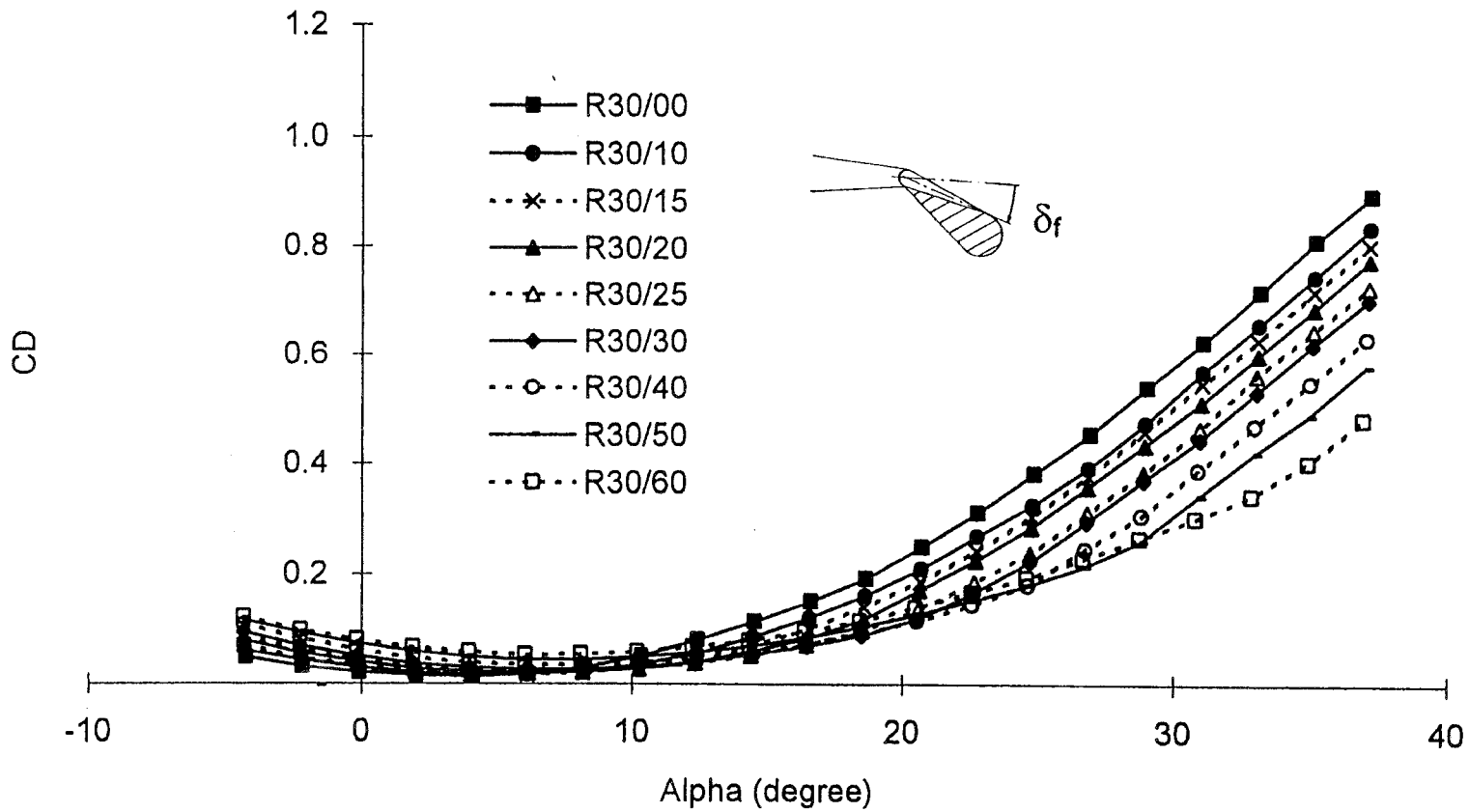

Fig.13b) C_D-α

Fig.13 Effect of Flap Deflection (R30)

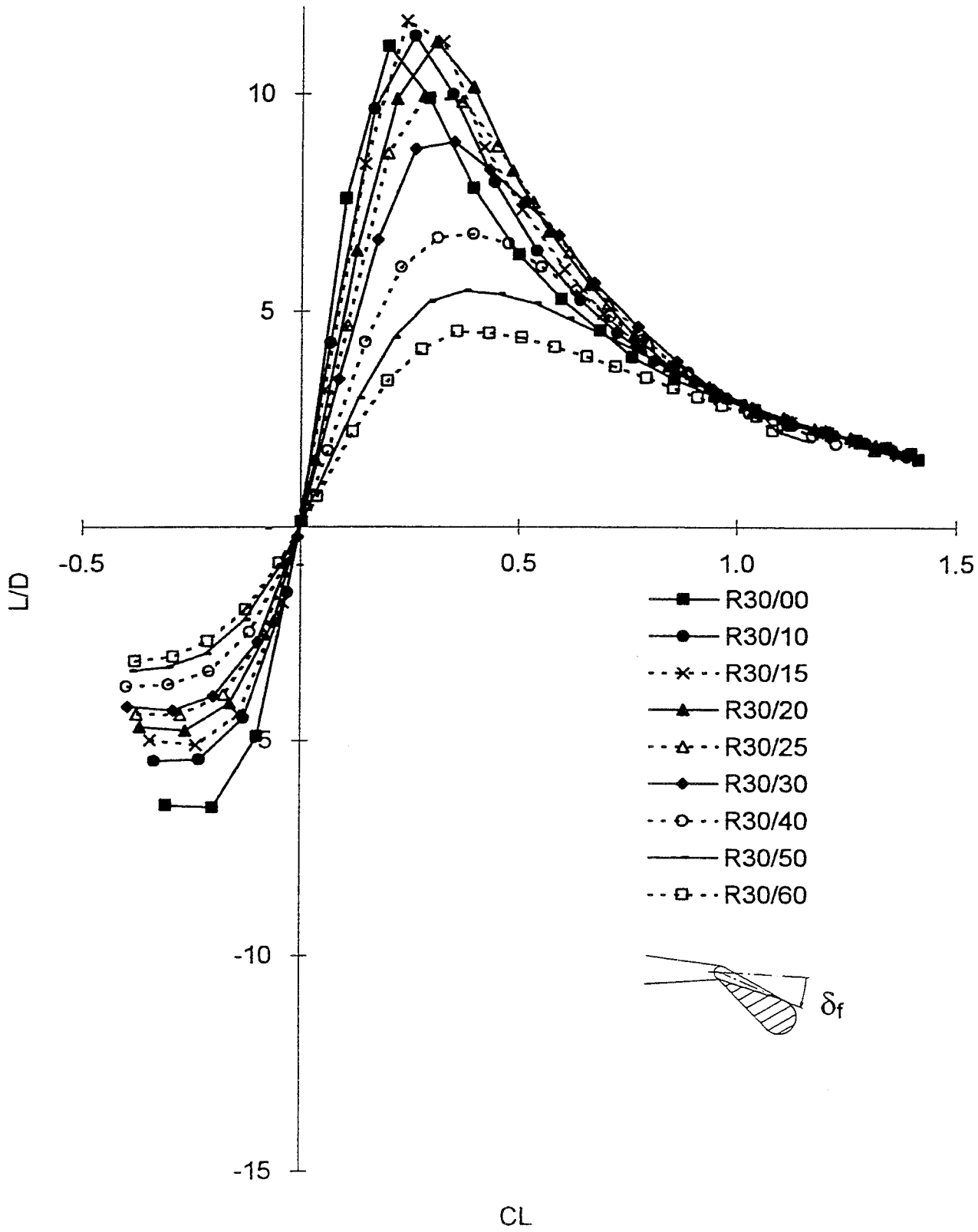

Fig.13c) L/D-C_L

Fig.13 Effect of Flap Deflection (R30)

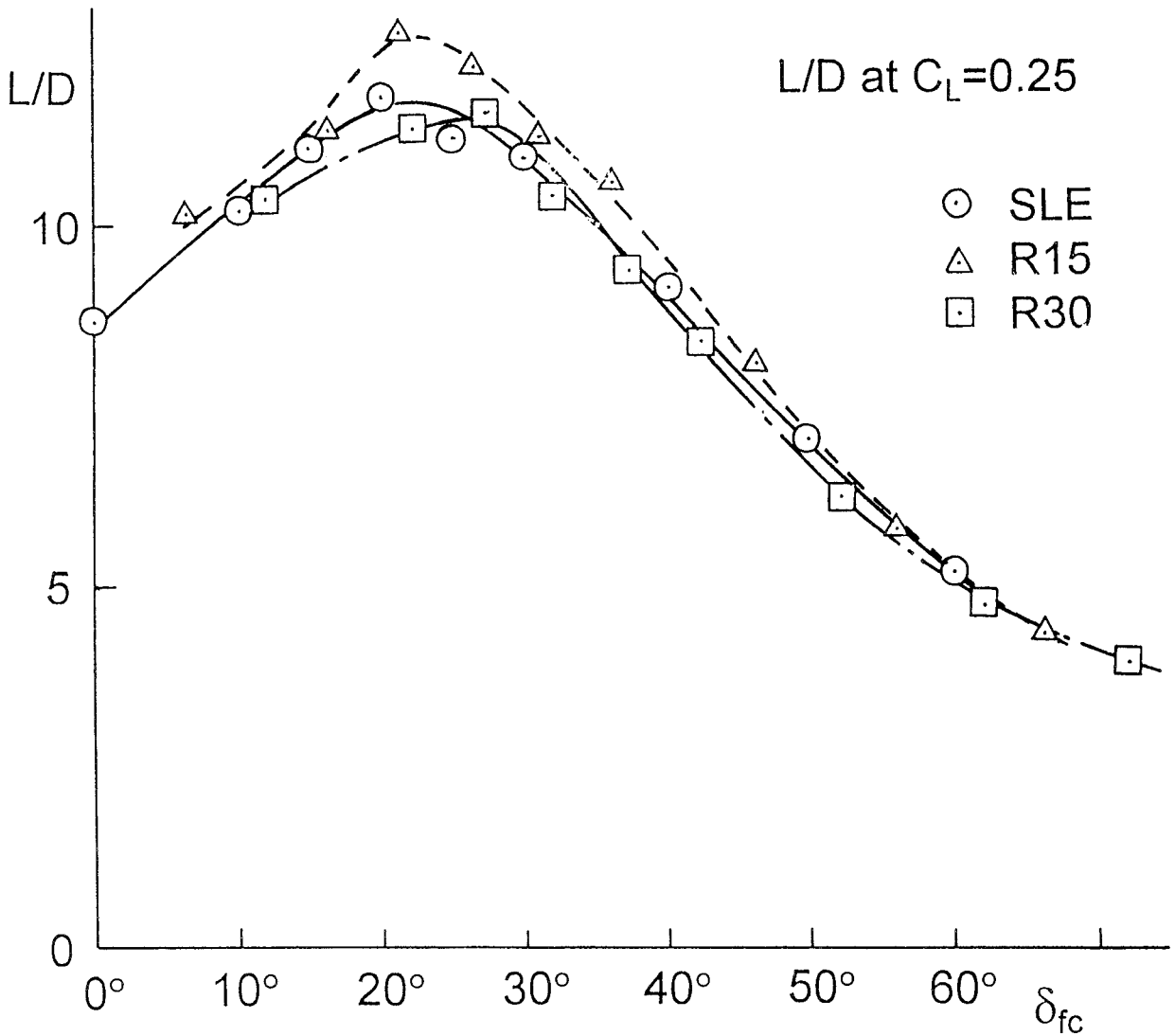

Fig.14a) *L/D* at C_L=0.25

Fig.14 *L/D* vs. Corrected δ_f at Constant C_L

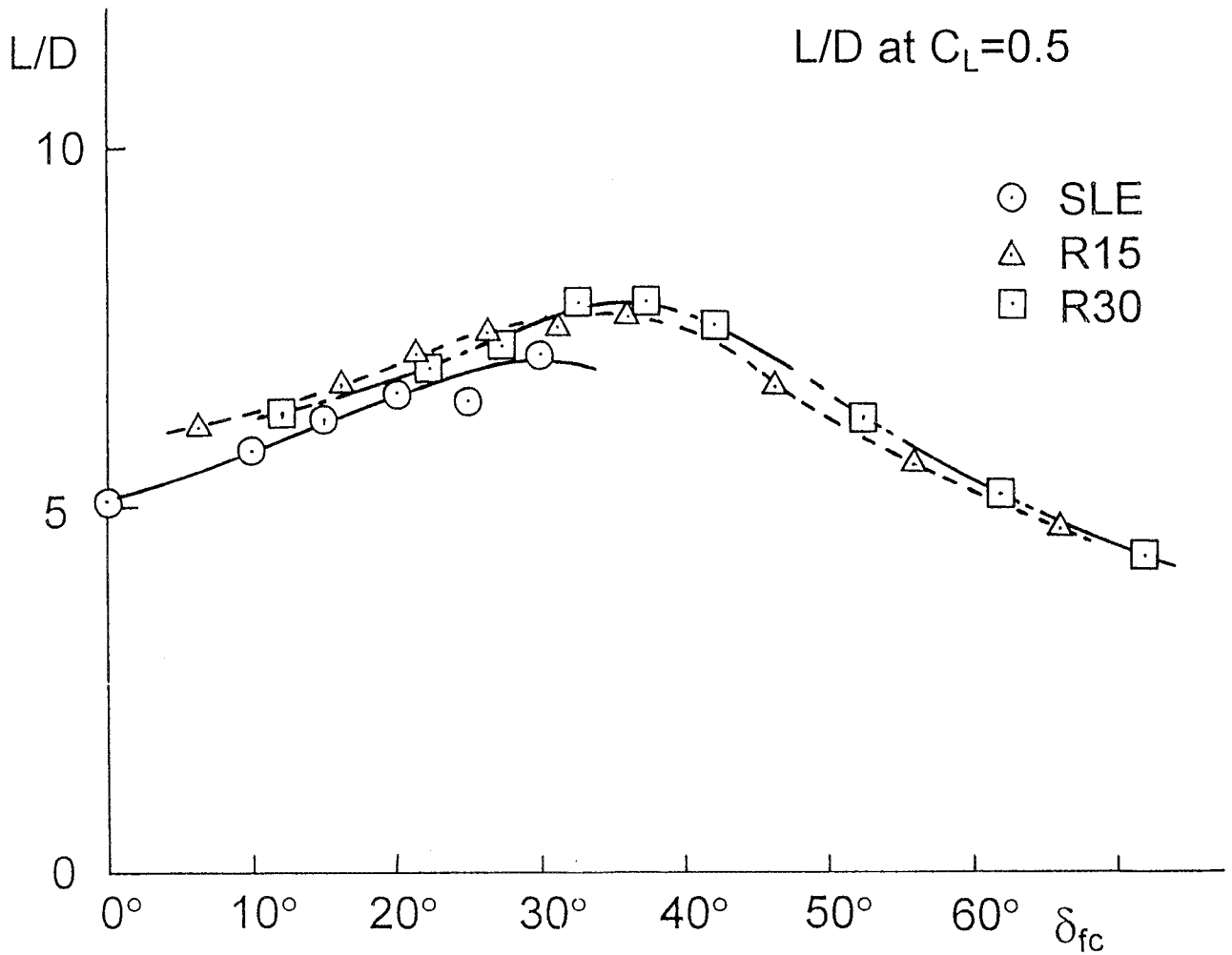

Fig.14b) *L/D* at C_L=0.5

Fig.14 *L/D* vs. Corrected δ_f at Constant C_L

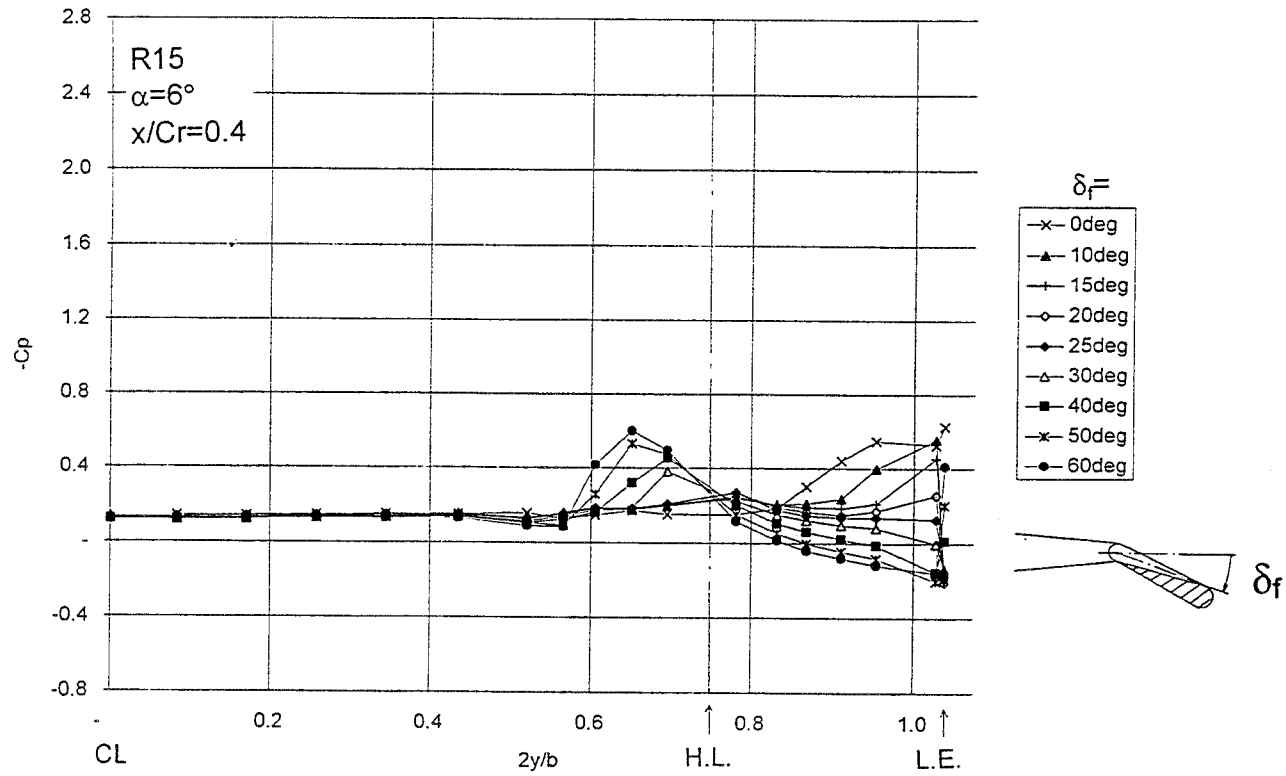

Fig.15a) R15

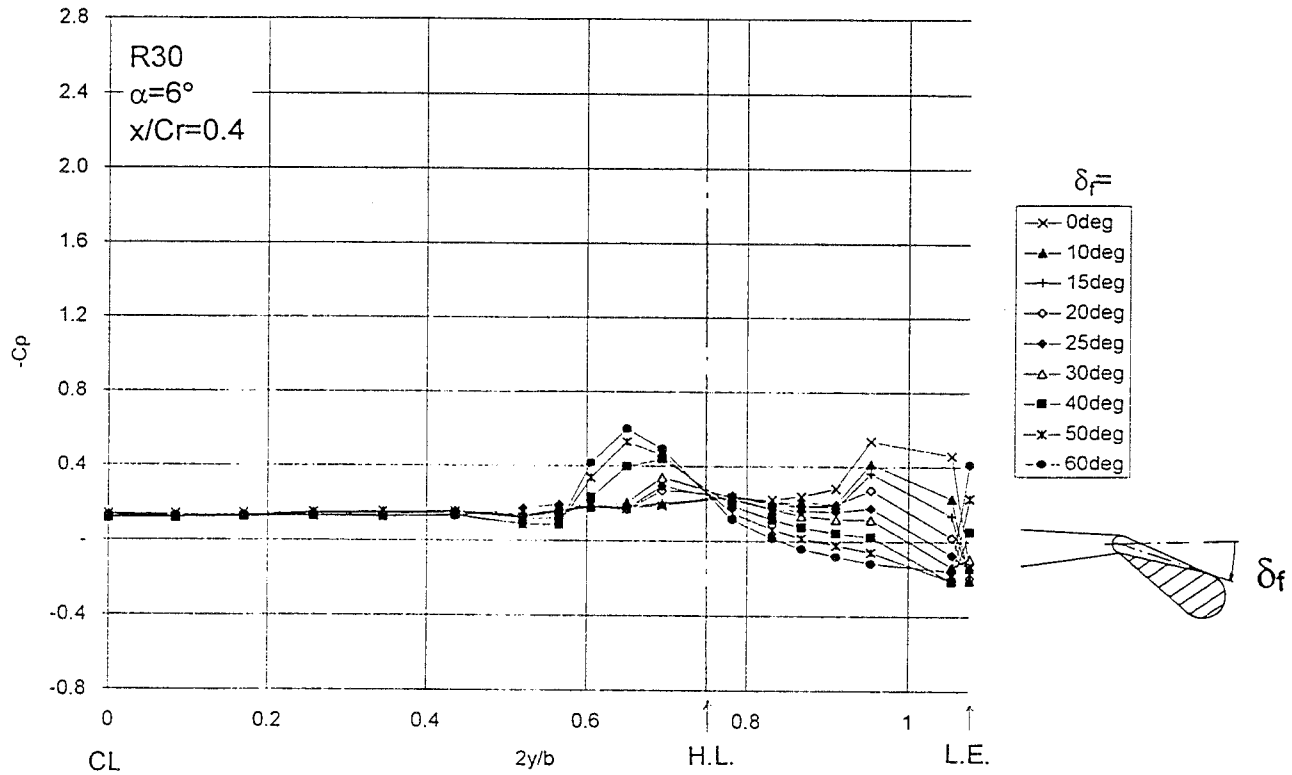

Fig.15b) R30

Fig.15 Surface Pressure Distributions at different δ_f (α=6°)

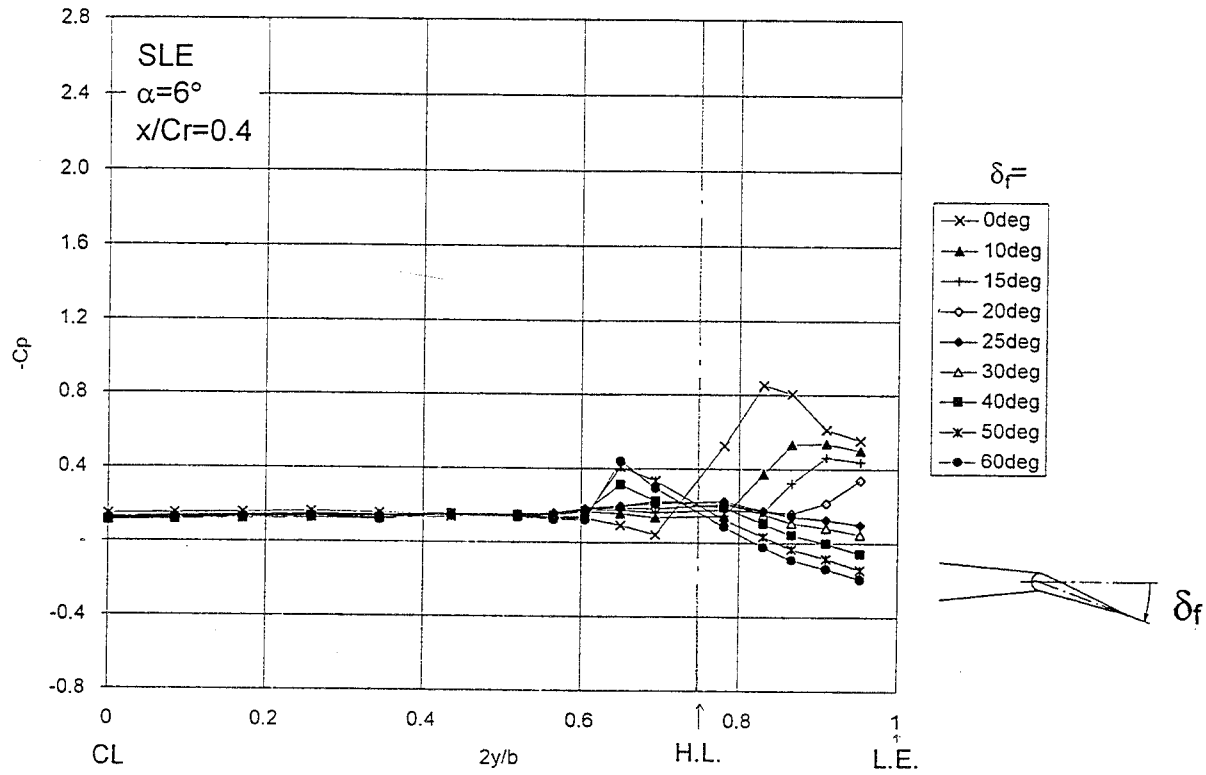

Fig.15c) SLE

Fig.15 Surface Pressure Distributions at different δ_f (α=6°)

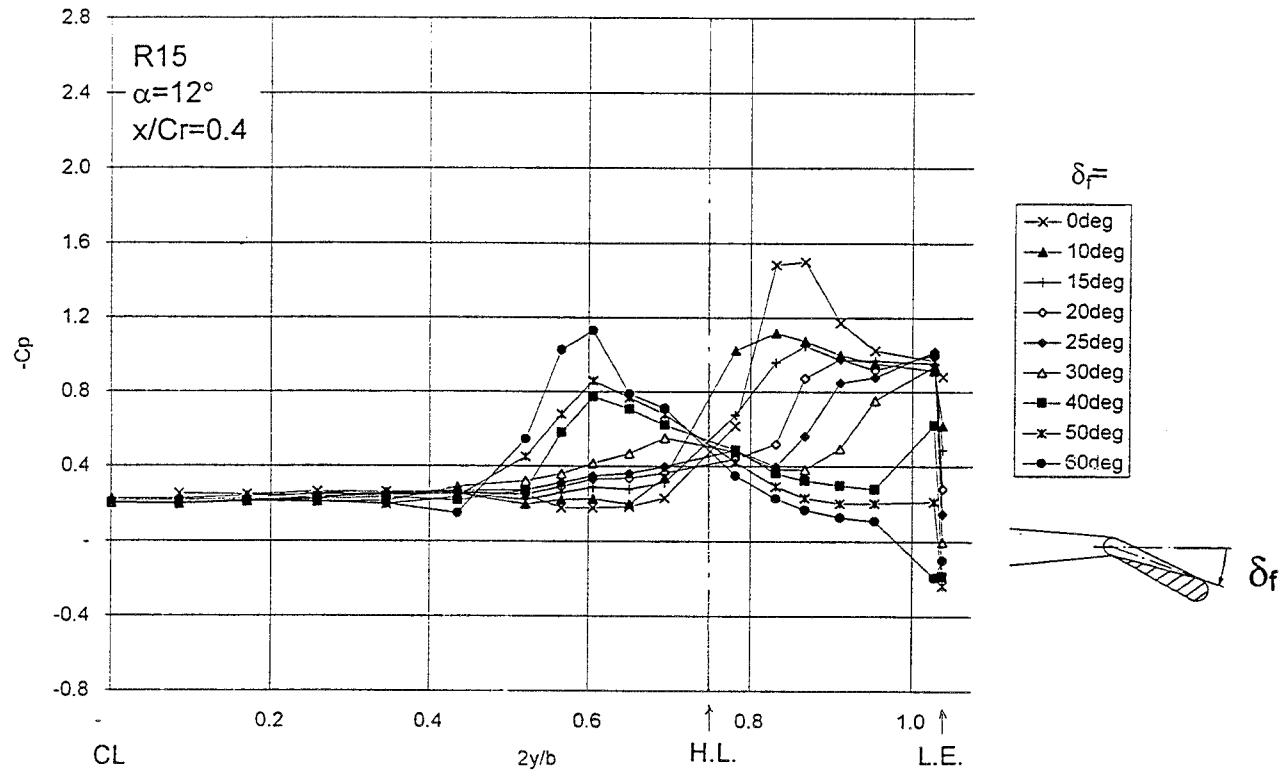

Fig.16a) R15

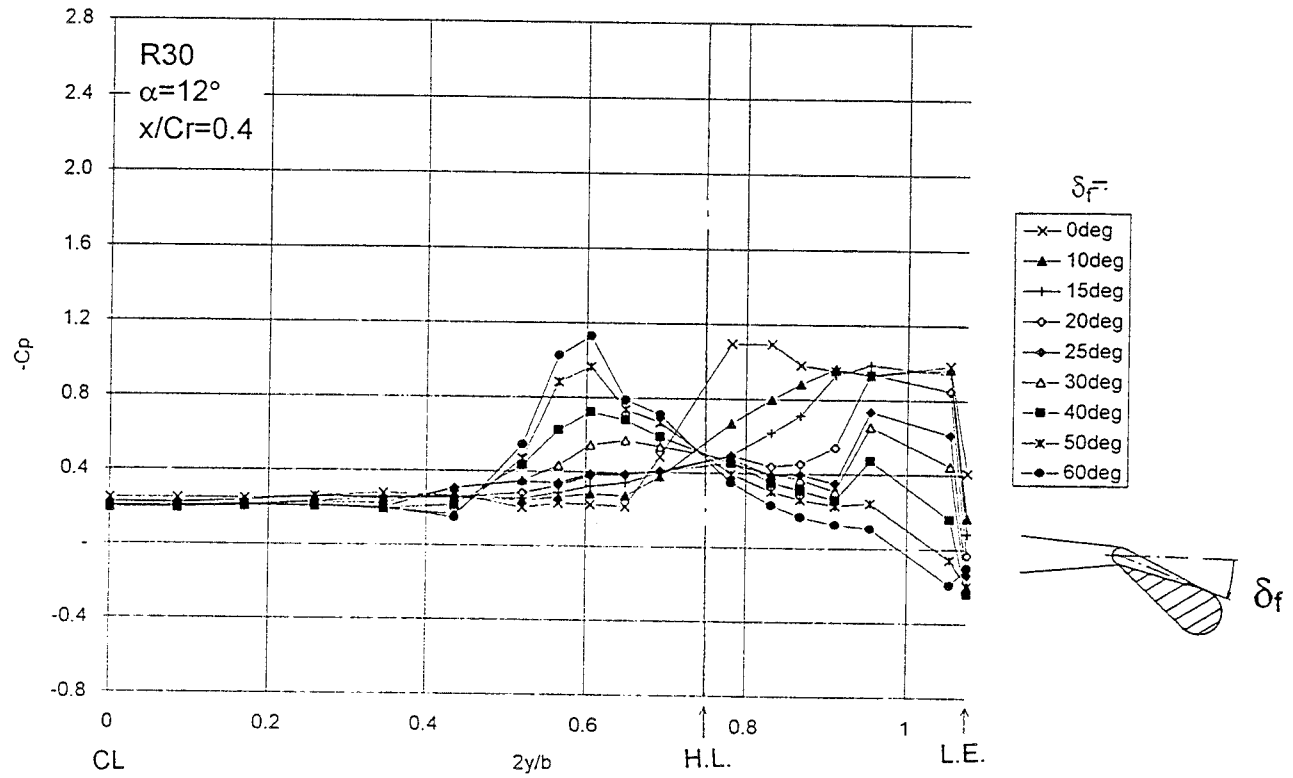

Fig.16b) R30

Fig.16 Surface Pressure Distributions at different δ_f (α=12°)

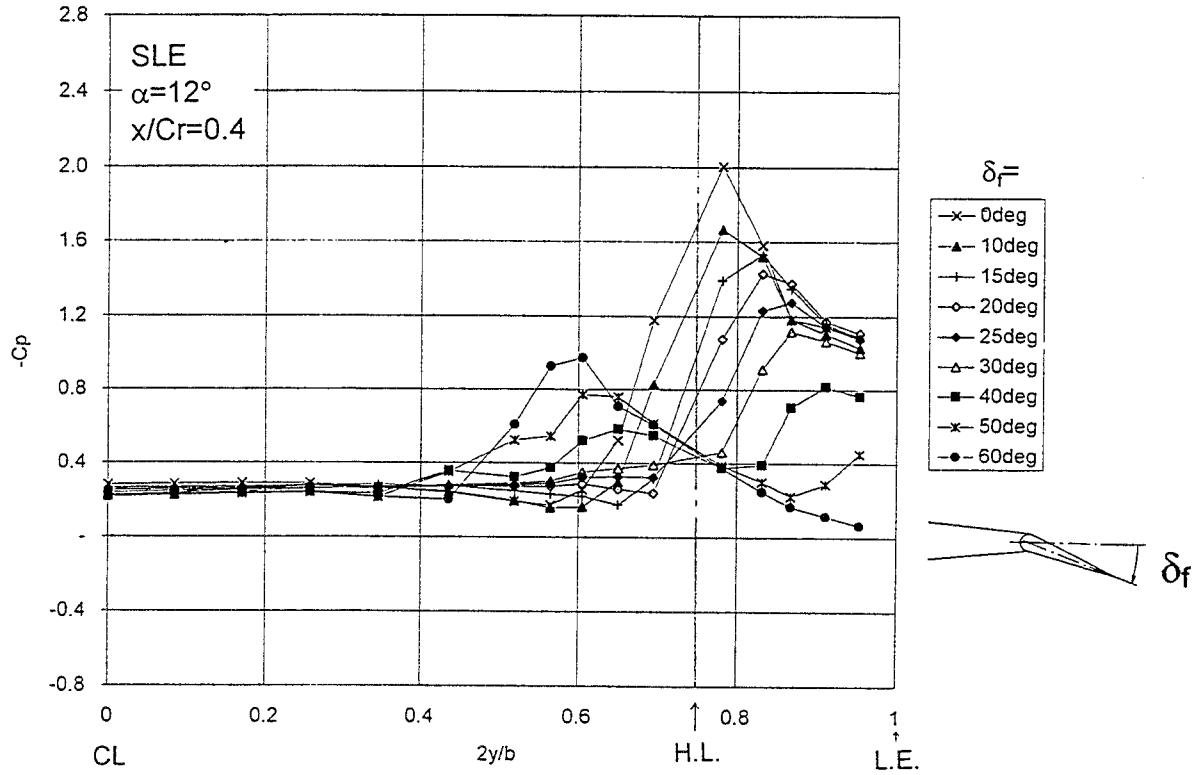

Fig.16c) SLE

Fig.16 Surface Pressure Distributions at different δ_f (α=12°)

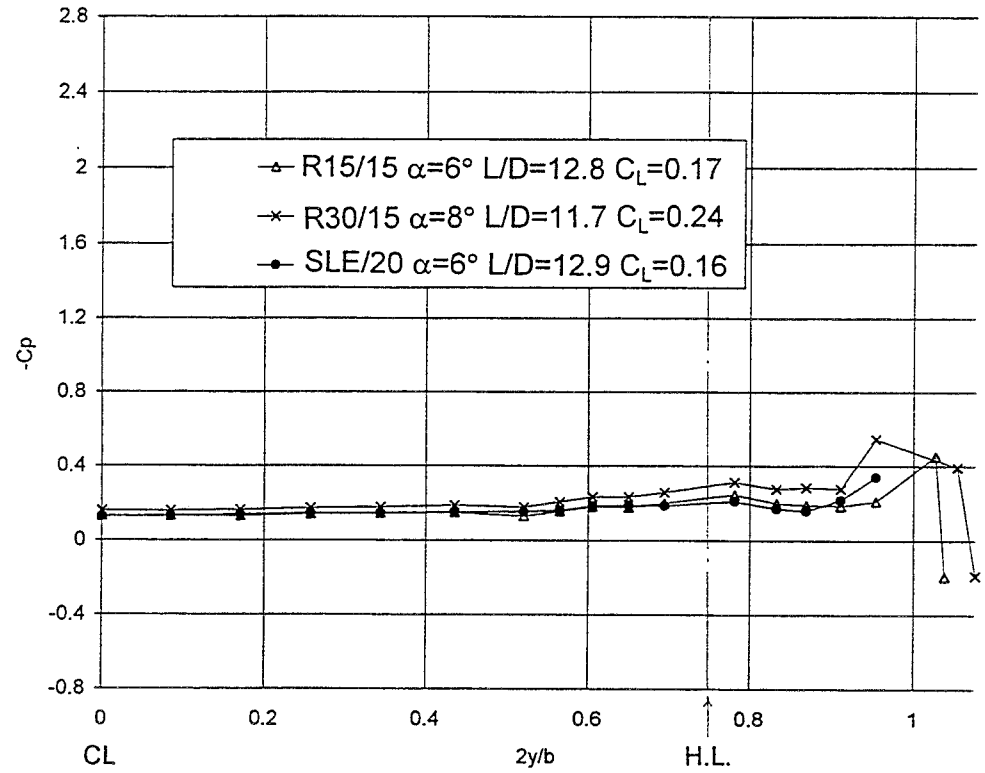

Fig.17a) Maximum *L/D*

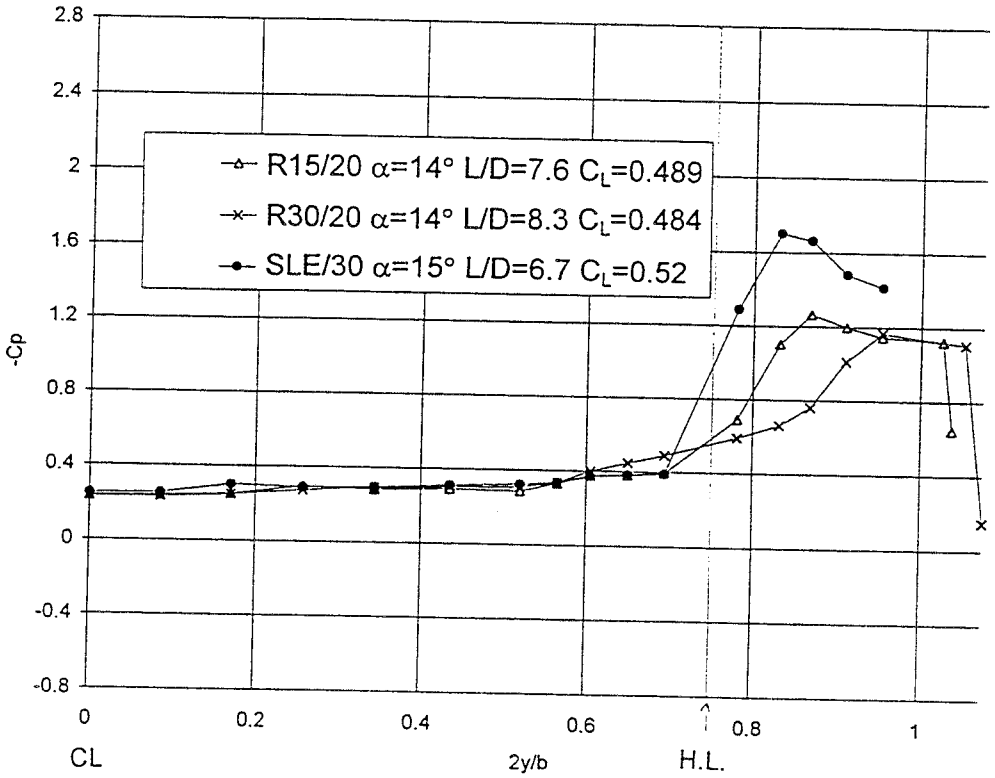

Fig.17b) Local Max. *L/D* at C_L= 0.5

Fig.17 Surface Pressure Distributions (*x/Cr*=0.4)

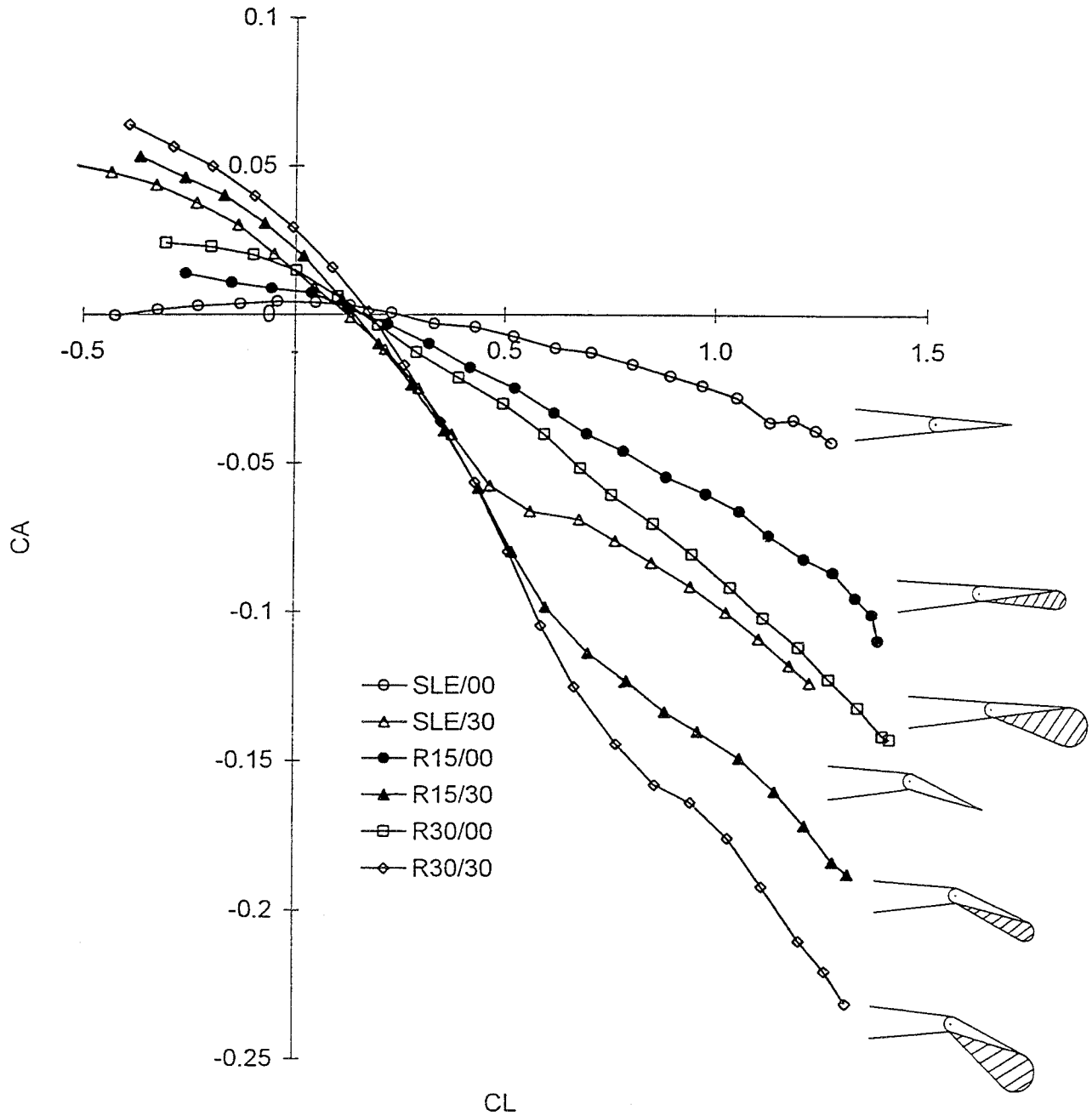

Fig.18a) Present results

Fig.18 Axial Force C_A vs. C_L

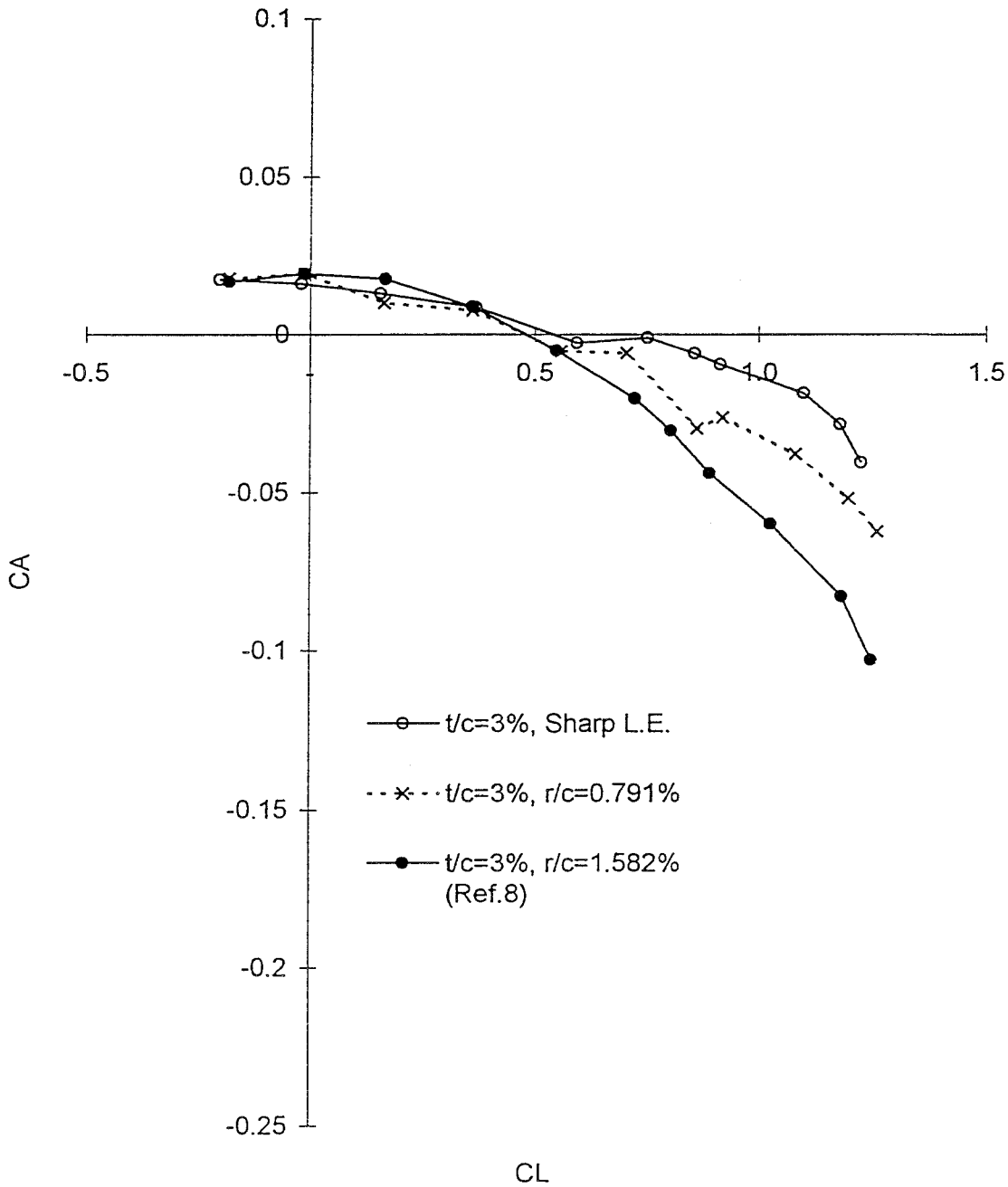

Fig.18b) from Ref.8

Fig.18 Axial Force C_A vs. C_L

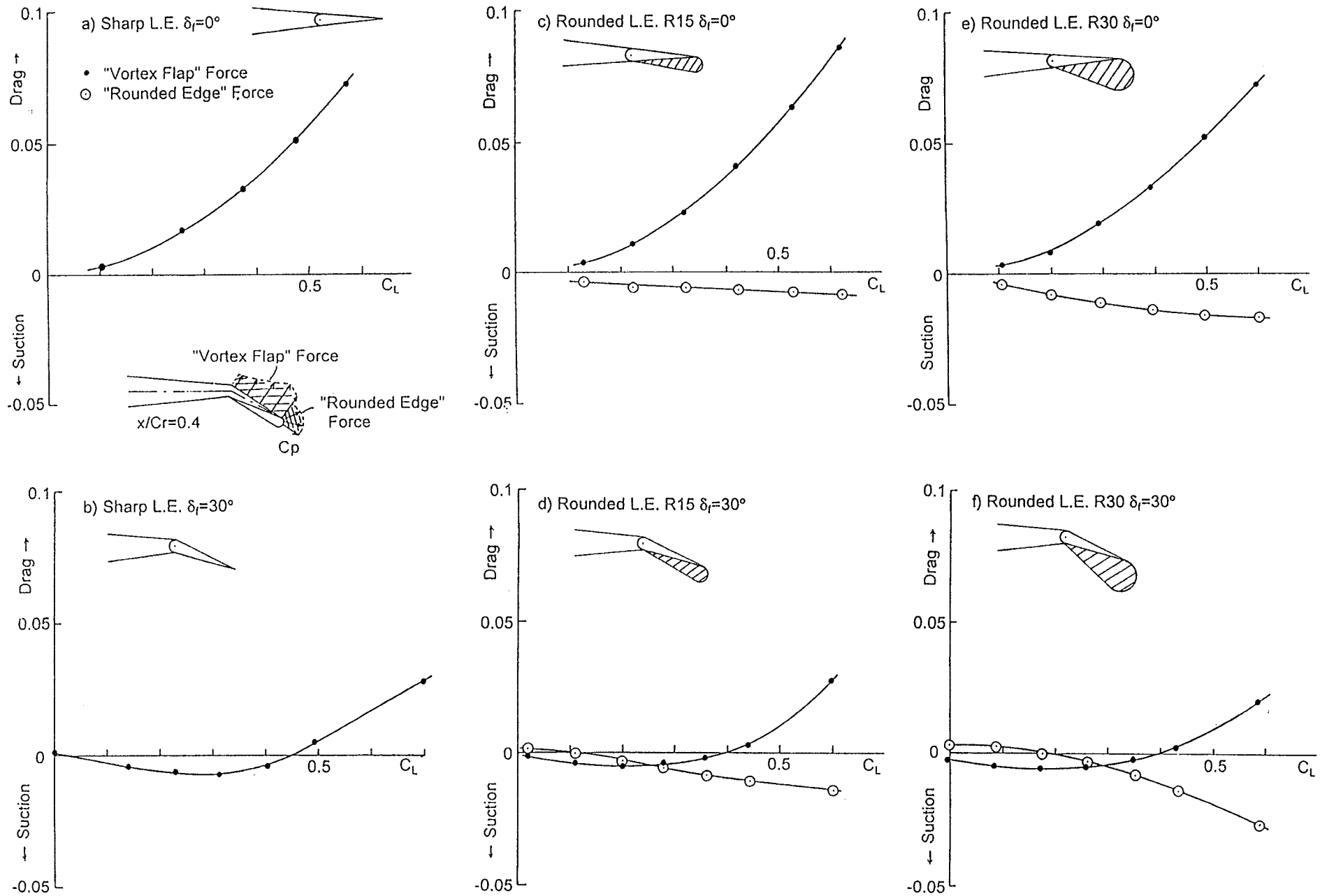

Fig.19 "Vortex Flap" Force & "Rounded Edge" Force

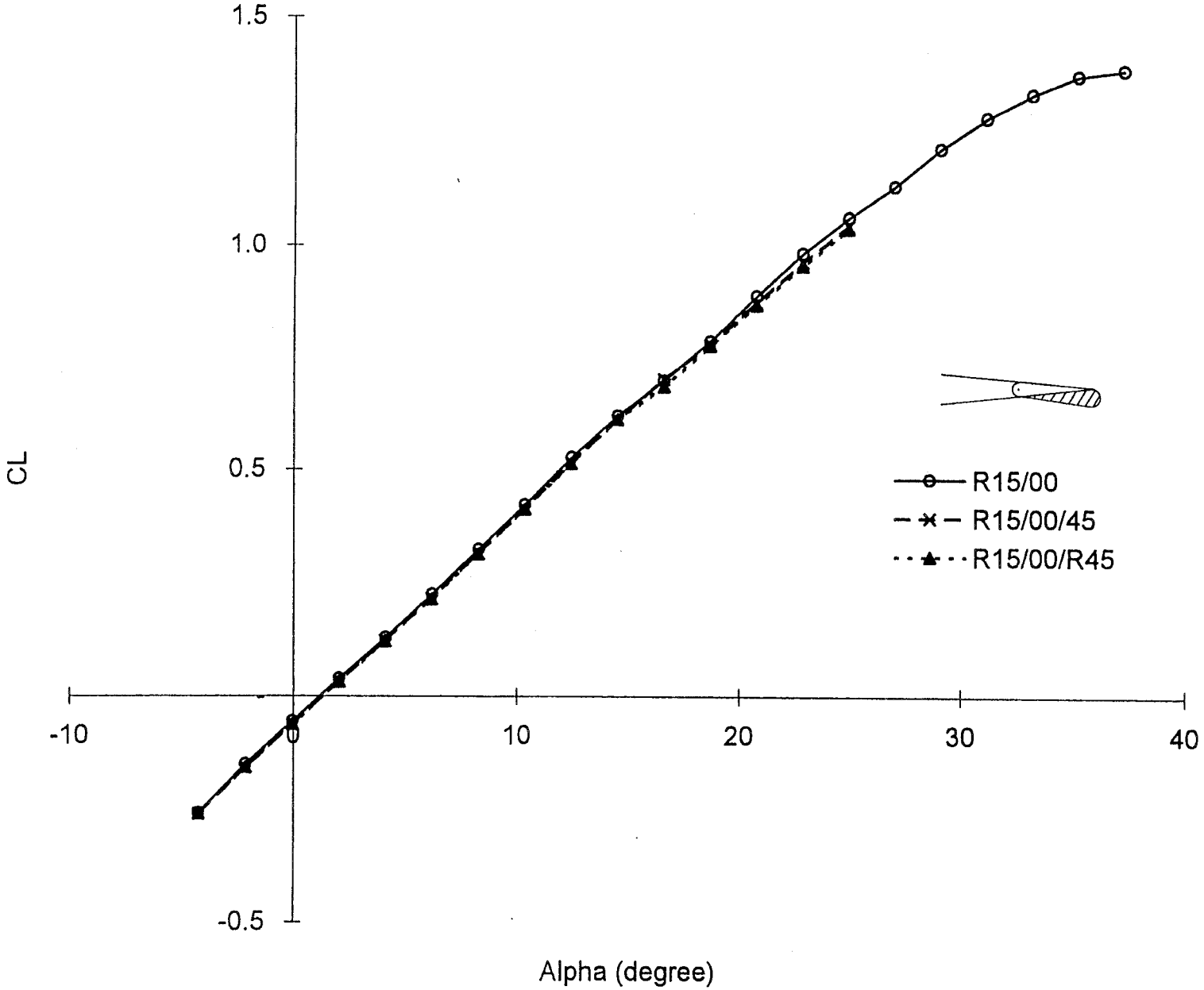

Fig.20a) C_L-α

Fig.20 Effect of Reynolds Number & Roughness (R15/00)

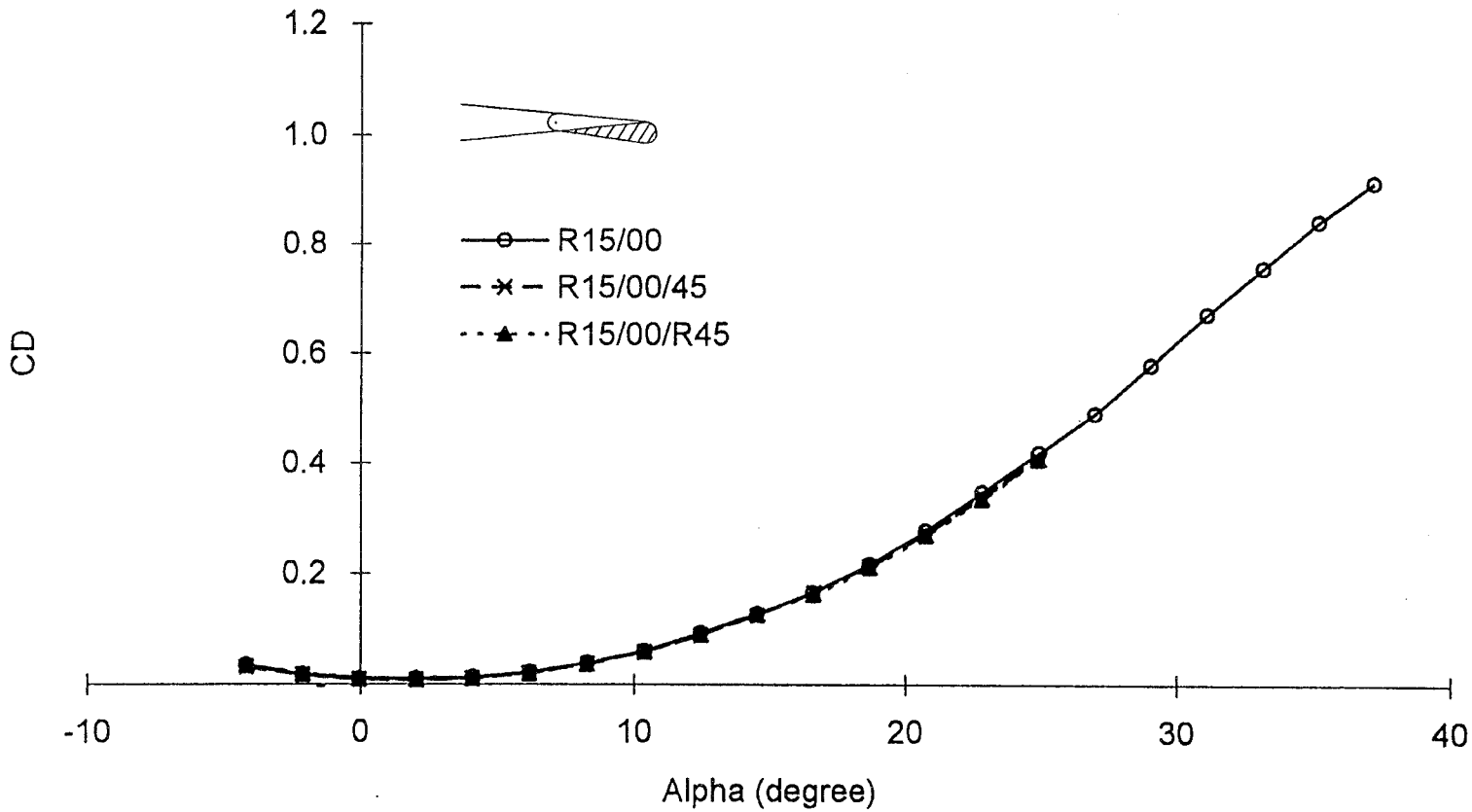

Fig.20b) C_D-α

Fig.20 Effect of Reynolds Number & Roughness (R15/00)

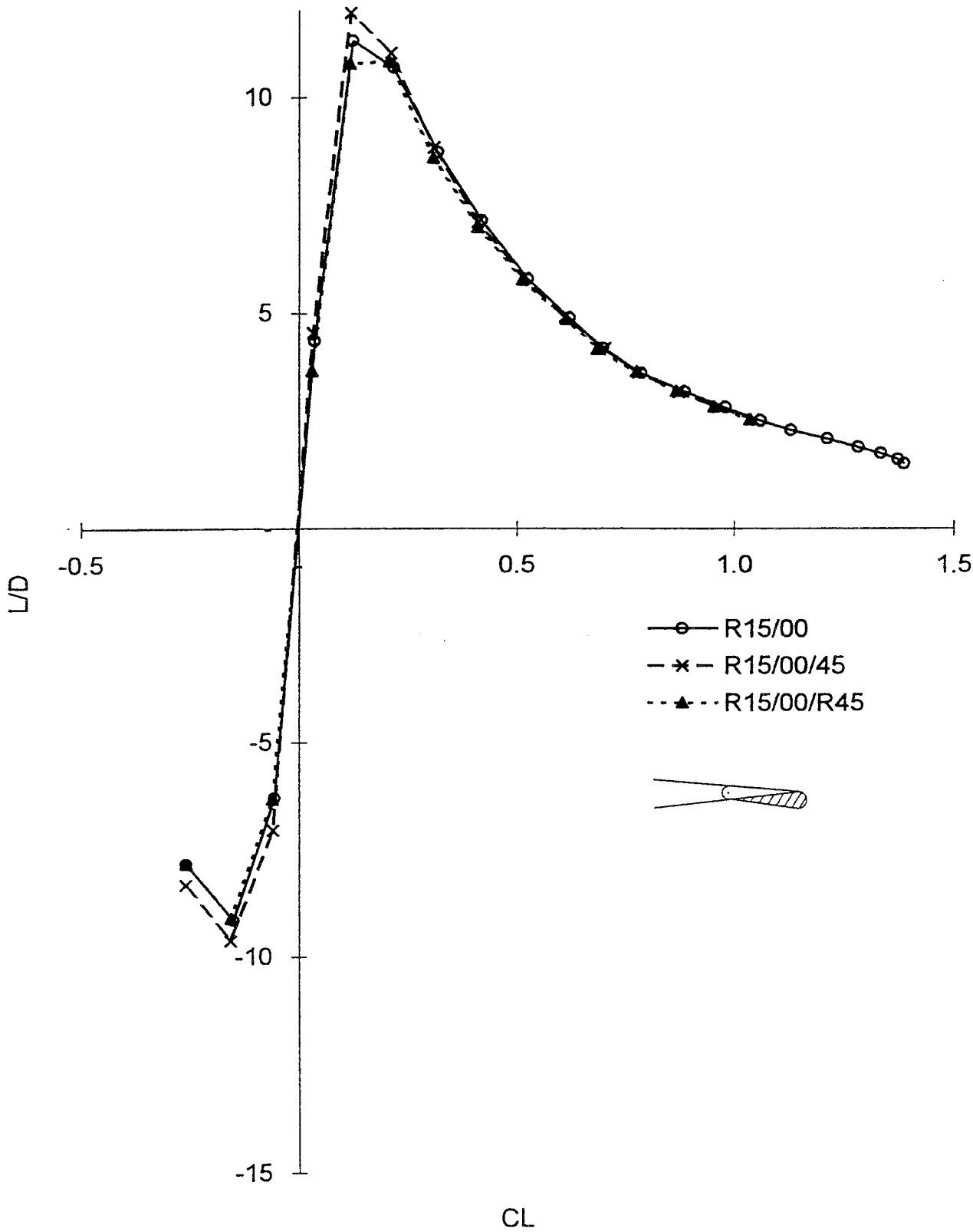

Fig.20c) L/D-C_L

Fig.20 Effect of Reynolds Number & Roughness (R15/00)

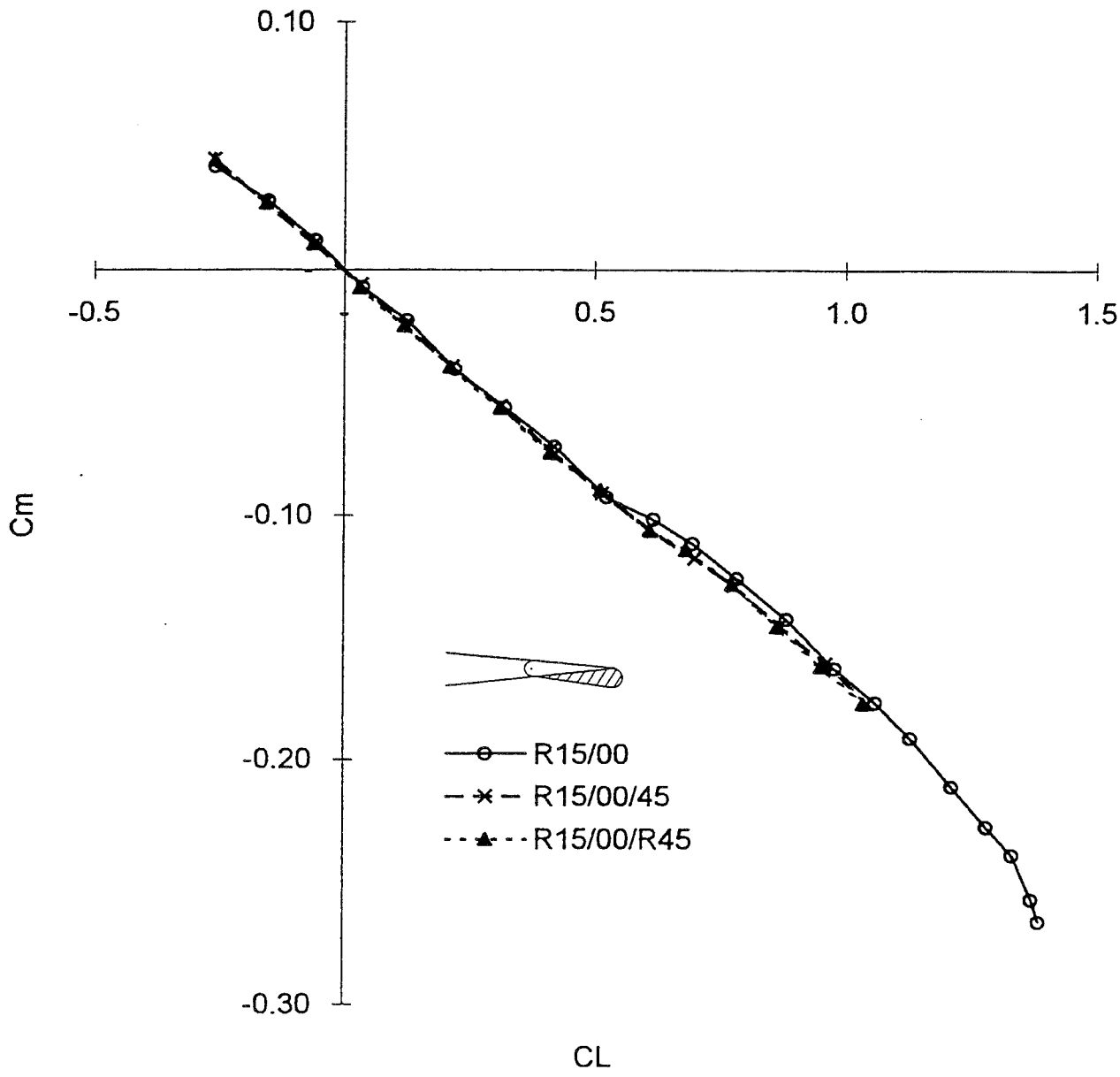

Fig.20d) C_m-C_L

Fig.20 Effect of Reynolds Number & Roughness (R15/00)

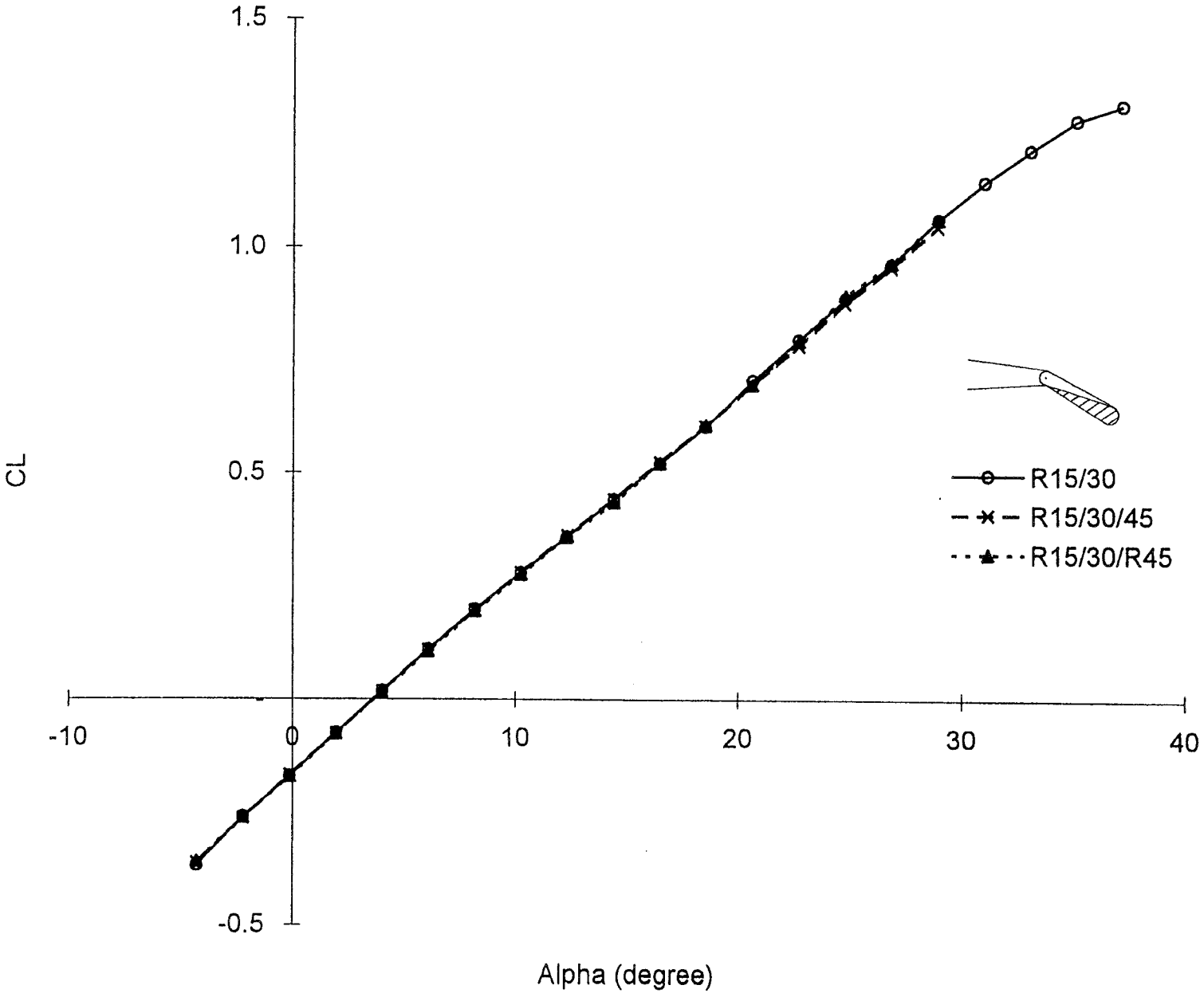

Fig.21a) C_L-α

Fig.21 Effect of Reynolds Number & Roughness (R15/30)

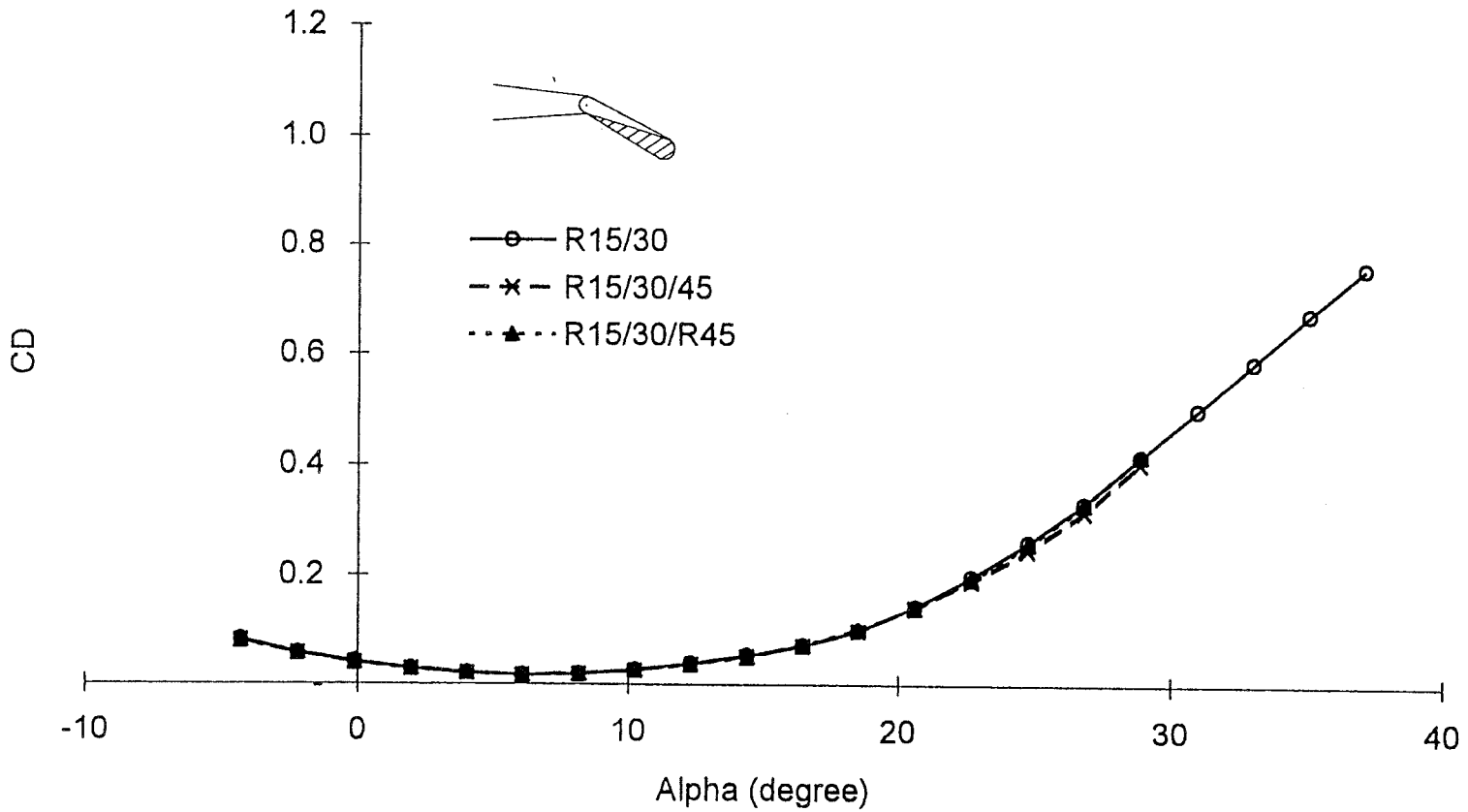

Fig.21b) C_D-α

Fig.21 Effect of Reynolds Number & Roughness (R15/30)

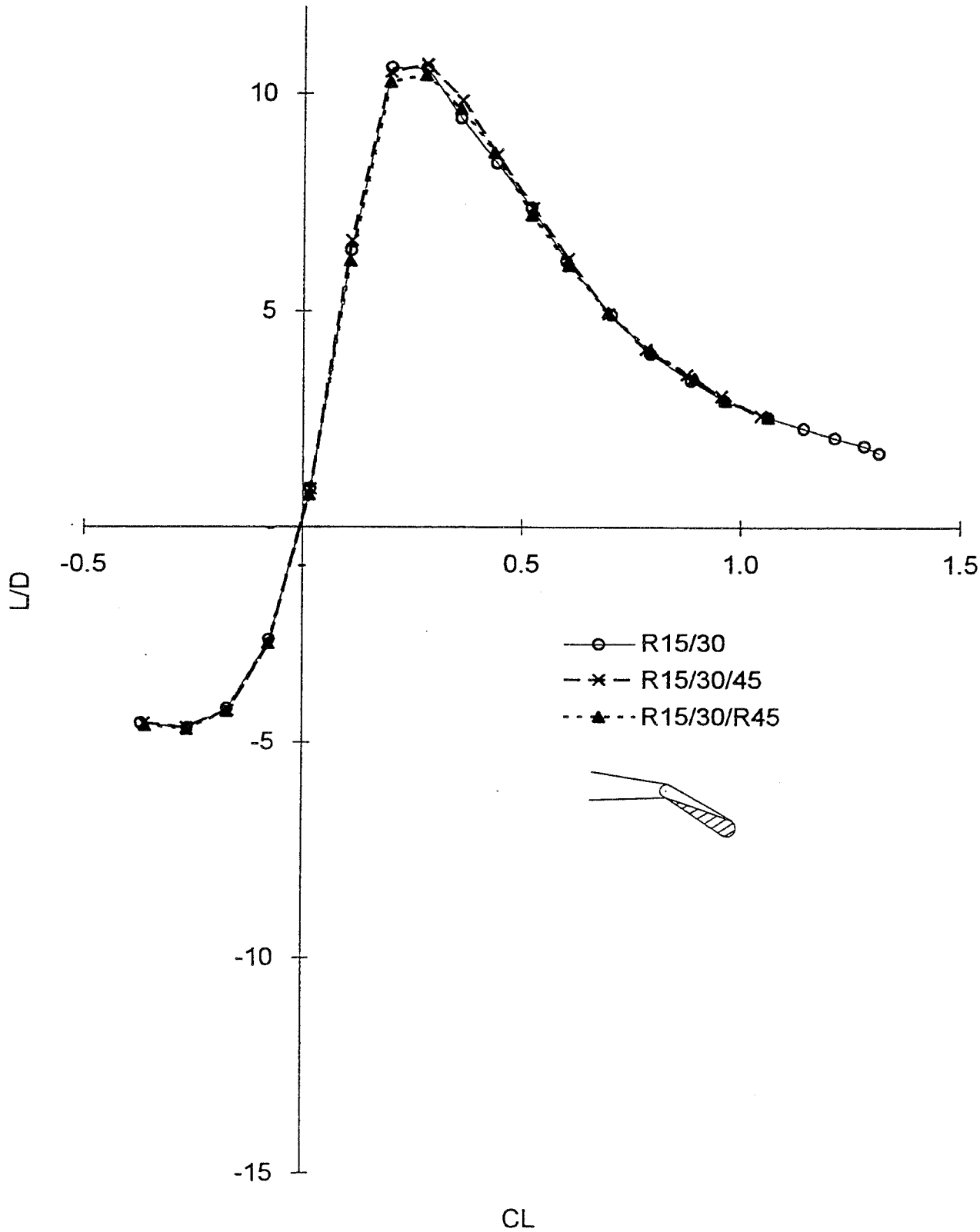

Fig.21c) L/D-C_L

Fig.21 Effect of Reynolds Number & Roughness (R15/30)

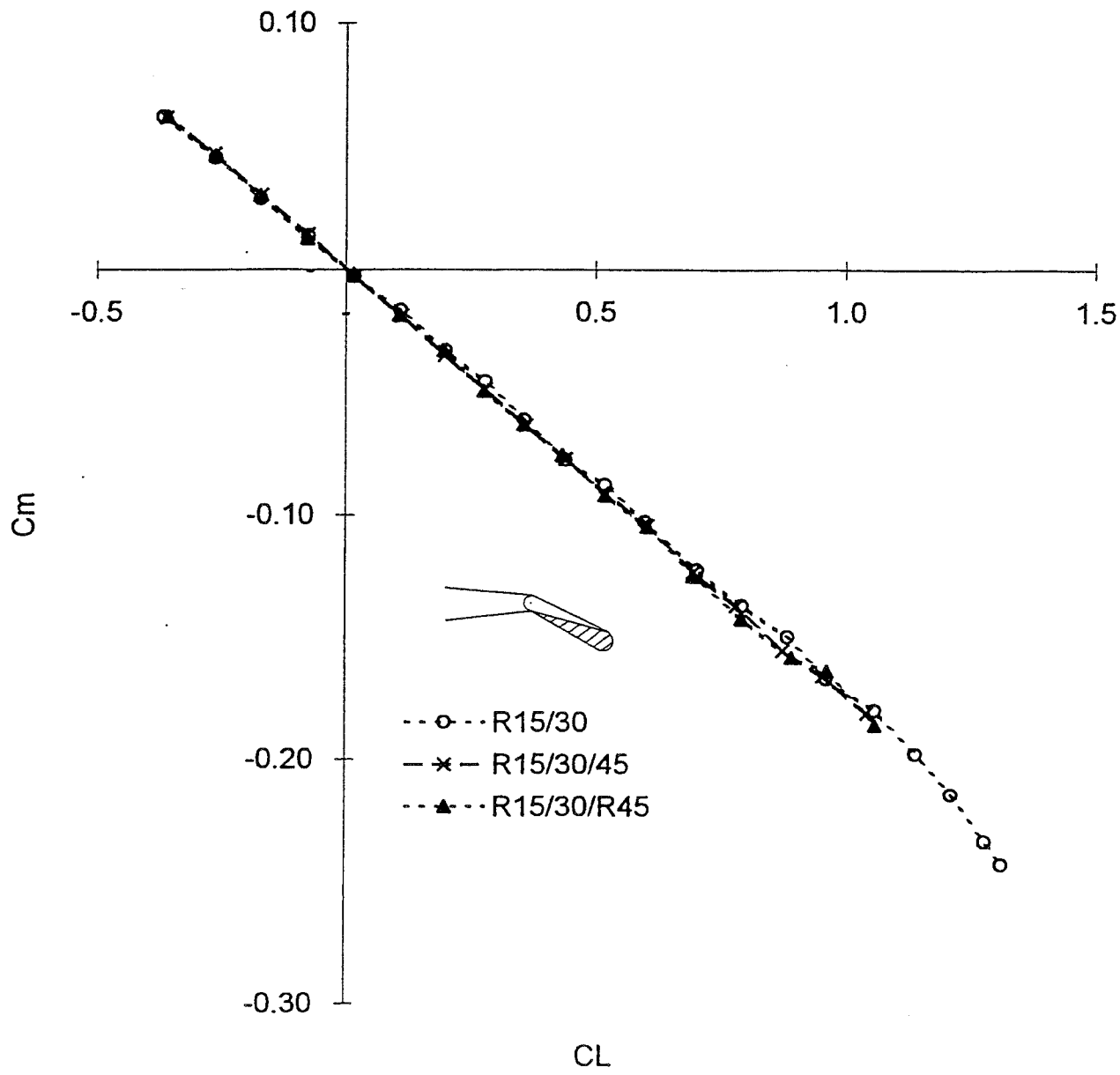

Fig.21d) C_m-C_L

Fig.21 Effect of Reynolds Number & Roughness (R15/30)

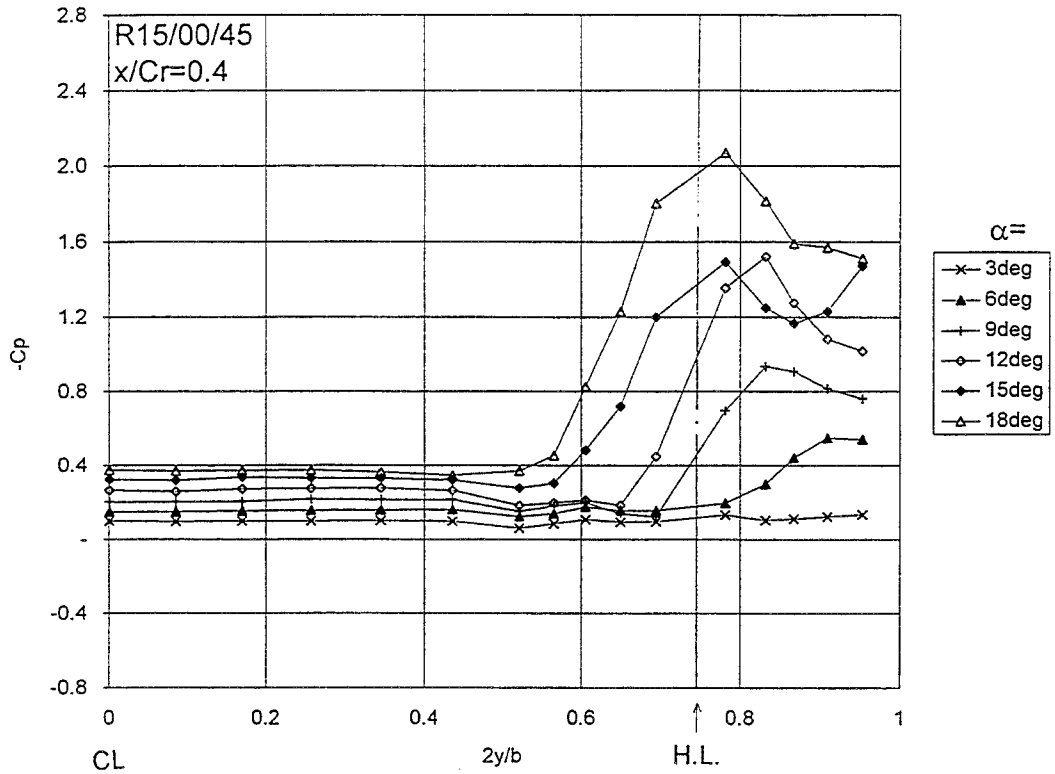

Fig.22a) R15/00/45, x/Cr=0.4

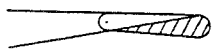

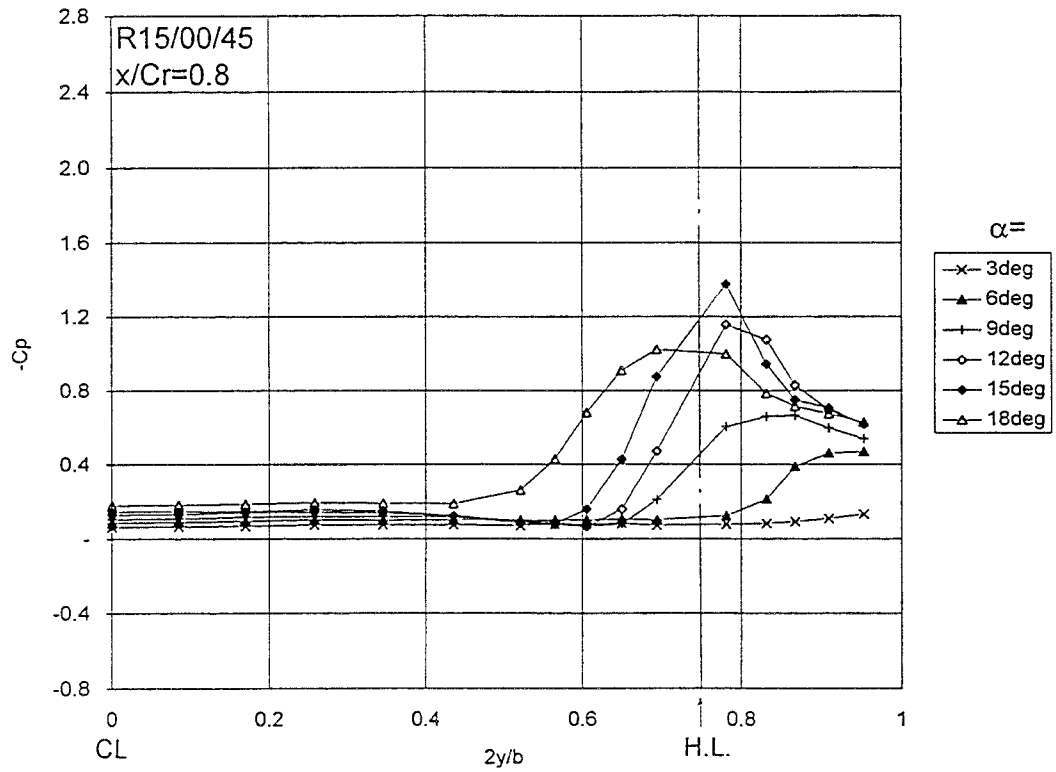

Fig.22b) R15/00/45, x/Cr=0.8

Fig.22 Surface Pressure Distributions at U_∞=45m/s

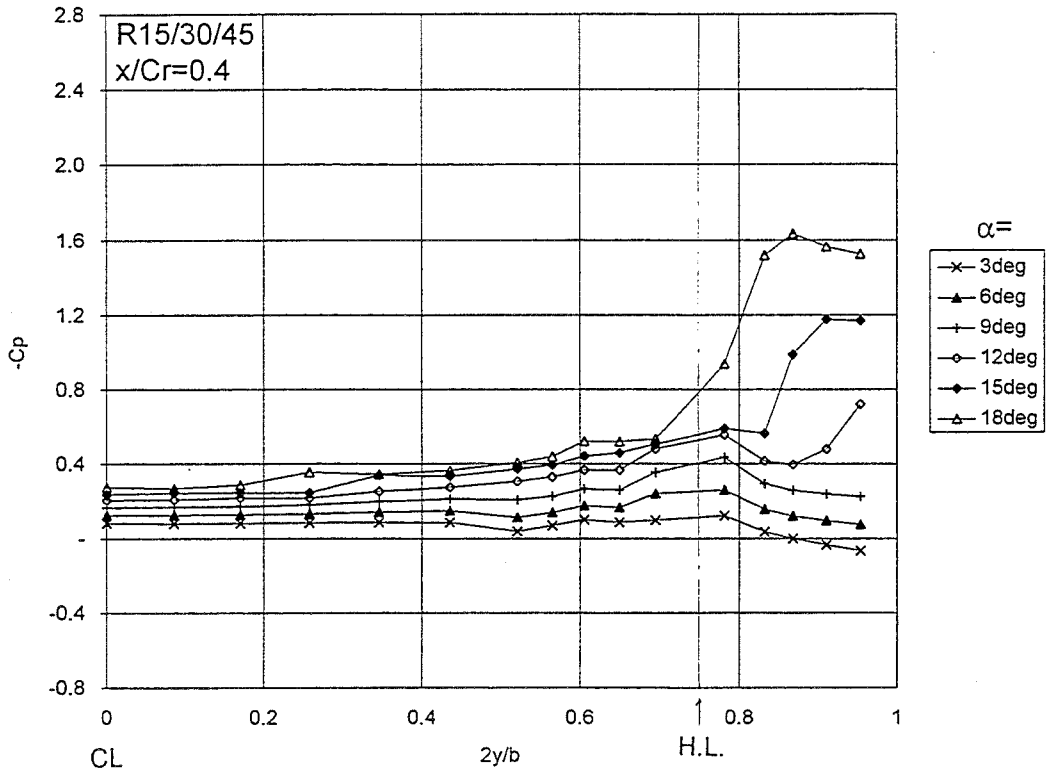

Fig.22c) R15/30/45, x/Cr=0.4

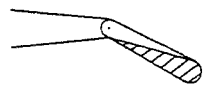

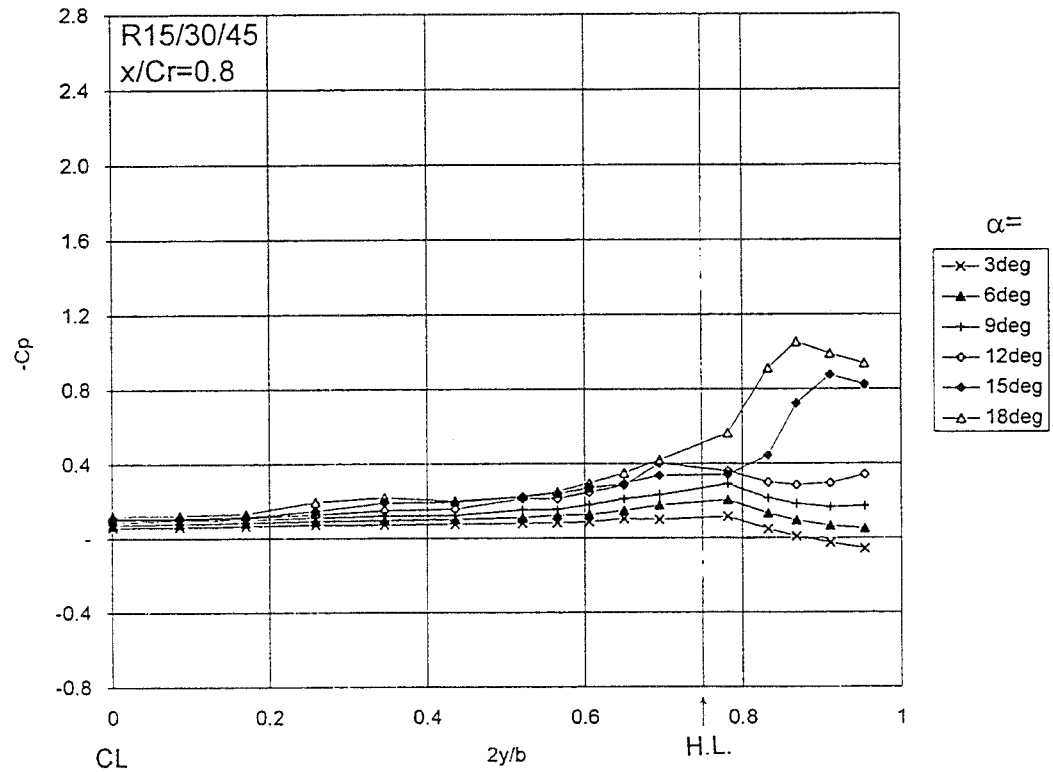

Fig.22d) R15/30/45, x/Cr=0.8

Fig.22 Surface Pressure Distributions at U_∞=45m/s

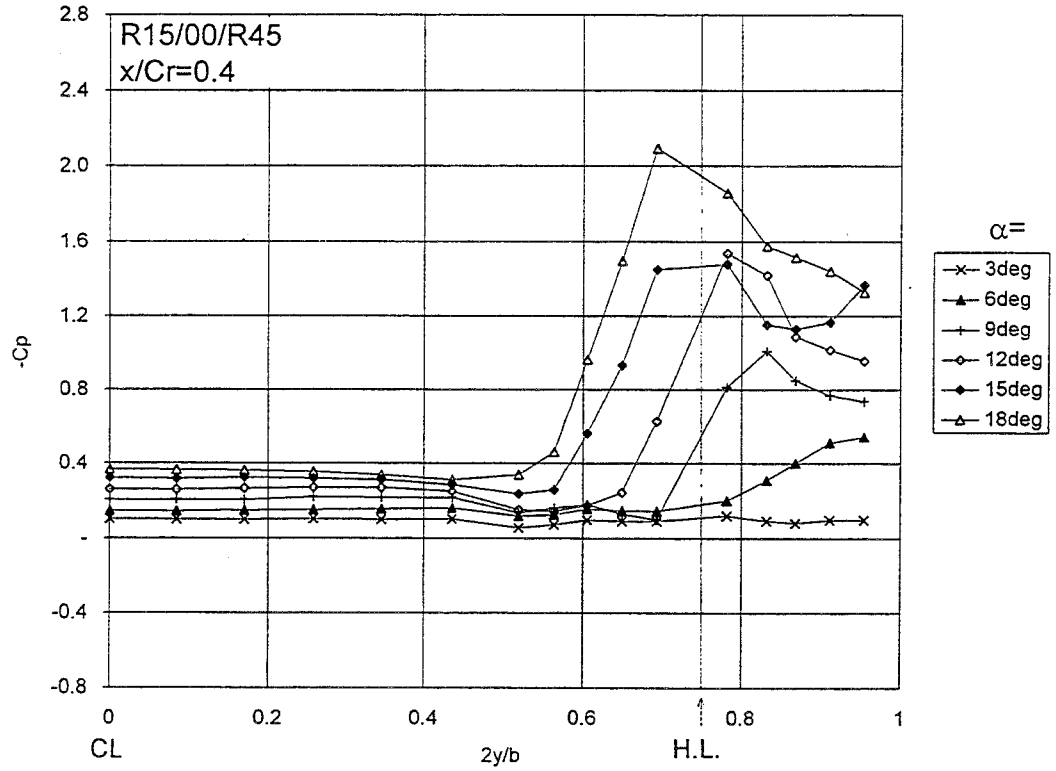

Fig.23a) R15/00/R45, x/Cr=0.4

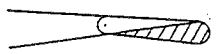

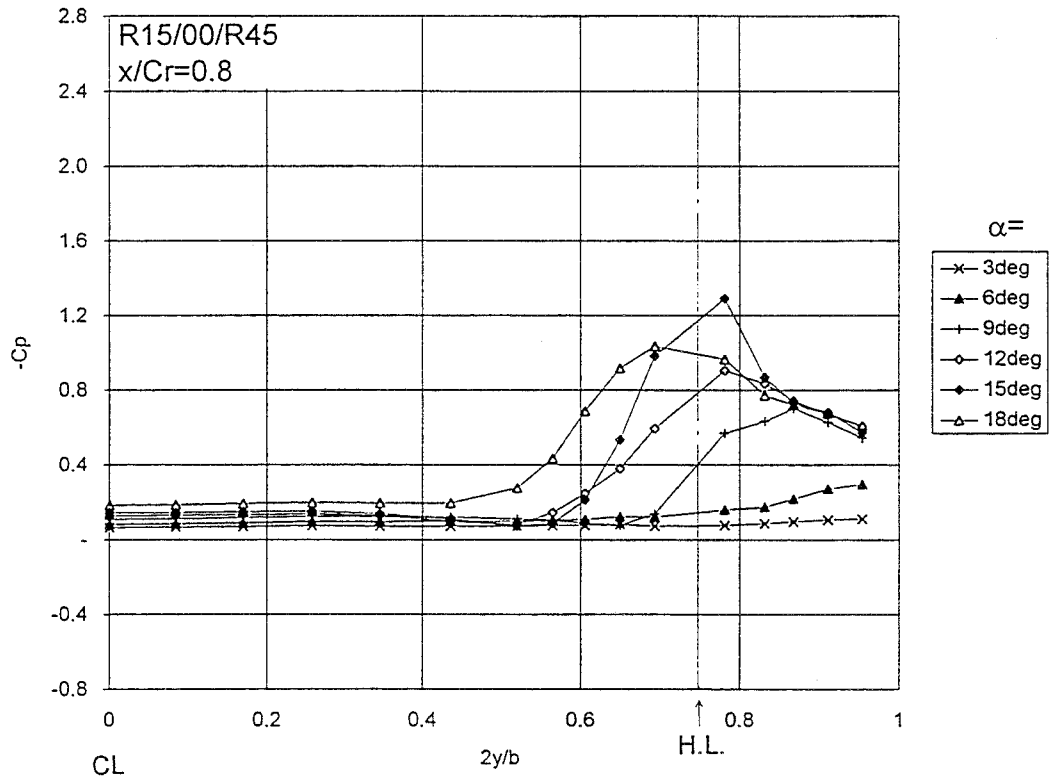

Fig.23b) R15/00/R45, x/Cr=0.8

Fig.23 Surface Pressure Distributions with Roughness at U_∞=45m/s

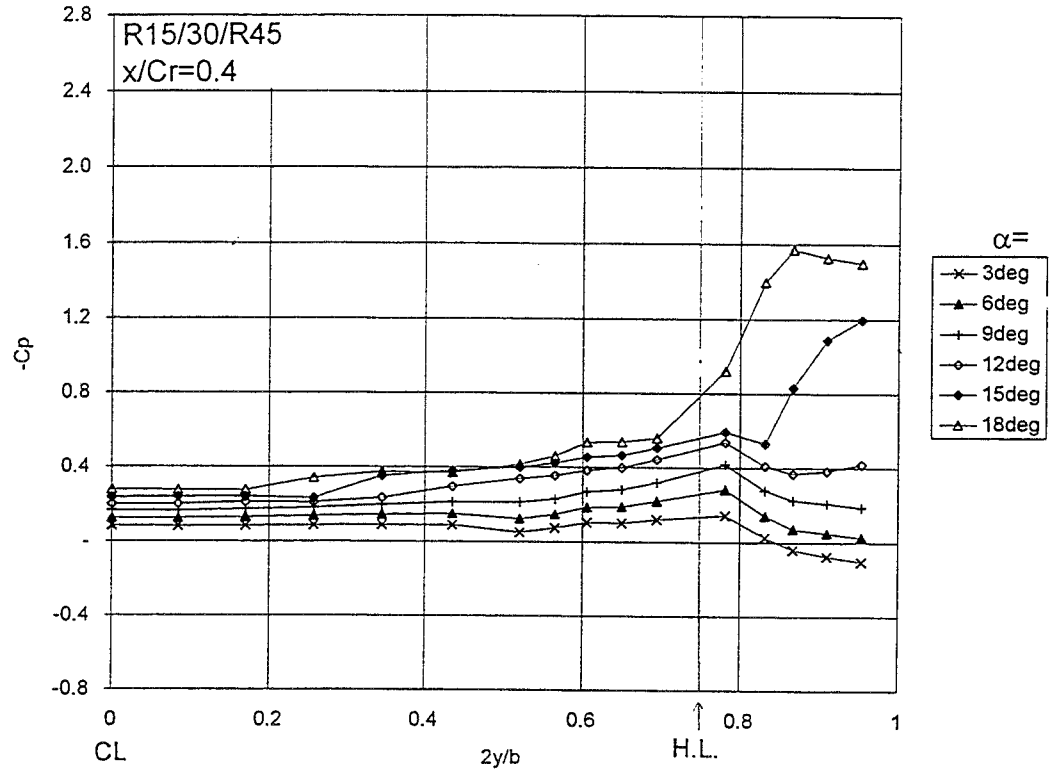

Fig.23c) R15/30/R45, x/Cr=0.4

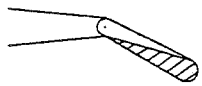

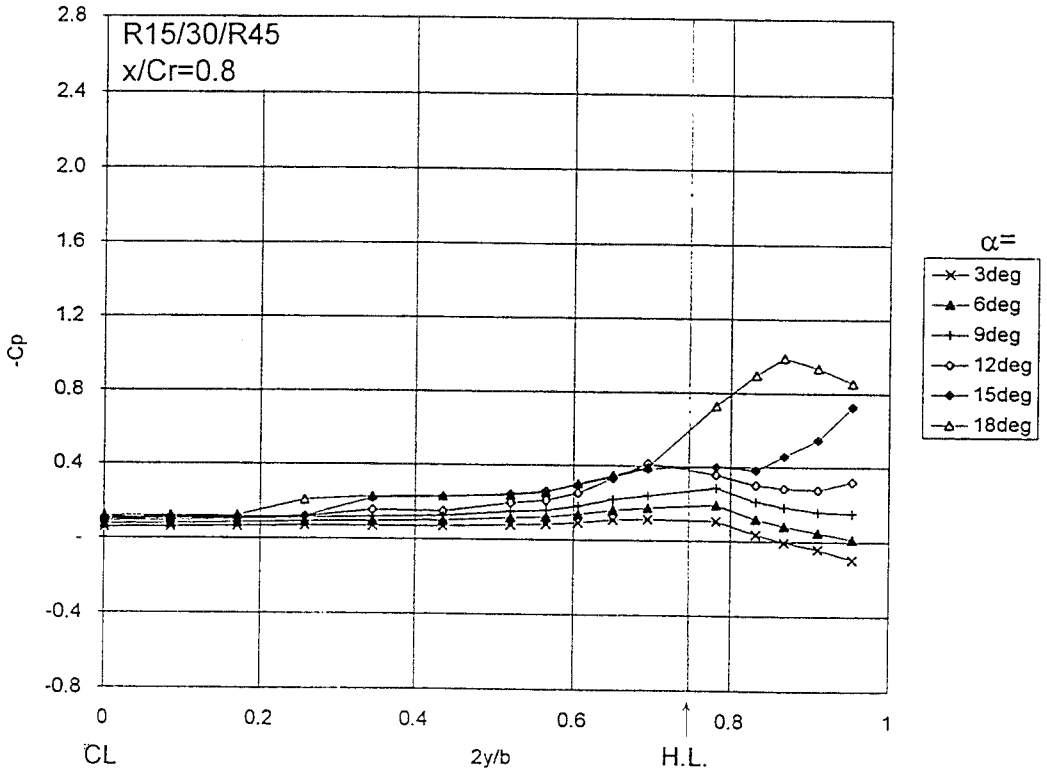

Fig.23d) R15/30/R45, x/Cr=0.8

Fig.23 Surface Pressure Distributions with Roughness at U_∞=45m/s

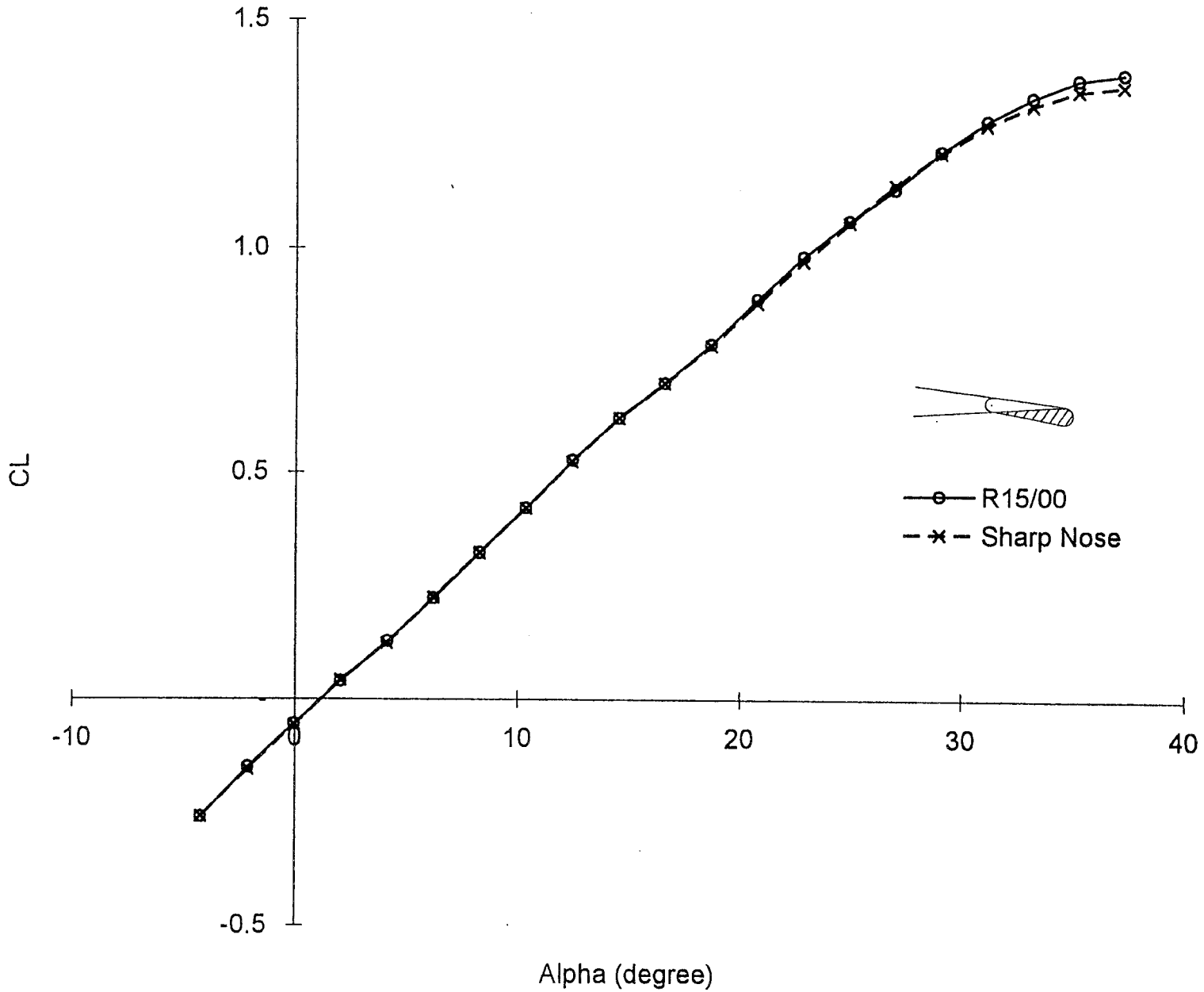

Fig.24a) C_L-α

Fig.24 Effect of Nose Leading-Edge Sharpness

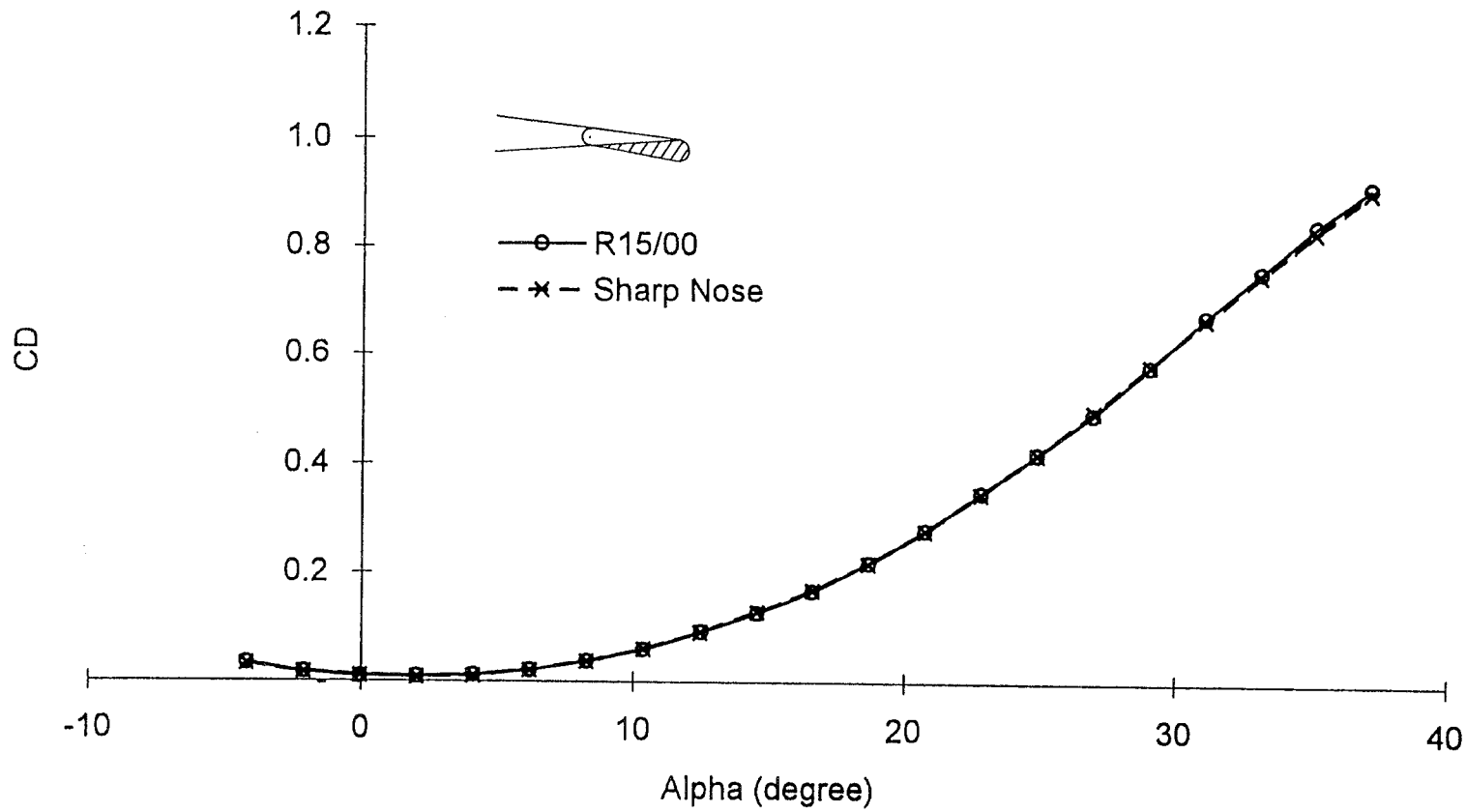

Fig.24b) C_D-α

Fig.24 Effect of Nose Leading-Edge Sharpness

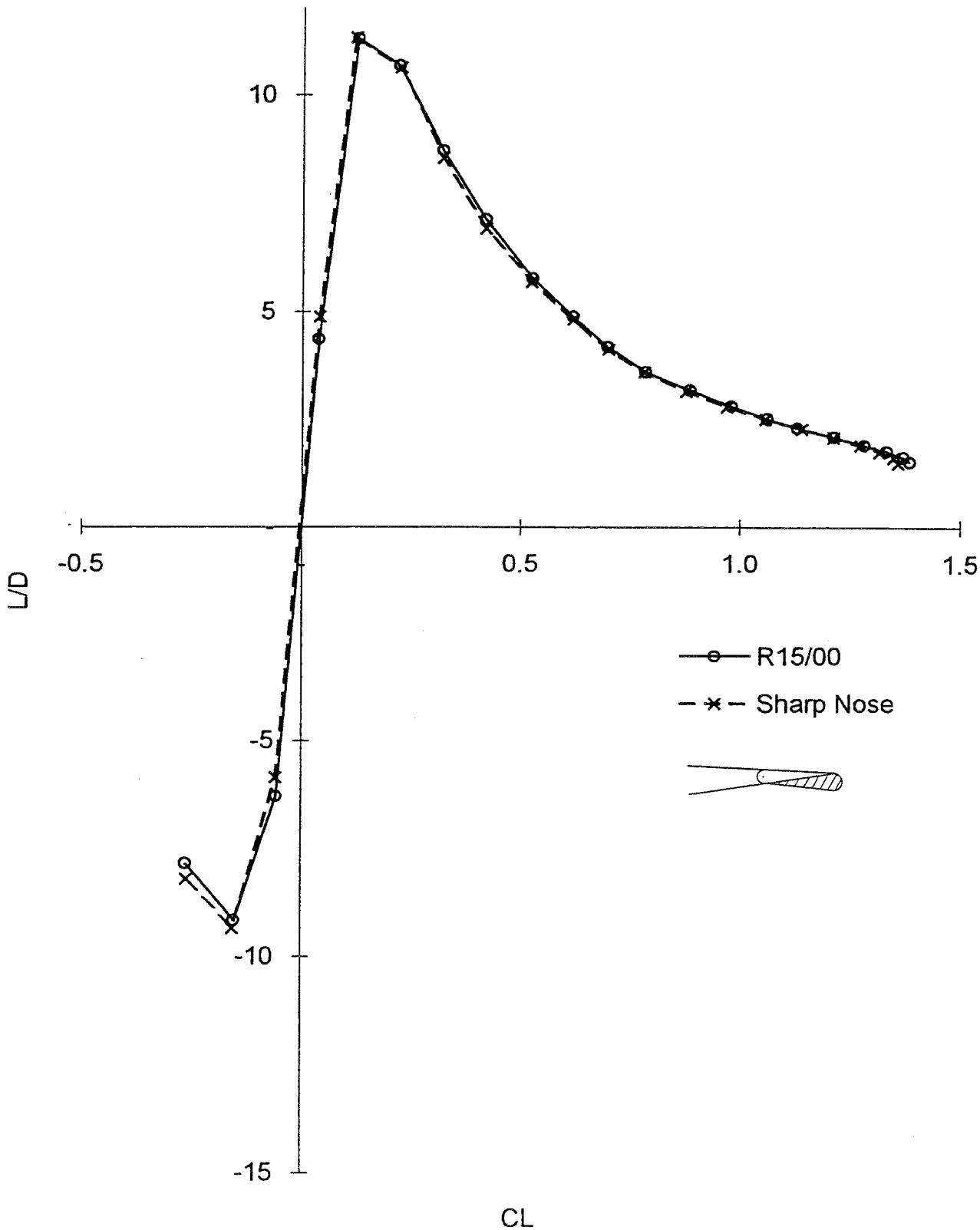

Fig.24c) L/D-C_L

Fig.24 Effect of Nose Leading-Edge Sharpness

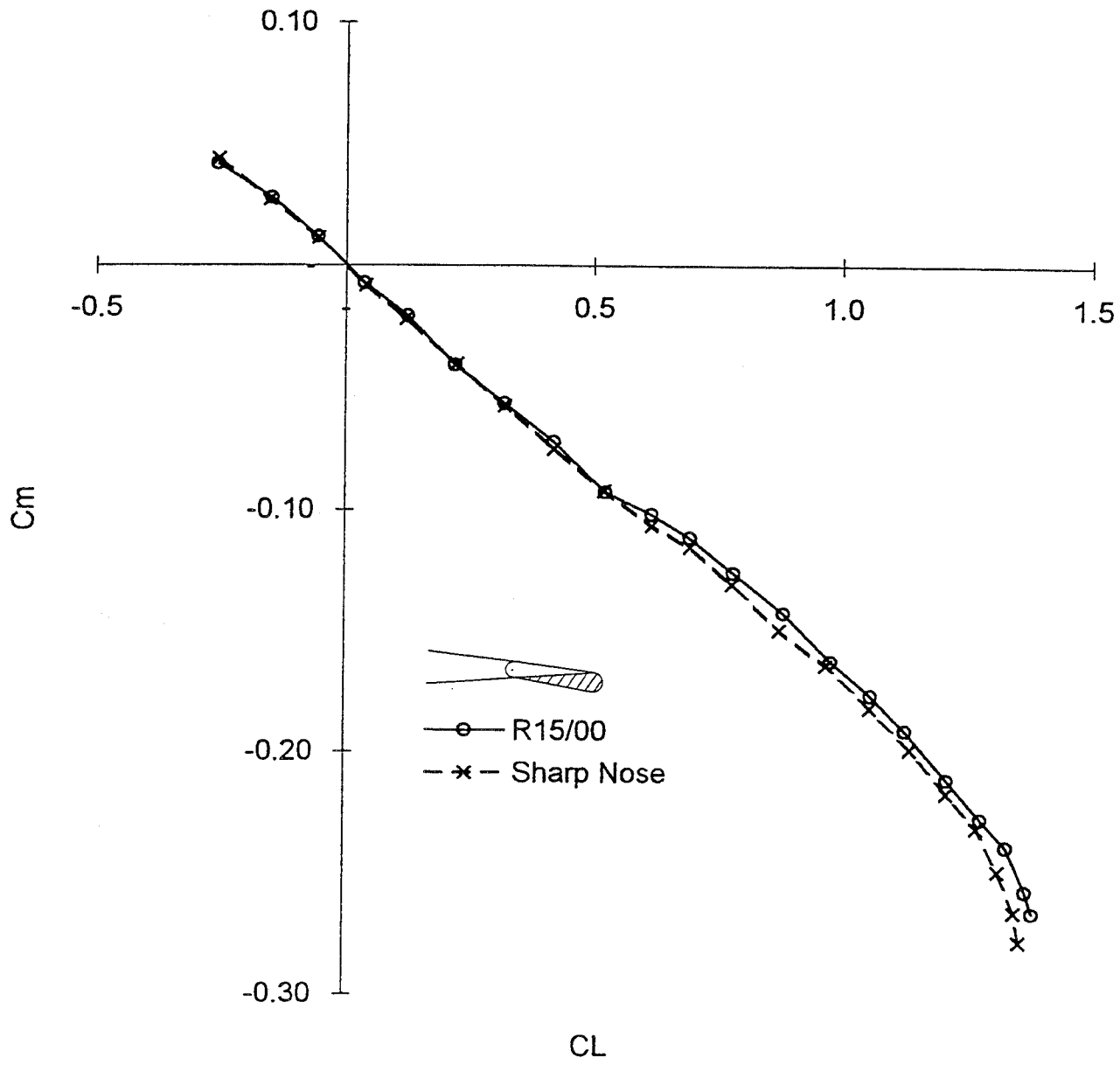

Fig.24d) C_m-C_L

Fig.24 Effect of Nose Leading-Edge Sharpness

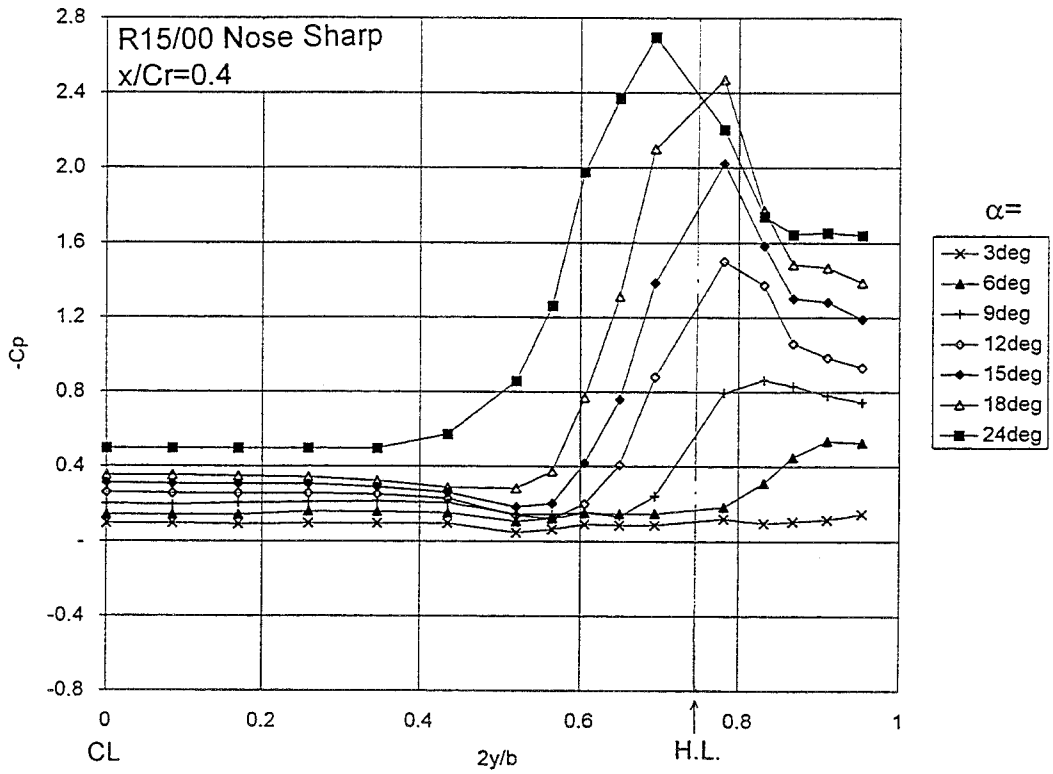

Fig.25a) R15/00, *x/Cr*=0.4

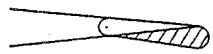

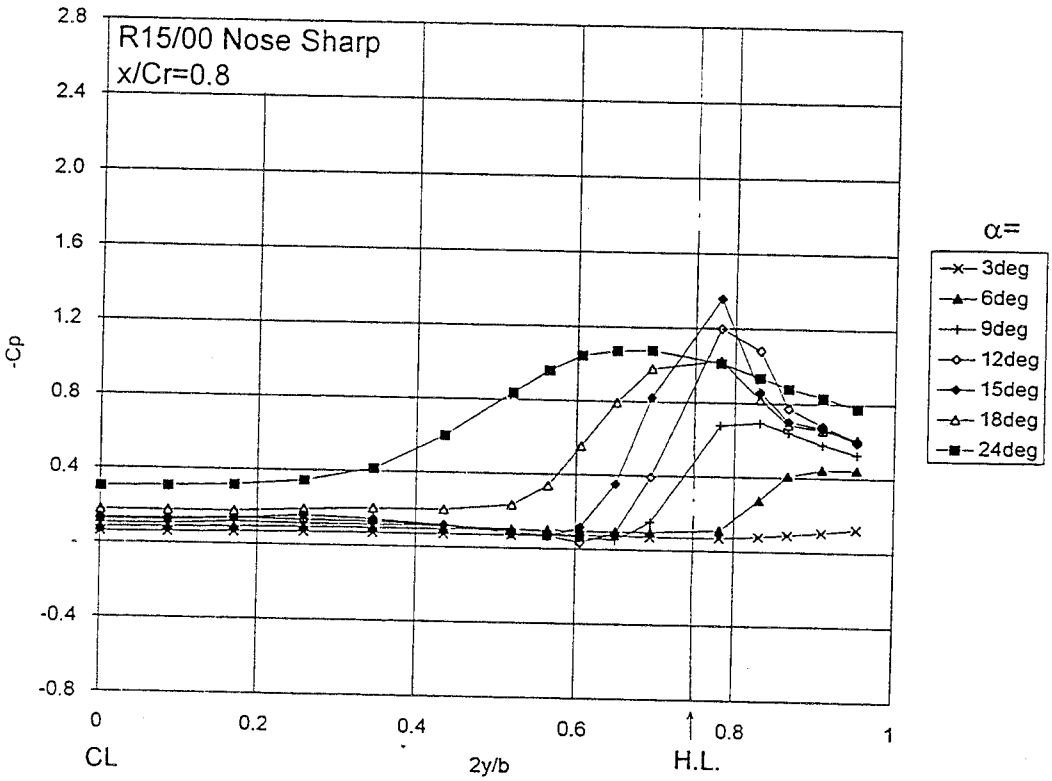

Fig.25b) R15/00, *x/Cr*=0.8

Fig.25 Surface Pressure Distributions (Nose Sharpness)